DEVELOPMENT OF MICROCHIP ELECTROPHORESIS BASED METHODS TO PROFILE CELLULAR NITROSATIVE STRESS

By

H. M. DULAN B GUNASEKARA

Submitted to the graduate degree program in Department of Chemistry and the Graduate Faculty of the University of Kansas in partial fulfillment of the requirements for the degree of Doctor of Philosophy.

_____

Chairperson- Prof. Susan M. Lunte

_____

Prof. Craig E. Lunte

_____

Dr. Cindy L. Berrie

_____

Prof. Richard S. Givens

_____

Dr. Prajna Dhar

Date Defended: 15th April 2014

The Dissertation Committee for H. M. Dulan B. Gunasekara

certifies that this is the approved version of the following dissertation:

DEVELOPMENT OF MICROCHIP ELECTROPHORESIS BASED METHODS TO PROFILE CELLULAR NITROSATIVE STRESS

_____

Chairperson- Prof. Susan M. Lunte

Date approved: 15th April 2014

Abstract

Nitric oxide (NO) is the main reactive nitrogen species (RNS) produced by immune cells. NO reacts with superoxide to produce peroxynitrite ($ONOO^-$). These two RNS are capable of nitration, nitrosylation and oxidation of intracellular biomolecules that can alter various biochemical processes. To help maintain cellular redox homeostasis in nitrosative and oxidative stress, antioxidant molecules are present in the cells. However, excessive nitrosative stress can alter the balance between antioxidants and prooxidants and therefore it plays an important role in cancer, cardiovascular and neurodegenerative diseases. A method for the simultaneous detection of prooxidants and antioxidants associated with nitrosative stress in biological samples would be beneficial for better understanding of their role in disease states. Therefore, in this dissertation a separation-based approach is described that makes it possible to detect and quantify cellular antioxidants and prooxidants such as NO, $ONOO^-$, glutathione and ascorbic acid.

Microchip electrophoresis (ME) was selected as the separation method due to its fast analysis times, compatibility with low sample volumes and potential future application to chemical cytometry. Most prooxidants and antioxidants are electrochemically active and therefore, electrochemical detection was used as the primary detection mode. First, a ME method with in-channel amperometric detection that employed an isolated potentiostat was developed for the detection of NO, $ONOO^-$, and other biologically important molecules associated nitrosative stress. Separation of these species was achieved in less than 35 s, which made it possible to detect prooxidants before they significantly degraded. Following this, two dual electrode configurations were developed and evaluated for better identification of reactive species in standard mixtures and cell lysates using voltammetric characterization.

The ME-amperometric method was then used for detection and quantification of NO_2^- and NO in macrophage cells under native and LPS stimulated conditions. Glutathione, a cellular antioxidant, was also measured in these studies and compared with the prooxidant levels in the cells. For further confirmation of NO production in these cells, ME with laser induced fluorescence detection was used for

the determination of NO using diaminofluorofluorescein. This same probe and separation was also used to investigate the heterogeneity of NO production in single cells using a cytometric device in collaboration with the Culbertson group. The main future goal of this project is to monitor macrophage cellular heterogeneity during nitrosative stress using an electrochemical cytometric device.

Dedication

To my loving parents

Acknowledgement

I owe my sincere gratitude to a great many people who helped and supported me during last few years.

I would like to express my sincere gratitude to my advisor Dr. Susan M. Lunte. I am indebted to her support, advice and all the help given in each and every step in my graduate career. She gave me the opportunity to join her lab and provided me with numerous opportunities to develop as a scientist. Her scientific thinking, writing and mentoring inspired me to become the person who I am today. Even with her busy schedule she was always available for meetings and discussions. She softly and steadily guided and mentored me to achieve my research goals. Also, writing this dissertation and publishing my research would not have been possible without her enormous guidance. I am also thankful for all the opportunities she has given me to attend various conferences that taught me to deliver good scientific talks as well as provided me with opportunities to network with scientific community. Also, she nominated me to several department and travel awards and this appreciation triggered me to explore more in research. I greatly appreciate the opportunity she gave me to write research proposals. It sharpened my knowledge and improved my writing and scientific thinking. Not to mention that she edited much of my writing, including my dissertation, and I am very thankful to her. Also, she gave me great opportunities to mentor young students and allowed me to form a single cell analysis group. Also, I am grateful for the many recommendation letters she wrote on my behalf.

Dr. Craig Lunte, Dr. Cindy Berrie, Dr. Richard Givens, Dr. Prajna Dhar and Dr. Karen Nordheden; I consider it an honor to have them in my oral comprehensive exam and dissertation committee. I am very thankful for their generous support given during the preparation of this dissertation, oral examination and my analytical division seminar. I want to thank Dr. Craig Lunte for serving as a reader and correcting my dissertation. I also want to thank Dr. Cindy Berrie for accepting my last minute invitation to serve as a reader. Further, I am immensely grateful to Dr. Cindy Berrie for serving as a reference and sending many recommendation letters through the years.

I am very lucky to be a member in Lunte research group. During my time, I met individuals with unique scientific, cultural and social experiences. It is my pleasure to share the credit of my work with postdoctoral fellows of Dr. Matt Hulvey and Dr. Philip Livanec; clean room director Ryan Grigsby; fellow graduate students Courtney Kuhnline Sloan, Tom Linz, Anne Regel, David Scott, Jessica Creamer, Rachel Saylor, Nate Oborny, Caitlin Schupp, Abdullah Al-Hossaini, Joe Siegel, Shamal Gunawardhana, Manjula Wejesinghe; undergraduate students Emilie Mainz, Pann Pichetsunnthorn, Keelan Trull (REU), Erin Reid, Derek Jensen, Jeff Bauman, Andrew Longanecker, Erin Evans, Christa Snyder (REU), Shannon Krauss (REU), Emer Duffy, Roy Meyler, Takara Bighorse; visiting scientists and scholars Dr. Fracassi da Silva, Giuseppe Caruso, Diogenes Meneses dos Santos, Bruno Lucca, Simon Pfeiffer and Richard Piffer. We always had good scientific conversations, helped each other with experiments, trained younger students, helped with oral exams and conference talks and shared good food and drinks. I will miss those happy times. Especially, I want to extend my appreciation to Dr. Matt Hulvey, Courtney Kuhnline Sloan, Dr. Fracassi da Silva, Tom Linz and Rachel Saylor, for many interesting scientific discussions as well as for the support given me during last few years.

I owe my deepest gratitude to single cell analysis group (Dr. Matt Hulvey, Dr. Fracassi da Silva, Emilie Mainz, Joe Siegel, Pann Pichetsunnthorn, Giuseppe Caruso, Keelan Trull (REU), Derek Jensen, Diogenes Meneses dos Santos, Jeff Bauman, Richard Piffer, Andrew Longanecker) in the Lunte research group. It gives me great pleasure to thank Dr. Matt Hulvey, who trained and mentored me when I joined the lab in 2009. Matt has generously provided me with many recommendation letters at various times. I am very thankful to Emilie Mainz who helped me to culture cells and she was a key to the success of the fluorescence detection part of this project. Also, I want to thank Giuseppe Caruso for cell protocol optimizations and Joe Siegel for working with me on the final nitrite and nitric oxide experiments. Pann Pichetsunnthorn is a great undergraduate student, who worked with me on voltammetric experiments and calculations. I considered it an honor to work with Dr. Fracassi da Silva and I am thankful to him for helping me with NONOate experiments and writing recommendation letters. I also greatly appreciate all the support given by Ryan Grigsby for microfabrication through the years. Also, I would like to thank Dr.

Christian Schöneich for sharing his expertise with us and providing peroxynitrite samples. I want to thank Pinnacle Technologies, Lawrence, KS for developing and providing isolated potentiostats over last five years.

Dr. Culbertson; it was a great honor to work with you in single cell experiments. I want to greatly appreciate all the help and support given by Dr. Chris Culbertson, Ane Culbertson and Eve Metto at Kansas State University. Ane Culbertson supplied Jurkat cells for us and helped culture them and Eve developed the single cell cytometric device. I am very grateful to Dr. Culbertson for serving as a reference and generously writing many recommendation letters for me.

I greatly appreciate and thank Nancy Harmony, Tom Linz, Rachel Saylor and Yamuna Ariyarathna for their editorial assistance. The Dr. Craig Lunte lab was always helpful with research. I want thank Dr. Jennifer Laurence group for letting us use the cell culture hood over the past five years. KU Chemistry Departmental staff and Higuchi Biosciences Center staff (some of the names are Donna Burruss, Gary Webber, Jan Akers, Beth Benfield, Beverly Johnson and Sonjia Payne) were very helpful with travel documentation and reimbursements, preparing posters, hiring, ordering and submitting proposals and I am very grateful to them. Especially I want to appreciate Gary Webber for his help during my stay at KU.

I greatly appreciate the support of the National Institute of Health, KU Chemistry Department and Adams Institute at KU the funding the research. Also, I am grateful to the sponsors of J. K. Lee award, Richard Givens Scholarship, McCollum Research Scholarship, The Charles and Beatrice Kulier Scholarship for their financial support. I was selected for Travel Awards by Society for Laboratory Automation, International Symposium on Capillary Chromatography, Society of Electroanalytical Chemistry, Ted Kuwana Travel Grant at KU, International Symposium on Electro- and Liquid Phase-Separation Techniques and KU Research and I appreciate their financial support that allow me to participate in various conferences.

I would like to appreciate all the teachers and mentors especially Prof. Gamini Rajapakse, Prof. Veranja Karunaratne, and Prof. Nedra Karunaratne at University of Peradeniya who guided me during my undergraduate studies. Also, I would like to appreciate all the help given by Prof. Amudhu Gopalan and Prof. Glenn D. Kuehn former Department Chairs of Chemistry and Biochemistry Department, New Mexico State University during my short stay at NMSU.

I cannot find words to express my gratitude to my family. Their support was enormous, especially in last five years. I am very fortunate to have my father H. M. Gunasekara, mother Sriyani Perera Gunasekara, my wife Yamuna Ariyarathna and my brother Chamath Gunasekara in my life. Since the day I born, my parents taught me to be a better person. Their constant support and devotion to my education have made me come this far. Their help, love and encouragement are enormous and I am very grateful to have them in my life. Yamuna, my wife is the driving force behind my success. She helped and encouraged me in every step of my graduate career and I am very grateful for all her efforts. Also, she takes care of me and lets me spend a lot of time on my research. I appreciate all her efforts. My brother fulfills all the family responsibilities, that I am supposed to do, giving me opportunity to study abroad and I greatly appreciate his support. Also, I appreciate all the help given by, and happy moments shared with my Sri Lankan friends in Lawrence, KS.

Table of Contents

List of Figures

Figure 3.2: Generation of NO using (A) DEA/NO and (B) PROLI/NO (The reaction schemes were adapted from www.caymanchem.com).

Figure 3.3: Monitoring the acid hydrolysis of DEA/NO at pH 7. Conditions: BGE: 10 mM boric acid, 2 mM TTAB, pH 11. Triangle – nitrite; solid circle – DEA/NO; open circle – NO. Gated injection: –2200 V at SR, –2400 V at BR, 1 s injection, 60 s run. The inset shows the magnification of the electropherogram from 750 to 950 s. The arrows indicate the sample injection. Baseline subtraction was accomplished using Origin

Figure 3.4: (A) DEA/NO peak decay fit into first-order rate law. (B) Peak heights obtained during DEA/NO acid hydrolysis as a function of sequential injections. (The data represented here obtain from the electropherogram in Figure 3.3)

Figure 3.5: (A) Monitoring the acid hydrolysis of PROLI/NO at pH 7.2–7.4. Triangle – nitrite; solid circle – PROLI/NO; open circle – NO. The arrows indicate sample injections. Other conditions as in (B) Peak heights in the part A as function of sequential injections. The *x*-axis can be converted to time by using the total separation time.

Figure 3.6: Comparison of the nitrite and NO migration times with a 100 µM nitrite and hydrogen peroxide standard solution

Figure 3.7: Monitoring the acid hydrolysis of PROLI/NO at pH 9.0. ▼– nitrite; ●– PROLI/NO. The arrows indicate sample injections. Other conditions as in Figure 3.3.

Figure 4.1: (A) Single (B) Dual-series and (C) Dual-parallel electrode configuration and pictures of these electrode alignments

Figure 4.2: The basis of generation of current ratios by hydrodynamic voltammetry

Figure 4.3: (A) Dual channel microchip design used for dual-parallel electrode configuration (Adapted from ref. 30) (B) An injection of a same sample into the two separation channels using normal polarity

Figure 4.4: The separation ground and Ag/AgCl reference electrode placement in (A) Dual-series and (B) Dual-parallel configuration

Figure 4.5: An example for characterization of dual-series configuration using nitrite, tyrosine and H_2O_2 standards. The sample was prepared in 10 mM boric and 2 mM TTAB buffer at pH 11 and the separation was also achieved using the same buffer. +1100 mV versus Ag/AgCl reference electrode was used for both end and in-channel electrodes.

Figure 4.6: An example for characterization of dual-parallel configuration using nitrite, tyrosine and H_2O_2 standards. The sample was prepared in 10 mM boric and 2 mM TTAB buffer at pH 11 and the separation was also achieved using the same buffer. (A) WE-1 = WE-2 = +1100 mV (B) WE-1 = +1100 and WE -2 = +950 mV versus Ag/AgCl reference electrode were used.

Figure 4.7: The degradation of contaminated $ONOO^-$ standards over several injections using the dual-series configuration. The sample was prepared in 10 mM boric and 2 mM TTAB buffer at pH 11 and the separation was also achieved using the same buffer. +1100 mV and +950 mV versus Ag/AgCl reference electrode was used for end and in-channel electrodes respectively.

NaCl) and high conductivity separation buffer (7.5 mM NaCl). (C) No change to the conductivity of the sample and separation buffer.

Figure 6.4: (A) Comparison of LPS-stimulated (top) and native (bottom) RAW 264.7 macrophage cell lysates using ME-EC. (B) Comparison of the ME-EC method and the Griess assay for determining the increase in nitrite concentration resulting from a 24 h LPS stimulation relative to the nitrite concentration produced from native cells. The sample was prepared in 10 mM boric acid and 2 mM TTAC buffer at pH 10.3 and the separation was achieved with a 10 mM boric acid, 7.5 mM NaCl and 2 mM TTAC buffer at pH 10.3

Figure 6.5: Detection of NO in macrophage cell lysate. LPS-stimulated cell lysate (top) and native cell lysate (bottom). Inset is a magnified portion of the LPS-stimulated cell lysate. The cells were lyzed using 500 µL of 10 mM boric acid and 2 mM TTAB buffer at pH 11 and the separation was achieved with a 10 mM boric acid and 2 mM TTAB buffer at pH 11.

Figure 6.6: Detection of NO in cell lysate. LPS-stimulated cell lysate (top) and native cell lysate (bottom). Inset is a magnified portion of the LPS-stimulated cell lysate. The sample was prepared in 10 mM boric acid and 2 mM TTAC buffer at pH 10.3 and the separation was achieved with a 10 mM boric acid, 7.5 mM NaCl and 2 mM TTAC buffer at pH 10.3.

Figure 6.7: Comparison of the nitrite and glutathione (GSH) levels as a result of LPS stimulation relative to that of the native cell lysate. The sample was prepared in 10 mM boric acid and 2 mM TTAC buffer at pH 10.3 and the separation was achieved with a 10 mM boric acid, 10 mM NaCl and 2 mM TTAC buffer at pH 10.7.

Figure 7.1: Eelectropherograms of native macrophage cell lysates using dual-parallel electrodes. The cells were lysed using 250 µL of 10 mM boric and 2 mM TTAB buffer at pH 11 and the separation was also achieved using the same buffer. WE-1 = +1100 and WE -2 = +950 mV versus Ag/AgCl reference electrode were used.

Figure 7.2: A schematic of modified single cell analysis device

Figure 7.3: (A) Comparison of LPS-stimulated and native Jurkat cell lysates using ME-EC. An LPS concentration of 3 µg/mL for 6 h was used in these experiments. The sample was prepared in 10 mM boric acid and 2 mM TTAB buffer at pH 11 and the separation was also achieved using the same buffer.

Figure 7.4: Proposed ME coupled bipolar electrode set up for conversion of an electrochemical signal into fluorescence signal

List of Tables

Chapter 1

Introduction

1.1 Cellular nitrosative stress

Excessive production of reactive nitrogen species (RNS) in cells is known as cellular nitrosative stress and has been linked to various diseases including atherosclerosis, Parkinson's disease, Alzheimer's disease, hypertension, arthritis and cancer [1-6]. RNS are exceedingly reactive and capable of nitration (formation of a nitro group), nitrosylation (addition of a nitroso group), oxidation and peroxidation of important biomolecules (e.g. proteins, thiols, DNA etc.) and metal centers [1-5]. These reactions can alter ongoing important biological processes and promote inflammation, apoptosis and necrosis [1-5]. The main reactive nitrogen species produced in the body is nitric oxide (NO), which can lead to the production of many other reactive species including dinitrogen trioxide (N_2O_3), nitrogen dioxide radical ($^{\cdot}NO_2$), and peroxynitrite ($ONOO^-$). When the physiological NO concentration is below 200 nM, only NO related biological reactions occur. However, physiological concentrations of NO higher than 400 nM can lead to nitrosative stress where formation of other RNS becomes significant [6]. The reaction of NO with O_2 (often referred to as NO autooxidation) generates nitrogen dioxide ($^{\cdot}NO_2$). Nitrogen dioxide can further react with NO to produce N_2O_3 that can degrade into nitrite (NO_2^-) and nitrate (NO_3^-) [7,8]. Nitrogen dioxide ($^{\cdot}NO_2$) is more reactive than N_2O_3 [4,7,8].

NO can react with thiols to produce nitrosothiols, and nitrosoglutathione and nitrosoalbumin are considered to be NO carriers that transport NO for cell signaling and various other biological functions [9]. NO can also react with $O_2^{-\cdot}$ (superoxide) to produce $ONOO^-$, which is harmful to the cellular environment due to its reactivity with macromolecules, and its ability to convert into the neutral species, peroxynitrous acid (ONOOH), which can cross membranes leading to the subsequent production of additional reactive radical species following degradation [1,5,10,11]. The formation of RNS from NO and some of the reactions of RNS with biomolecules are summarized in Figure 1.1 [12].

NO is a highly diffusible species and can travel to sites where superoxide is generated such as mitochondria [1]. The partial one electron reduction of O_2 forms the $O_2^{-\cdot}$ radical in the cellular

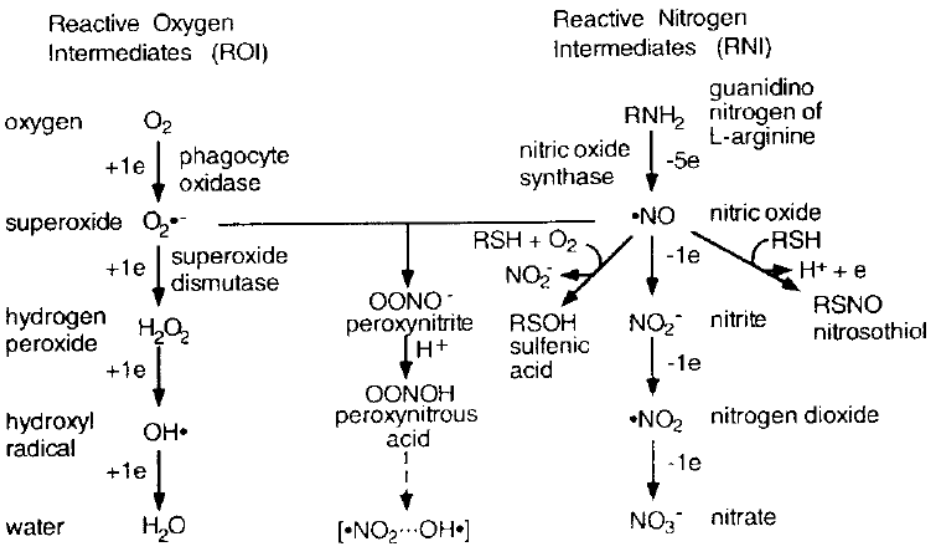

Figure 1.1: Formation of RNS and their reactions with intracellular biomolecules. (reproduced with permission from Nathan, C.; Shiloh, M. U.; *Proc Natl Acad Sci U S A*, 2000, 97, 8841-8848 Copyright (2000) National Academy of Sciences, U.S.A.)

environment. Mitochondrial dysfunction and NADPH oxidase activation are two common sources of superoxide *in vivo* [13]. Superoxide is converted inside the cells into H_2O_2 by the enzyme superoxide dismutase (SOD) [14]. The reaction of NO and $O_2^{-\cdot}$ is close to diffusion limit; therefore, NO can react with $O_2^{-\cdot}$ before it is converted to H_2O_2 by superoxide dismutase [1].

1.2 Physical and chemical properties of NO

NO is a gaseous molecule, soluble in water at a concentration of approximately 2 mM and has a very high diffusion coefficient (3.4×10^{-6} cm^2/s at 37 ºC) [15]. It is more soluble in organic than aqueous solvents and therefore, NO can be trapped in cellular membranes. It has been shown that oxidation of NO in these hydrophobic environments is faster than that in aqueous environments [15]. NO oxidation to NO_2^- follows the second order rate law and therefore it degrades slowly when present at low nanomolar concentrations. Therefore, NO can participate in important biological reactions at low concentrations (<200 nM) [6,7,15]. The main pathway of NO oxidation is by reaction with O_2 (autooxidation) and metal ions. Therefore, NO is very stable in an oxygen or metal ion free environment.

1.3 Production of RNS in cells

NO is produced in cells by the enzyme nitric oxide synthase (NOS), which converts L-arginine into L-citrulline [16,17]. NOS has a reductase and oxygenase domain and these two sites come together when calmodulin binds the enzyme leading to activation [16,17]. There are three specific isoforms of NOS; endothelial (eNOS), neuronal (nNOS) and inducible NOS (iNOS). Endothelial and neuronal cells primarily contain eNOS and nNOS and immune cells express iNOS [16]. eNOS and nNOS activation depend on the calcium binding protein calmodulin [16]. Both eNOS and nNOS depend on the intracellular calcium concentration. However, the third isoform, iNOS is structurally different and does not depend on intracellular calcium concentration and is activated as part of the immune response [16-18].

There are many different types of immune cells in the human body. Macrophages are the primary cell type and they express iNOS following immune system activation. At the same time, there are macrophages specific to different organs (e.g. macrophages in cardiac, kidney, lungs and eye) that have

unique functions. Several of these macrophage cell types have particular names (e.g. microglia: brain macrophages, Alveolar: lung macrophages, and Kupfter cell: clear debris from blood) [19]. In addition, it is well known that monocytes can be differentiated into macrophages. For example, monocytes in blood are known to migrate into the intima of a blood vessel and can be differentiated to macrophages during atherosclerosis [20,21]. Other immune cell types such as T-lymphocytes, dendritic cells and cancer cells also express iNOS [22,23]. Once iNOS is activated, it can lead to generation of large amounts of NO over an extended period of time.

1.4 Biological properties of NO

Guanylate cyclase (GC) is activated by low nanomolar concentrations of NO and produces cyclic guanosine monophosphate (cGMP) from guanosine triphosphate (GTP) [24]. This is the main role of NO in biological reactions and the GC pathway is involved in vasodilation as well as long term memory formation in the brain [24,25]. Shear force on the endothelial layer of a blood vessel, due to blood flow, induces NO release through the activation of eNOS. NO then binds with GC to produce cGMP, which can relax the smooth muscle leading to vasodilatation [24]. NO also inhibits platelet aggregation and monocyte adhesion [26]. Immune cells produce NO as a part of their defensive action through the activation of iNOS. As described previously, NO can subsequently produce other RNS such as $ONOO^-$, $^{\cdot}NO_2$ and N_2O_3. These RNS are used by immune cells to kill foreign objects such as bacteria, pathogens or cancer cells.

1.5 Cellular redox state and cellular redox balance

Oxidation of glucose generates ATP, which is the main biological energy source. During glucose oxidation, oxygen is reduced (accepts electrons) by cytochrome oxidase in mitochondria. Often there can be a leak of intermediate species such as $O_2^{-\cdot}$ that are involved in the reaction into the cellular environment (Figure 1.2) [27-29]. To mitigate this, superoxide dismutase is present in the cell and converts $O_2^{-\cdot}$ to H_2O_2. Catalase, another key enzyme present in cells, then converts the H_2O_2 into H_2O

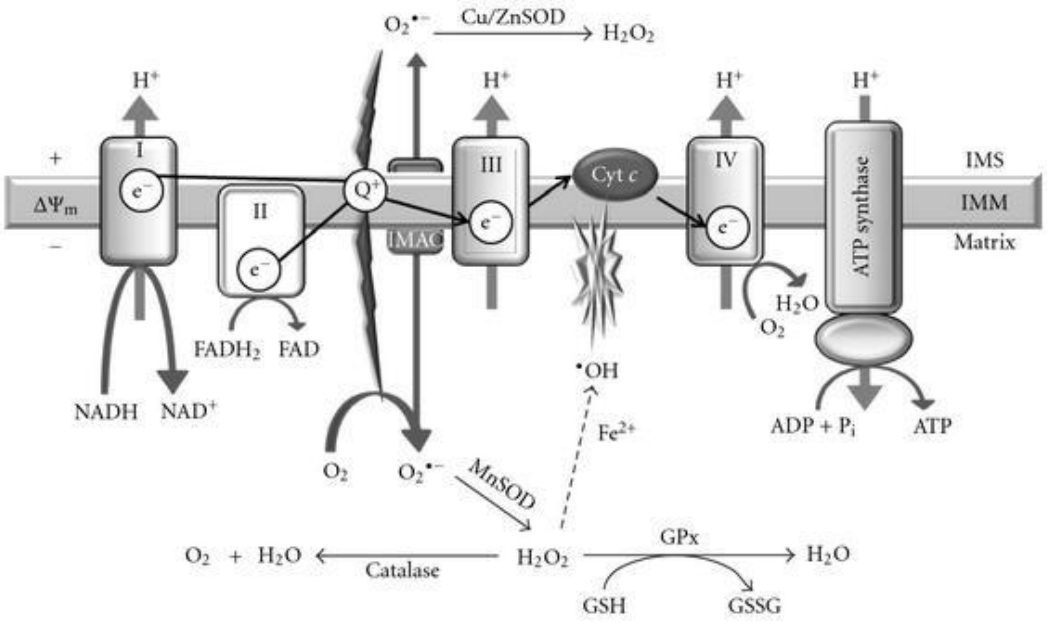

Figure 1.2: Formation of ROS in mitochondria and neutralization of ROS by antioxidant enzymes and biomolecules (reproduced with permission from Ma ZA, Zhao Z, Turk J *Experimental diabetes research*, Vol. **2012**, Article ID 703538, 11 pages, 2012 doi:10.1155/2012/703538)

(Figure 1.2) [30]. Therefore, in general, a healthy cellular environment is more reductive to facilitate these processes. There are several other molecules and enzymes present in a cell that maintain the cellular redox state including glutathione, cysteine, NADPH and glutathione peroxidase. Conversely, there are many other mechanisms that contribute to production of prooxidants. Some of these include radiation, exposure to toxins and heavy metals, cigarette smoke, high glycemic conditions and obesity [28].

The most common antioxidants and prooxidants found in cells are listed in Table 1.1. When cellular redox homeostasis is maintained, prooxidants and antioxidants are in a near balance and maintain a reduced cellular environment [31]. One key redox couple that participates in this process is glutathione and glutathione disulfide (GSH/GSSG). GSH is the reduced species and is present in millimolar concentrations inside cells to maintain a reducing environment while GSSG is present in micromolar concentrations [32]. GSH can be oxidized to GSSG in the presence of prooxidants such as H_2O_2 and $ONOO^-$ [30]. Therefore, the GSH/GSSG ratio has been used as an indicator of the cellular redox state [27].

The total cellular redox state of a cell includes a collection of reducing potentials of all the compounds along with their intracellular concentrations [27]. Schafer et al. has developed a method to determine the cellular redox state based on the concentration of the reduced and oxidized form of intracellular biomolecules (e.g. GSH/GSSG and $NADP^+$/NADPH) [27]. Due to its high concentration in the cell they calculated cellular redox potential based on GSH using the Nernst equation. It is represented by the following equation [27].

[-180 mV (GSH); 3.5 mM]

GSH provides a good representation of the cellular redox state because GSH is the main component that dominates $E_{1/2}$ in the cell. Also, a model that predicts cell proliferation, differentiation, apoptosis and necrosis have been developed using the GSH/GSSG redox couple [27]. This model shows that cell proliferation starts when the cell has a high reduction potential and differentiation begins when the reduction potential drops. This is because during differentiation more energy and oxygen are

Table 1.1: A list of common processes of generation of cellular oxidative and nitrosative stress, and antioxidants defenses

Oxidative and nitrosative stress	**Antioxidant defenses**
Overproduction of RNS (e. g. NO and $ONOO^-$) due to inflammation	Glutathione
Cytokines (e.g. interferon gamma)	Ascorbic acid
Superoxide production due to mitochondrial dysfunction NADPH oxidase	Superoxide dismutase
Generation of hydroxyl radical	Catalase
	Cytokines (e.g. Interleukin 1 and 10)
	Glutathione peroxidase

required. Following the same trend, cell apoptosis and necrosis occur when cell potential shifts to more oxidizing potentials [27].

1.6 Cellular heterogeneity of RNS production and macrophage phenotypes

In general, cells are heterogeneous in nature and this heterogeneity can be biochemical, genetic, behavioral or physiological [33,34]. Macrophage cells have been shown to exhibit heterogeneity following activation with different classes of cytokines and endotoxins [20,35]. There are two main pathways of activation that produce different macrophage phenotypes. Macrophage cells can be activated by bacterial lipopolysaccharide (LPS) and interferon gamma (IFN-Ɣ) to produce pro-inflammatory M1 macrophages. This activation pathway is known as classical activation. In contrast, alternative activation results in anti-inflammatory M2 macrophages following exposure to interleukins (IL) 4, 10 or 13 (Figure 1.3) [35-38]. These two phenotypes have opposite biochemical characteristics. M1 macrophages express iNOS and produce large amounts of RNS. They attack bacteria but can also promote cytotoxicity and tissue injury. In contrast, arginase is expressed in M2 macrophages (not iNOS) and these cells produce growth factors such as vascular endothelial and epidermal growth factors that promote immune suppression and tissue repair (Figure 1.3) [35-38]. The balance between these two types of macrophages is important for maintenance of cellular homeostasis [39,40]. The shift of this balance towards the M1 can lead to cardiovascular or neurodegenerative disease, which could be due to generation of reactive oxygen and nitrogen species (RNOS) and subsequent cellular and tissue injury. In contrast, the shift of this balance towards the M2 phenotype can lead to cancer by supporting unnecessary cell growth and proliferation (Figure 1.3). Aside from these two main phenotypes, the presence of other macrophage phenotypes such as M3 and M4 has also been reported [35-38].

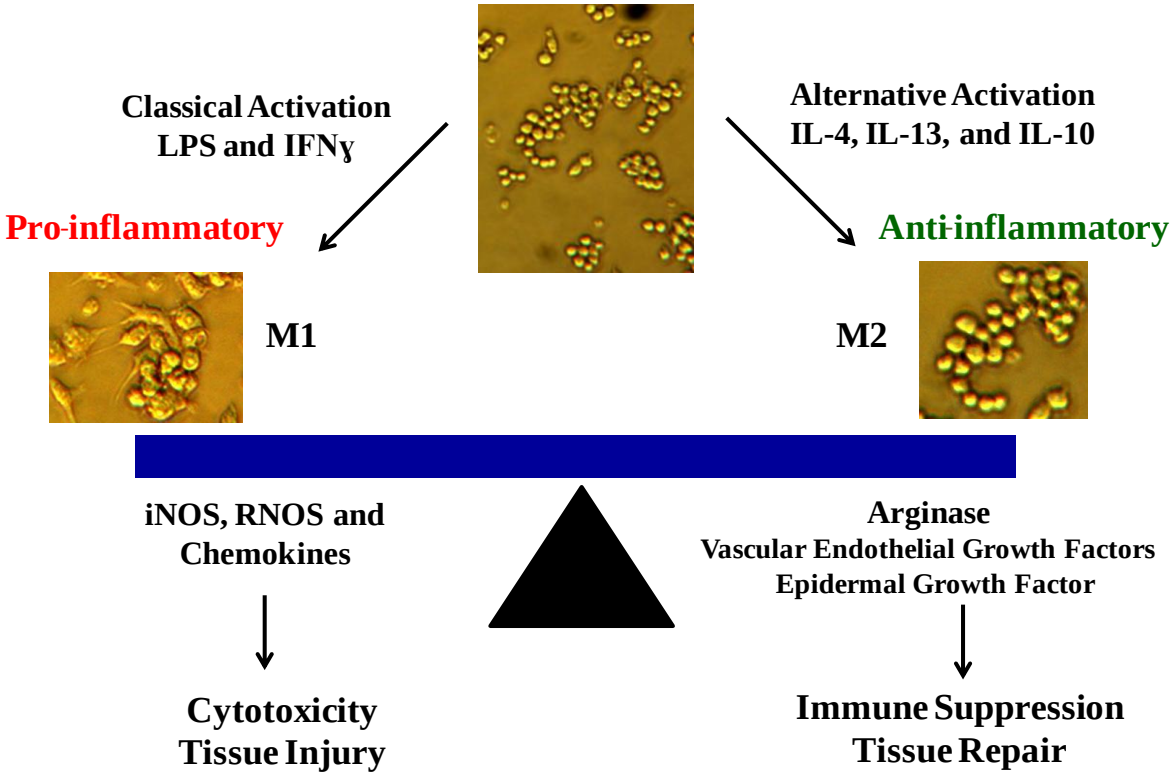

Figure 1.3: Heterogeneity of macrophage cells and the importance of the balance between the M1 and M2 phenotypes (adapted from Laskin, D. L.; *Chem. Res. Toxicol.* **2009**, *22* (8),1376-1385.)

1.7 Biological implications of cellular nitrosative stress

Macrophage cells are implicated in the development of many disease states due to their *in vivo* production of large amounts of RNS and reactive oxygen species (ROS), and existence of multiple phenotypes. Therefore, the macrophage connection to cardiovascular and neurodegenerative diseases and cancer is briefly reviewed.

1.7.1 Atherosclerosis

Atherosclerosis is a plaque buildup in arteries due to chronic inflammation that can lead to cardiovascular disease and myocardial infarction. When the concentration of LDL in the blood is elevated, it can infiltrate into the intima of the vessel and cause inflammation [3,21,36,41]. The infiltrated LDL can then undergo oxidation and nitration (Apo protein B-100) by $O_2^{-\cdot}$ and $ONOO^-$, respectively [42]. These modified LDL molecules then recruit monocytes to the intima through the release of leukocyte adhesion molecules [21,36]. The recruited monocytes are differentiated into macrophages that take up the modified LDL molecules and ultimately produce foam cells, leading to plaque buildup (Figure 1.4) [21,36,43]. During this chronic inflammation process, a cocktail of cytokines is released by T cells, macrophages, and smooth muscle cells that can activate iNOS and NADPH oxidase. This causes excessive production of NO and $O_2^{-\cdot}$ leading to cell death [3,36,44,45]. These dead cells are normally removed by the regulatory anti-inflammatory M2 macrophages but, if it is out of control, will lead to plaque buildup [36,45]. The evidence for excessive $ONOO^-$ production in these plaques is provided by the observation of protein tyrosine nitration in the arteries of patients with atherosclerosis [43,46].

The initial immune response mediated by pro-inflammatory macrophages due to the inflammation caused by oxidized LDL is balanced by the presence of anti-inflammatory macrophages [21,37,39,43]. This balance of M1 and M2 is important for the regulation of LDL concentrations in the blood of healthy individuals. However, during chronic inflammation, there is an overproduction of pro-inflammatory macrophages and foam cells. Apoptosis of these foam cells also contributes to

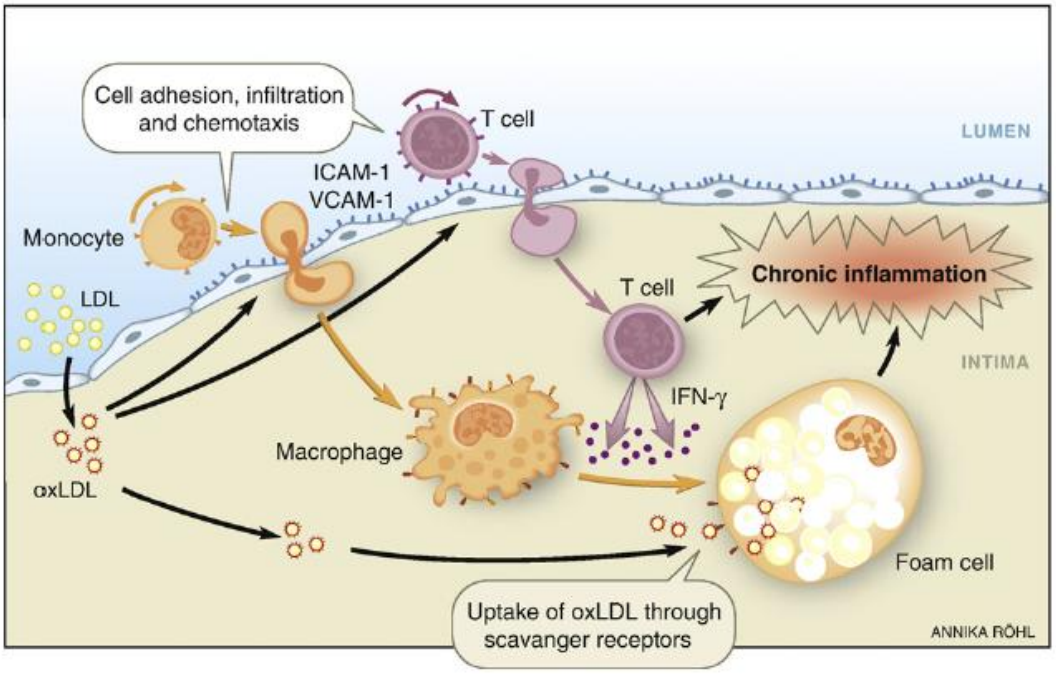

Figure 1.4: Plaque buildup in arteries due to chronic inflammation during atherosclerosis (reproduced with permission from Andersson, J.; Libby, P.; Hansson, G. K., Adaptive immunity and atherosclerosis. *Clin. Immunol.* **2010,** *134* (1), 33-46.)

accumulation of cellular debris at the intima of blood vessel. Therefore, both the pro-inflammatory macrophages and the resulting apoptosis ultimately determine the amount of plaque buildup [21,37,39,43]. Hyperglycemic conditions have been shown to facilitate the generation of $O_2^{-\cdot}$ and the oxidation of LDL, and therefore cause for cardiovascular diseases through the production of $ONOO^-$ at the blood vessel wall [47].

1.7.2 Neurodegenerative diseases

Neurodegenerative diseases such as Alzheimer's and Parkinson's (PD) disease are caused by the death of specific types of neurons. The occurrence of these diseases increases with age and progresses rapidly as the patient becomes older [48-51]. Several causes have been proposed for these neuronal death in neurodegenerative diseases. These include genetic mutation, protein misfolding and aggregation, mitochondrial dysfunction, oxidative and nitrosative stress and the presence of iron and other transition metals [48-51]. In Alzheimer's disease, an increase in amyloid β-peptide aggregation in the brain with age is common and it is believed to be a potential cause of neuronal death and dysfunction [48,51]. The death of dopamine neurons due to accumulation of misfolded proteins (extracellular) is a main cause of Parkinson's disease [50]. Many of these the misfolded proteins are nitrated and oxidatively damaged, providing evidence of a role for $ONOO^-$ and other ROS in these diseases states [52]. It has also been shown that misfolded proteins such as, amyloid β, can induce chronic inflammation to produce RNS [48,53].

Microglia are brain macrophages that are activated by pathogens, bacteria, and proteins such as β-amyloid. They also clear cellular debris from the brain extracellular space through phagocytosis [48,54]. Like macrophages, microglia also exhibit phenotypic and structural differences. It has been shown that there are three distinct states of microglia. Microgial are normally present in a resting state when there is no inflammation. However, during inflammation of brain tissue due to pathogens or the presence of abnormal proteins, NADPH oxidase is activated in these cells, producing an acute state. During this acute state, microglia release pro-inflammatory cytokines that result in the activation of iNOS to produce NO

[54]. This second activation state is known as chronic activation. In the chronic state, $ONOO^-$ can be produced due to the reaction of NO with superoxide and result in neuronal death [54]. Microglia cells have a third state of activation that involves phagocytosis of intracellular debris that is produced from chronic activation and apoptosis. This state of microglial cells is known as the resolution state [54].

1.7.3 Cancer

Association of NO and other RNS in cancer is quite complex because these species can be both toxic as well as help the progression of tumors [22,55]. RNS such as $ONOO^-$ and N_2O_3 can modify and damage DNA [8,22,26,55]. N_2O_3 can deamidate nucleic acids through nitrosation [55] and peroxynitrite can oxidize guanine [56,57]. RNS can also produce toxic nitrosoamines that are known carcinogens [22,55].

On the other hand, immune cells can kill tumor cells through the production of RNS. Both NO and iNOS activation have been investigated as therapeutic strategies for cancer by inducing and avoiding cytotoxicity [23,58,59]. These strategies are highly dependent on the type and nature of the cancer [23]. One of these strategies is to supply large amounts of NO through NO releasing molecules to induce apoptosis of cancer cells [23,60]. Leukemia cells (e.g. Jurkat cells) show low viability with induction of iNOS and therefore NO generating molecules have been used to kill these cancer cells [61,62]. In contrast, inhibition of iNOS itself or its transcription pathway (e.g. inhibit nuclear factor kappa β) to reduce the NO-based cancer progression has also been reported [23].

1.8 Probing cellular nitrosative stress

Cellular nitrosative stress pathways have been widely explored due to their biological implications and follow–up development of therapeutic strategies. There are many conventional analytical methods available for direct detection of NO and $ONOO^-$ [63]. However, the instability of NO and $ONOO^-$ in biological fluids is a challenge for those methods. Therefore, in general, NO_2^- and NO_3^-, which are metabolites of NO and $ONOO^-$, have been used for the indirect detection of NO. *In vivo* NO is oxidized to NO_2^- and then further oxidized to NO_3^- [63]. Also, $ONOO^-$ can isomerize into NO_3^-.

Peroxynitrite also can react with tyrosine residue on proteins to produce nitrotyrosine. Therefore, detection of protein bound nitrotyrosine has been used as an indirect measurement for $ONOO^-$ production [64].

1.8.1 NO detection methods

NO can be directly detected using electron paramagnetic resonance spectroscopy (EPR), fluorescent probes, chemiluminescence and electrochemical methods [63,65-68]. NO is an odd electron species and therefore produces an EPR signal. To stabilize the signal, NO is captured using a spin trap during EPR studies [63]. Fluorescence and chemiluminescence detection have low nM to pM low limits of detection (LOD) for NO; however, NO needs to be reacted with a fluorophore or luminescence agent prior to detection [63,64,68]. The 4-amino-5-methylamino-2',7'-difluorofluorescein (DAF-FM) family of probes are popular for detection of NO using fluorescence and these probes have been widely used for biological studies [69-72]. The main disadvantage of DAF-FM is its reaction with dehydroascorbic acid (DHA) to produce a spectrally similar species (DAF-FM DHA) to that produced with NO (DAF-FM T). Therefore, DAF-FM DHA needs to be separated from DAF-FM T for better quantification. In addition to DAF-FM probes, there are other fluorescent probes such as 2,3-diaminonaphthalene and diaminorhodamine that have been reported for NO [68,69,71,72]. However, a common disadvantage of all these probes is cross reactivity with other RNOS, and cellular biomolecules. An in-depth discussion of DAF-FM for NO detection, its cross reactions and the care needed to be taken for accurate quantification can be found in chapter 6.

For chemiluminescence detection, NO is reacted with H_2O_2 to produce $ONOO^-$ and then the resultant $ONOO^-$ is reacted with luminol [63,68]. However, both H_2O_2 and $ONOO^-$ can interfere with this assay. An alternative approach is to react NO with O_3 to produce an excited state nitrogen dioxide [63,64,71].

NO is electrochemically active and amperometric NO biosensors are widely used in biological applications [63,73,74]. There are several NO biosensors that are commercially available. However,

despite their low LOD, biosensors can suffer from interferences and also lack of the ability to detect multiple analytes simultaneously. Some common interferences include NO_2^-, ascorbic acid, glutathione, dopamine, uric acid, and carbon monoxide. To avoid those interferences, biosensors are equipped with a membrane (e.g. nafion and xerogel) that allows selective detection of NO [63]. Therefore the selectivity of NO biosensors depends on the membrane and the potential applied to the sensor.

NO_2^- is the major product of NO oxidation and it is more stable than NO. Therefore, NO can be detected indirectly using NO_2^-. NO_2^- in acidic conditions reacts with sulfanilamide and forms its diazonium salt that further reacts with N-(1-napthyl)-ethylenediamine to produce a colored product. This reaction is commonly referred to as the Griess reaction and the product absorbance is measured at 548 nm [64]. This assay is heavily used for the indirect detection of NO. However, NO_2^- can slowly oxidize into NO_3^-. One approach for combined detection of NO_2^- and NO_3^- is to reduce NO_3^- back into NO_2^- using a Cd or nitrate reductase. This procedure has also been employed with the Griess assay for accurate determination of NO production [64]. NO can undergo various other reactions including formation of GSNO and $ONOO^-$. Therefore, the development of a method that can detect multiple nitrosative stress makers such as nitrotyrosine, GSNO and other nitrosothiols in biological sample would be advantageous for understanding cellular nitrosative stress.

1.8.2 Peroxynitrite detection methods

Currently, UV absorbance spectroscopy is the main method employed for $ONOO^-$ detection. Peroxynitrite produces a characteristic absorbance at 302 nm and absorbance spectroscopy is widely used for quantitation of $ONOO^-$ in aqueous samples [75,76]. In UV absorbance, transmittance is measured and then absorbance is calculated indirectly. Therefore, absorbance has higher limits of detection compared to fluorescence detection where photon emission following excitation is directly measured from a non background. Therefore, $ONOO^-$ selective fluorescent probes such as dihydrorhodamine 123 have also been reported, but these probes can cross-react with other RNOS, which can be problematic for *in vivo* monitoring applications [64,69]. Recently, highly selective $ONOO^-$ probes have been reported but they

are not currently commercially available [77,78]. Similar to NO, $ONOO^-$ can be detected using chemiluminescence by the reaction of $ONOO^-$ with luminol [63,64].

Peroxynitrite is electrochemically active and can be directly detected using electrochemical methods. Therefore, amperometric detection methods have been developed for the detection of $ONOO^-$ [79-81]. One of the disadvantages of amperometric detection is that it does not provide information on other species that might be present in the sample. Also, other electroactive compounds present in the cells can interfere with the analysis. To monitor multiple species, it is possible to perform amperometric detection at several different voltages. These voltages are selected based on voltammetric behavior of analytes of interest. With this method, the concentration of each species is calculated mathematically. Therefore, amperometric detection at several voltages has been used for detection of $ONOO^-$, H_2O_2 and NO from standard solutions and cells (extracellular release) by Amatore's group [76,81]. This method allows some degree of identification of multiple species when it employs for extracellular RNOS detection [76,81]. However, there are many interfering compounds that are also electrochemically active such as AA and GSH present inside the cell, making it difficult to quantitate multiple species using this method.

1.9 Separation-based approach for RNS detection

The main drawback of the common analytical methods for NO and $ONOO^-$ is the interference of other species during analysis. Thus, these methods cannot distinguish the signal for NO or $ONOO^-$ from interferences or side products [69,70,82,83]. Similarly, most methods only measure a single analyte and therefore multiple methods need to be employed for obtaining information on other species. In order to measure several species simultaneously in a single sample, separation-based approaches such as liquid chromatography (LC) and capillary electrophoresis (CE) have become popular for the determination of NO and other RNS [65,83].

CE has many advantages over liquid chromatographic methods for biological studies, including very low sample volume requirements, higher separation efficiencies, and faster separations. Therefore,

CE has been used for determination of NO from various biological samples [84-88]. CE with laser-induced fluorescence (LIF) detection has been extensively used for the direct monitoring of NO using NO selective fluorescent probes in neurons [83,88]. Conductivity and UV detection have also been employed for the indirect detection of NO by monitoring its degradation products, NO_2^- and NO_3^- [84-87,89].

1.9.1 Microfluidic-based approaches

More recently, microfluidic devices have been employed to monitor the production of NO and its metabolites [90-95]. These devices have many advantages over classical methods for the study of NO production, including the possibility of performing on-chip cell culture, simulating the cellular response in constricted blood vessels, modeling *in vivo* environments (by immobilizing cells in a microchannel), and single cell analysis that can be difficult to achieve using classical methods [90-95]. Fluorescence detection is predominantly used in these devices, and methods for monitoring NO production from erythrocytes [95], endothelial [96], and macrophage cells [93] have been reported.

1.9.2 Microchip electrophoresis (ME)

Separations with microfluidic devices are most commonly performed using electrophoresis. The use of high field strengths with short channels in the planar format makes it possible to routinely perform subminute separations using this technique. Therefore, this method is especially useful for the detection of chemically labile species since they can be separated and detected quickly before significant degradation occurs. The simple-T microchip design is the most common design used for ME where both sample and separation buffer are electrokinetically transported (Figure 1.5). Sample introduction into the separation channel is most commonly achieved using gated injection [97-99]. Double-T and dual channel microchip designs have also been used for ME, and injection schemes such as pinched and hydrodynamic injections can be used for sample introduction [99-102]. An advantage of ME is that the chip design can be customized for a particular application. For example, double-T microchips have been used for integration

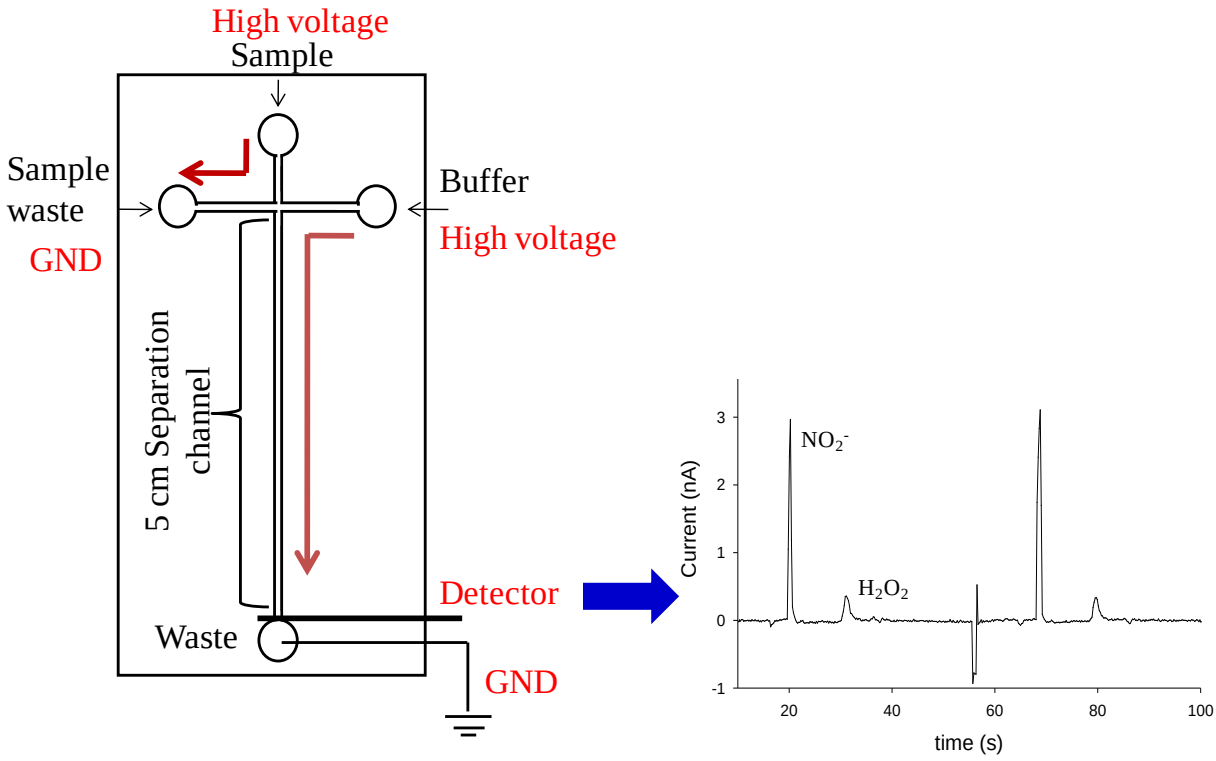

Figure 1.5: A schematic of simple-T microchip design used for ME

of microdalysis sampling into ME, where high salt microdialysis samples are introduced into the separation channel using hydrodynamic injection [100,103].

1.9.3 Separation mechanism in microchip electrophoresis

The separation mechanism in ME is identical to that of capillary zone electrophoresis. In CE, there is a negatively charged layer on capillary surface due to ionized silanol groups (a surfactant can also be used for obtaining the surface charge). Ions in the solution close to the capillary surface segregate into two layers for balancing the surface charge. This phenomenon is known as electrical double layer formation. The closest layer to the charged surface is the adsorbed layer where positively charged ions such as H^+ and Na^+ are adsorbed onto the surface. The next layer also contains extra positive ions to balance the rest of the surface charge and this layer is known as the diffusive layer [104]. Once a positive electric field gradient is applied between two ends of the capillary, positively charged ions in the diffuse layer migrate toward the cathode (negative/ground electrode), creating a bulk flow called the electroosmotic flow (EOF). The EOF carries all analytes regardless of charges toward the cathode and does not separate species. EOF generates a plug flow profile and therefore the band broadening is less compared to pressure driven flows [104].

There is an electrostatic force from the electric field on ions when ions are introduced into a capillary under an electric field. This generates their electrophoretic mobility. This force is balanced by the solution frictional force (F), which is velocity dependent (equation 1). Therefore, the ions move through the capillary with a constant velocity.

The force from the electric field on the ion = Eq

Solution frictional force for spherical particle $F = 6\pi\eta a v$

$$Eq = 6\pi\eta a v \qquad (1)$$

Where E is the electric field gradient, q is the charge of the analyte, η is the viscosity of the buffer, a is hydrodynamic radius of the analyte and v is the velocity of the species.

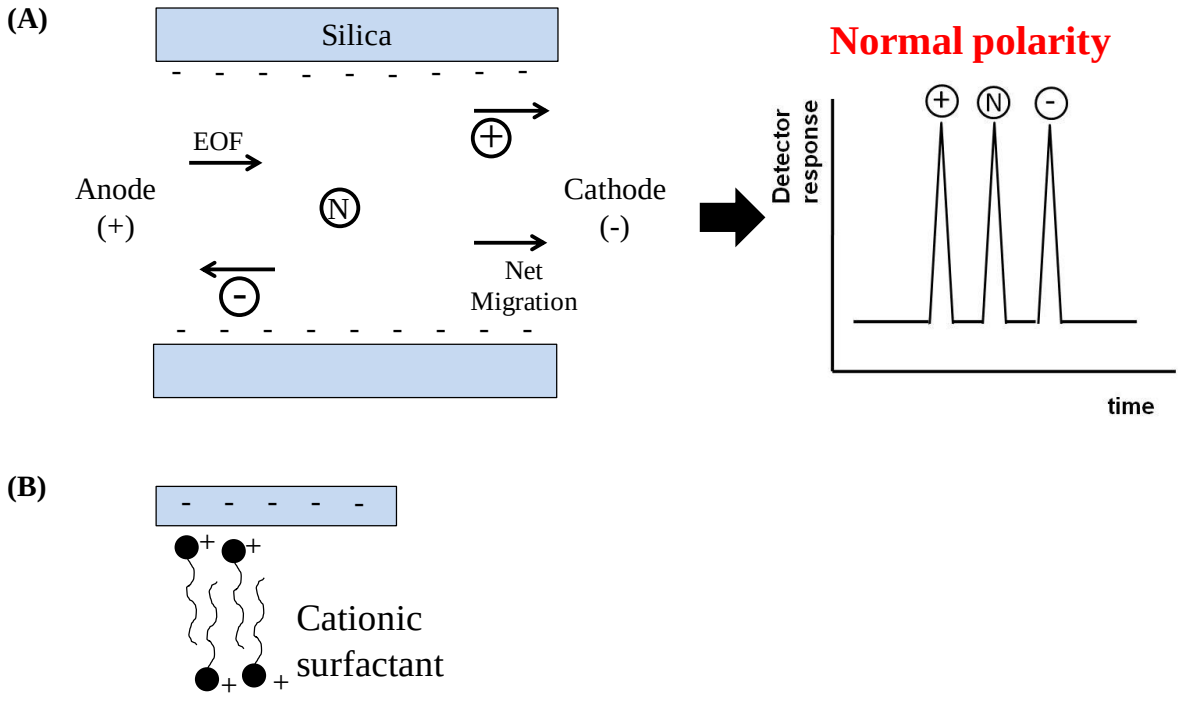

Figure 1.6: The separation mechanism of CE (A) The direction of electrophoretic mobilities of ions and a sample electropherogram in CE with normal polarity (B) A modified silica surface using a cationic surfactant for reverse polarity

In the equation 1 the factor $q/6\pi\eta a$ is defined as the electrophoretic mobility (μ) and is a constant for an analyte in a given buffer system (η is constant). Therefore, μ only depends on charge to hydrodynamic radius ratio. The mobility of the ion (μ) is the parameter that allows for the separation. When an EOF is present the mobility of the ion is the vector sum of μ_{EOF} and μ_{ion}.

$$\mu_{total} = \mu_{EOF} + \mu_{ion} \qquad (2)$$

Application of a positive voltage gradient over negatively charged capillary is called normal polarity (Figure 1.6A). In normal polarity, positive ions and the EOF move toward the cathode [104]. The negatively charged anions have their mobility toward the anode; however, the EOF pushes them toward the cathode. Therefore, the total or "apparent" mobility of an ion is the vector sum of mobility of the EOF and mobility of the ion (equation 2).

For small negative ions with high negative electrophoretic mobilites, reverse polarity is often used. The capillary surface is modified to generate a positively charged layer (Figure 1.6B). In this case, the negatively charged molecules in the diffuse layer move toward the anode (the ground electrode) with the application of negative high voltage gradient between the two capillary ends [104].

In capillary electrophoresis, fused silica capillaries are used. The surface of these capillaries is composed of siloxane groups (pK_a 6) [104]. This fused silica capillary surface can be chemically treated with NaOH or KOH to convert siloxane into the silonyl group (Si-OH) that can be further deprotonated to produce a negatively charged surface [104]. In contrast, ME is performed using various materials such PDMS, glass, PMMA and ceramics [105]. In some cases, such as when using PDMS, the surface needs to be modified with a negatively or positively charged surfactant to generate EOF due to a lack of surface charge. Also, this lack of surface charge facilitates the adsorption of hydrophobic molecules onto the PDMS surface and therefore, hydrophobic molecules can cause channel clogging when PDMS is used in biological studies. The choice of the material for ME is highly depend on the application and the cost.

1.10 Detection strategies for ME

Laser induced fluorescence (LIF) and electrochemical detection are the most common detection strategies in ME. LIF detection has lower LODs; however, analytes typically need to be derivatized before analysis. Amperometry and conductometry are the two main electrochemical strategies used in ME [106]. Conductometry is a universal detection method and capacitively coupled contactless conductivity detection (C4D) is becoming popular as the universal detection method in ME. UV absorbance detection is commonly used as a universal detector in both LC and CE. However, absorbance detection depends on the path length of the detection cell. Microchannel dimensions used for ME are in the low micron range (~15 μm), which is even smaller than that of the CE capillary diameters (~2 x 75 μm). Therefore, absorbance detection in ME is less common. Amperometry is the most widely used electrochemical detection method in ME and the selectivity of an amperometric detector can be controlled through the applied potential at the working electrode or modification of the electrode material. Also, only electroactive compounds give a signal with amperometric detection.

1.10.1 Electrochemical detection (EC) in ME

Various amperometric detection strategies have been developed for CE and these methods were then transferred into microchips when ME become popular. Integration of an electrode into ME is easier compared to CE due to the planar format of ME. However, the electrode cannot be directly placed inside the channel/capillary for amperometric detection because of the electric field used for separation. That is, the separation current can easily ground through the potentiostat and damage its electronic circuitry if the working electrode is in the separation field [107,108]. A common strategy to prevent this is to place the electrode in the ground reservoir 10-15 μm away from the separation channel [107-109]. This configuration is known as the end-channel electrode configuration (Figure 1.7A). However, in this case, analytes diffuse into the waste reservoir when they exit from the channel leading to band broadening and a decrease of signal [107-109].

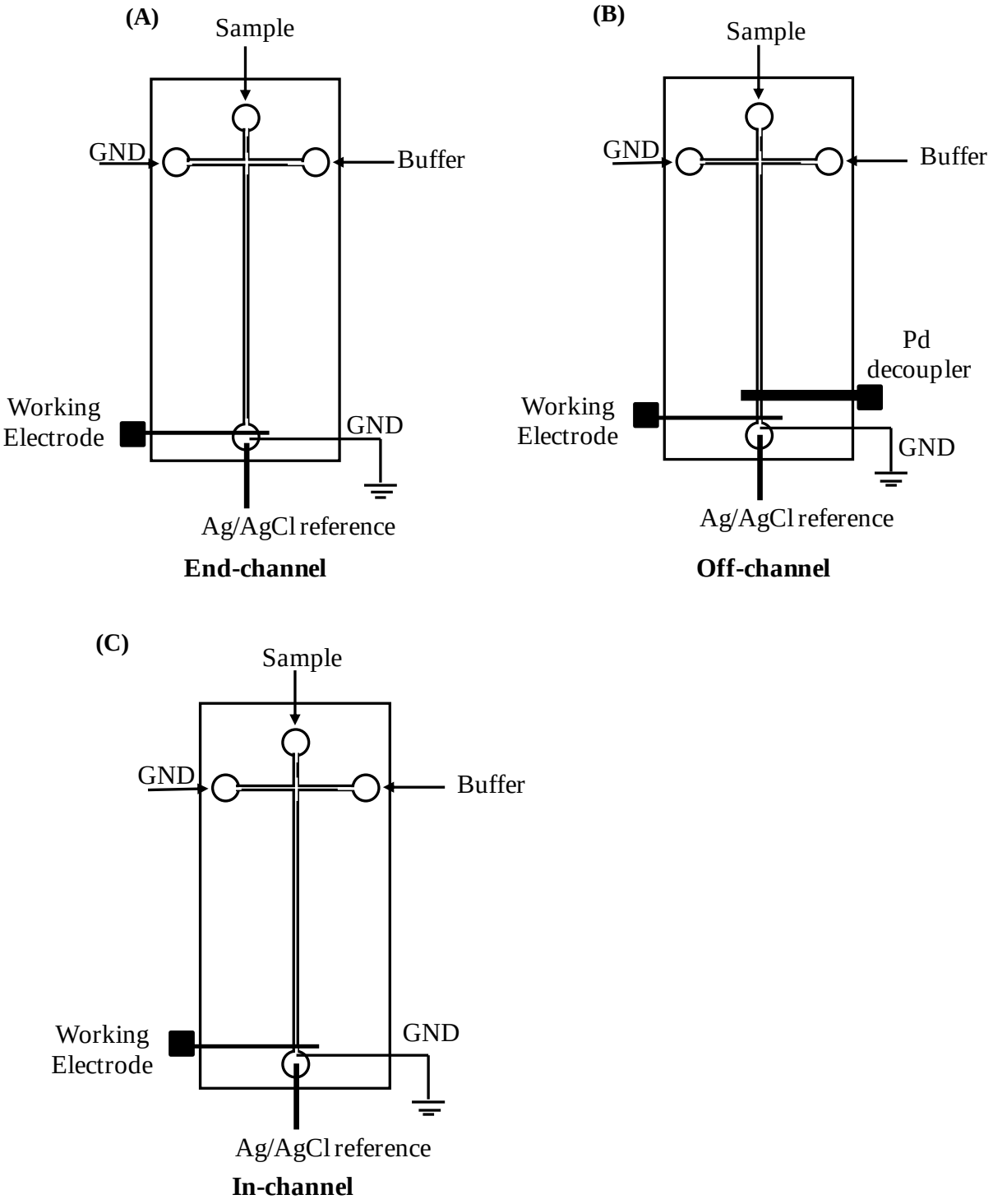

Figure 1.7: Electrode configurations in ME (A) End-channel (B) Off-channel (C) In-channel (Adapted from ref. 107 and 108)

Another approach for ME-EC is to place the electrode inside the channel but ground the separation field prior to the electrode using a decoupling electrode (Figure 1.7B) [109,110]. A metal band electrode such as Pd is commonly employed for this purpose in ME [110]. Unfortunately, these metal band electrodes are microfabricated and they may not very stable under high voltage conditions. In the case of CE-EC, the decoupler can be made by making a facture in the capillary, which is covered by a membrane such as cellulose acetate or nafion and then placed in the ground reservoir [111-113]. The separation current grounds through this fracture and the membrane while the solution continues to flow towards the electrode by the EOF. The same approach has been investigated by the C. Lunte group for ME and they observed lower noise (< 1 pA) and excellent LOD for dopamine (25 nM) [114]. The primary advantage of the decoupler or off-channel alignment is it is free from the noise induced by the separation field. However, the flow profile changes to parabolic once the separation field is grounded by the decoupler, which causes band broadening leading to lower resolution especially if the working electrode is far away [108].

The third approach to perform amperometric detection in ME is to use an isolated or "floating" potentiostat where the potentiostat is not grounded. This approach allows placing an electrode inside the channel (Figure 1.7C). The S. Lunte group has reported an in-channel amperometric detection method using a homemade isolated potentiostat for normal polarity conditions [115]. More recently, the same group has reported an in-channel detection method for reverse polarity with an isolated potentiostat design by Pinnacle technologies [107]. The advantage of using in-channel detection is that it avoids band broadening and therefore, higher resolution and sensitivity can be obtained. However, noise from the separation voltage fluctuation affects the LODs. To reduce noise observed with in-channel detection due to the separation voltage, a dual-channel/dual-electrode approach was reported by Hahn's group [102,116]. In their approach, reference and working electrodes were placed inside two parallel separation channels of a dual-channel microchip. The noise due to high voltage (used for separation) fluctuation was the same at both electrodes and therefore the noise cancels out [102,116]. A more thorough discussion

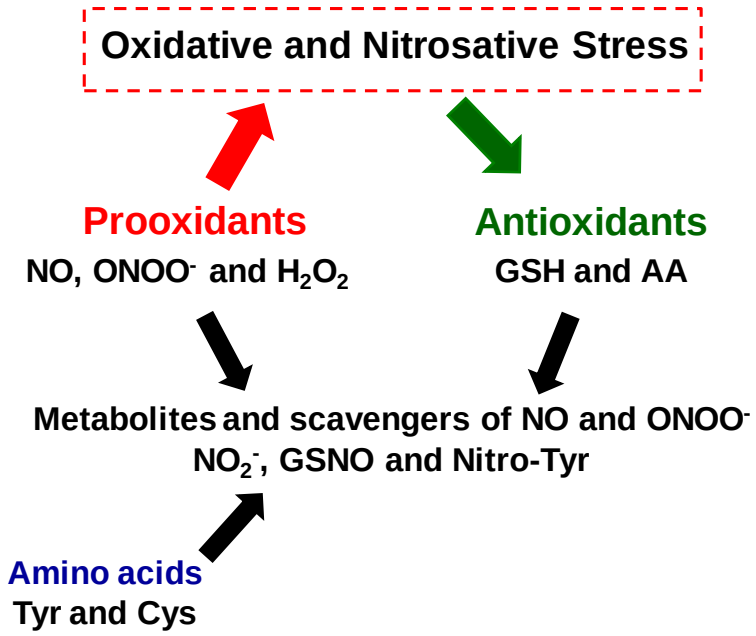

Figure 1.8: Intracellular electroactive species related to cellular oxidative and nitrosative stress

on electrochemical strategies and considerations for reverse polarity conditions is provided in chapter 2.

ME-EC has been used for detection of RNS. Recently, we reported ME-EC methods for the detection of NO and $ONOO^-$ from NONOate salts, commercially available $ONOO^-$ standards (Chapter 3 and 4) and $ONOO^-$ releasing molecules [107,117,118]. Indirect detection of NO based on nitrate and nitrite has also been reported [119-123]. Since nitrate is not electroactive, a method using an on-chip Cu^{2+}/Cd reductor was used to reduce nitrate into nitrite, which permits the detection of both species by ME-EC [119]. Nitrate and nitrite can also be monitored using ME using combined conductivity and amperometric detection [120]. In addition to these methods, there are several reports of ME coupled to amperometric or conductivity detection for determination of nitrite and nitrate in food, biological and environmental samples [121-123].

1.10.2 Electrode materials

For RNS and most oxidizable compounds found in cells (Figure 1.8), a metal electrode such as Pt can be used. Pt black electrodes are known to produce much higher response for NO than bare carbon or Pt electrodes [63]. Therefore, Pt and Pt black electrodeposited electrodes have been widely used for RNS detection [63,74]. For better detection of specific analytes such as thiols, additional electrodes materials are needed. For example, Au/Hg amalgam electrodes have been widely used for the detection of GSH and other thiols [124,125]. The concentration of GSH in the intracellular environment is in the mM range, and therefore, GSH can be easily detected without modifying the electrode. Additionally, a modified electrode can be used for selective detection of GSH [126]. In addition to using a single electrode, a second electrode can also be integrated into ME systems to gain selectivity for compounds undergoing chemically reversible oxidation reactions.

1.11 Detection of cellular antioxidants and other important biomolecules during nitrosative stress

Some electroactive species of interest when probing cellular nitrosative stress include cysteine, tyrosine, nitrotyrosine, nitrosoglutathione and other nitrosothiols, hydrogen peroxide, oxidized forms of

thiols such as cystine and glutathione disulfide, and guanine (Figure 1.8). Some of these species can be detected while detecting RNS, providing more detailed information on the cellular redox state. However, to accomplish this, a separation of all the related species must be developed and optimized. In this case, fast highly efficient separation conditions are necessary because reactive species are labile and need to be separated and detected before they significantly degrade (less than 30 s).

1.11.1 Detection of cellular antioxidants

Thiols are endogeneous antioxidants and methods based on CE and ME with amperometric detection have been developed for the detection of GSH, cysteine and homocysteine [124-128]. Most of these methods employed Au/Hg electrodes. As mentioned previously, the GSH/GSSG ratio can be used as a measure of the redox state of the cell and is an important biomarker. Therefore, the simultaneous detection of thiols and disulfides has been achieved in CE [126]. In those methods, a dual electrode configuration was commonly employed. Disulfides in the sample are reduced to their corresponding thiols at one electrode and the generated thiols are detected at the second electrode. At the second electrode Hg is oxidized in the presence of thiols and forms $Hg(SR)_2$ that generates the signal (corresponding to 2 electrons) [124,128]. Disulfides are commonly reduced at a gold electrode and detected downstream at a mercury gold amalgam electrode. However, both electrodes can also be gold amalgam electrodes [124]. Ascorbic acid is an exogenous anti-oxidant and exhibits a dual role where it can reduce or enhance NO production [129,130]. Ascorbic acid and polyphenolic compounds have also been separated and detected using CE and ME with electrochemical detection [106].

1.10.2 Detection of ROS and other intracellular electroactive molecules

Three important ROS are hydroxyl radical, $O_2^{-\cdot}$ and H_2O_2. H_2O_2 is more stable than both $O_2^{-\cdot}$ and the hydroxyl radical. H_2O_2 can be easily detected by ME-EC; however, it is a neutral compound at low pH and migrates with the EOF. Under high pH conditions (pH>11.6) H_2O_2 is ionized and can be separated from neutral compounds [117]. Other intracellular electroactive biomolecules such as uric acid,

tyrosine, guanine and 8-oxoguanine can also be separated and detected using ME and CE with amperometry.

1.11 Conclusions and thesis goals

The cellular redox state can be changed due to actions of nitrosative and oxidative stress and the depletion of intracellular antioxidants levels. Various analytical methods have been developed to detect individual single analytes that are involved in nitrosative stress. However, the development of methods to detect multiple analytes involved in the cellular redox state would be useful to obtain a better understanding of the diseases caused by RNS as well as for the development of new therapeutic strategies. Microfluidics has the advantage of the possibility of integrating various aspects of bench top analytical methods into a single device for biochemical analysis. Therefore, the goal of this dissertation is to develop microfluidic separation-based methods to detect multiple species that affect the cellular redox state under cellular nitrosative stress conditions. Microchip electrophoresis was chosen as the separation method in these studies. Detection has mainly been accomplished by electrochemical and LIF detection. This dissertation includes the development and application of ME-based methods to probe cellular nitrosative stress in macrophage cells.

1.12 Summary of thesis chapters

1.12.1 Chapter 1: Introduction

This chapter introduces cellular nitrosative stress and its implications in diseases. This chapter also discusses RNS, their production and reactions. Analytical methods used for detection of RNS and their advantages and disadvantages are discussed. Advantages of using ME to probe nitrosative stress are summarized. Electrochemical detection in ME and detection of nitrosative stress markers and other cellular electroactive molecules are also discussed.

1.12.2 Chapter 2: Microchip electrophoresis coupled with in-channel electrochemical detection for the separation and detection of nitrosative and oxidative stress markers

This work has been published in the following journal publication:

D. B. Gunasekara, M. K. Hulvey, S. M. Lunte, "In-channel amperometric detection for microchip electrophoresis using a wireless isolated potentiostat," *Electrophoresis*, **2011**, 32, 832-837 (Feature article)

The combination of ME with amperometric detection leads to a number of analytical challenges that are associated with isolation of the detector from the high voltage used for the separation. While methods such as end-channel alignment and the use of decouplers have been employed, they have limitations. A less common method has been to utilize an electrically isolated potentiostat. This approach allows placement of the working electrode directly in the separation channel without using a decoupler. This chapter explores the use of ME-EC with an electrically isolated potentiostat for the separation and in-channel detection of $ONOO^-$ and several biologically important anions.

1.12.3 Chapter 3: Microchip electrophoresis with amperometric detection for the study of the generation of nitric oxide by NONOate salts

This work has been published in the following journal publication:

D. B. Gunasekara, M. K. Hulvey, S. M. Lunte, J. A. F. da Silva, "Microchip electrophoresis with amperometric detection for the study of generation of nitric oxide by NONOate salts," *Anal. Bioanal. Chem.*, **2012**, 403, 2377-2384

This chapter explores ME with electrochemical detection to monitor NO production from diethylammonium (Z)-1-(N,N-diethylamino)diazen-1-ium-1,2-diolate (DEA/NO) and 1-(hydroxyl-NNO-azoxy)-L-proline disodium salt (PROLI/NO). NO was generated through acid hydrolysis of the NONOate salts. The products of acid hydrolysis were introduced into a 5 cm long separation channel using gated injection. The separation was accomplished using reverse polarity and electrochemical detection was achieved using an isolated potentiostat in an in-channel configuration.

1.12.4 Chapter 4: Evaluation of microchip electrophoresis with dual-series and dual-parallel electrode configurations for identification of chemically labile species

Analytes are normally identified based on their migration times in ME with amperometric detection. However, for complex samples such as cell lysates, migration time may not be adequate for peak identification. In this case, voltammetric characterization can also be used and can be accomplished by determining the current ratio at two different working electrode potentials. In this chapter, two separate dual-electrode configurations that can be employed for voltammetric characterization in real time are described. The first uses a single channel simple-T microchip with two platinum electrodes set at two different potentials in a series configuration (one in in-channel configuration and second electrode in end-channel configuration). An alternative approach involves a ME-EC system that contains two distinct separation channels each containing a platinum working electrode set at a different potential. Both dual-electrode configurations were used to evaluate the purity of peroxynitrite standards using voltammetric characterization.

1.12.5 Chapter 5: Comparison of cellular nitric oxide production in single and bulk cells using microchip electrophoresis with laser induced fluorescence detection

This work has been reported in the following journal publications and a conference proceeding:

E. R. Mainz, **D. B. Gunasekara**, G. Caruso, D. Jensen, M. K. Hulvey, J. A. F. da Silva, E. C. Metto, A. H. Culbertson, C. T. Culbertson, S. M. Lunte, "Monitoring of intracellular nitric oxide production by microchip electrophoresis and laser induced fluorescence detection," *Anal. Methods*, **2012**, 4, 414-420

E. C. Metto, K. Evans, K. Barney, A. H. Culbertson, **D. B. Gunasekara**, G. Caruso, M. K. Hulvey, J. A. F. da Silva, S. M. Lunte, C. T. Culbertson, "Integrated microfluidic device for monitoring nitric oxide production in single cells," *Anal. Chem.*, **2013**, 85, 10188–10195

S. M. Lunte, **D. B. Gunasekara**, E. C. Metto, M. K. Hulvey, E. R. Mainz, G. Caruso, J. A. F. da Silva, D. T. Jensen, A. H. Culbertson, R. J. Grigsby, C. T. Culbertson, "Microchip electrophoresis devices for the

detection of nitric oxide: Comparison of bulk cell and single cell analysis," *Proceedings of μTAS*, Seattle, USA, **2011**, 0536.

CE with laser-induced fluorescence detection has been used previously to separate and quantitate the fluorescent derivatives of NO from potential interferences in single neurons. In this chapter, ME coupled to laser-induced fluorescence (LIF) detection is evaluated as a method for measurement of the NO production by Jurkat cells under native and stimulated conditions. In these studies, 4-amino-5-methylamino-2',7'-difluorofluorescein diacetate (DAF-FM DA) was employed for the detection of NO, and 6-carboxyfluorescein diacetate (6-CFDA) was employed as an internal standard. Intracellular NO concentrations were calculated using a calibration curve and total cell count. The average estimated NO concentration observed in these bulk cell studies were then compared with average NO production in single cell analysis.

1.12.6 Chapter 6: Cellular nitrosative stress profiling using microchip electrophoresis coupled to electrochemical detection

This work has been published in the following journal publication:

D. B. Gunasekara, J. M. Siegel, G. Caruso, M. K. Hulvey, S. M. Lunte, "Development of a microchip electrophoresis method with amperometric detection for profiling cellular nitrosative stress markers," Analyst, **2014**, 139 (13), 3265 – 3273

In this chapter, a ME method with electrochemical detection for the separation of intracellular nitrosative stress markers in macrophage cells is described. The separation of nitrite, azide (interference), iodide (internal standard), tyrosine, glutathione, and H_2O_2 (neutral marker) was achieved in under 40 s. Initially, NO production was monitored by the detection of nitrite (NO_2^-) in cell lysates. The concentration of NO_2^- inside a single unstimulated macrophage cell was estimated to be 1.54 mM using the method of standard additions. ME-EC was then used for the direct detection of NO and glutathione in stimulated and native macrophage cell lysates. NO was identified in these studies based on its migration time and rapid

degradation kinetics. The intracellular levels of GSH in native and stimulated macrophages were also compared, and no significant difference was observed between the two conditions.

1.12.7 Chapter 7: Conclusions and future directions

The main conclusions are discussed in this chapter. These conclusions include development of ME-based electrochemical and LIF methods, their use for detection of reactive species and application to probe cellular nitrosative stress. Immediate future goals include identification of intracellular electroactive compounds using dual electrodes and development of single cell electrochemical cytometer. Long term goals include application of above methodologies for investigation of monocyte derived macrophages and their implications in cellular nitrosative stress. Further, long term goals include investigation of bipolar electrodes for indirect fluorescence detection in ME and other biochemical assays.

1.13 References

1. Pacher, P.; Beckman, J. S.; Liaudet, L., Nitric oxide and peroxynitrite in health and disease. *Physiol. Rev.* **2007,** *87* (1), 315-424.

2. Radi, R.; Cassina, A.; Hodara, R.; Quijano, C.; Castro, L., Peroxynitrite reactions and formation in mitochondria. *Free Radical Biol. Med.* **2002,** *33* (11), 1451-1464.

3. Pacher, P.; Szabo, C., Role of the peroxynitrite-poly(ADP-ribose) polymerase pathway in human disease. *Am. J. Pathol.* **2008,** *173*, 2-13.

4. Calabrese, V.; Cornelius, C.; Rizzarelli, E.; Owen, J. B.; Dinkova-Kostova, A. T.; Butterfield, D. A., Nitric Oxide in Cell Survival: A Janus Molecule. *Antioxid. Redox Signaling* **2009,** *11* (11), 2717-2739.

5. Torreilles, F.; Salman-Tabcheh, S.; Guerin, M. C.; Torreilles, J., Neurodegenerative disorders: the role of peroxynitrite. *Brain Res. Rev.* **1999,** *30* (2), 153-163.

6. Thomas, D. D.; Flores-Santana, W.; Switzer, C. H.; Wink, D. A.; Ridnour, L. A. In *Determinants of nitric oxide chemistry: impact of cell signaling processes*, Elsevier Inc.: 2010; pp 3-25.

7. Moller, M. N.; Li, Q.; Lancaster, J. R., Jr.; Denicola, A., Acceleration of nitric oxide autoxidation and nitrosation by membranes. *IUBMB Life* **2007,** *59* (4-5), 243-8.

8. Liu, X.; Miller, M. J. S.; Joshi, M. S.; Thomas, D. D.; Lancaster, J. R., Jr., Accelerated reaction of nitric oxide with O2 within the hydrophobic interior of biological membranes. *Proc. Natl. Acad. Sci. U. S. A.* **1998,** *95* (5), 2175-2179.

9. Hess, D. T.; Matsumoto, A.; Kim, S.-O.; Marshall, H. E.; Stamler, J. S., Protein S-nitrosylation: purview and parameters. *Nat. Rev. Mol. Cell Bio.* **2005,** *6* (2), 150-166.

10. Szabo, C.; Ischiropoulos, H.; Radi, R., Peroxynitrite: biochemistry, pathophysiology and development of therapeutics. *Nat. Rev. Drug Discovery* **2007,** *6* (8), 662-680.

11. Radi, R.; Peluffo, G.; Alvarez, M. N.; Naviliat, M.; Cayota, A., Unraveling peroxynitrite formation in biological systems. *Free Radical Biol. Med.* **2001,** *30* (5), 463-488.

12. Nathan, C.; Shiloh, M. U., Reactive oxygen and nitrogen intermediates in the relationship between mammalian hosts and microbial pathogens. *Proc Natl Acad Sci U S A* **2000,** 97(16), 8841-8848.

13. Bylund, J.; Brown, K. L.; Movitz, C.; Dahlgren, C.; Karlsson, A., Intracellular generation of superoxide by the phagocyte NADPH oxidase: How, where, and what for? *Free Radical Biol. Med.* **2010,** *49*, 1834-1845.

14. Valentine, J. S.; Doucette, P. A.; Potter, S. Z., Copper-zinc superoxide dismutase and amyotrophic lateral sclerosis. *Annu. Rev. Biochem.* **2005,** *74*, 563-593.

15. Lancaster, J. R. J., The physical properties of nitric oxide: determinants of the dynamics of NO in tissue. *Nitric oxide* **2000**, 209-224.

16. Bryk, R.; Wolff, D. J., Pharmacological modulation of nitric oxide synthesis by mechanism-based inactivators and related inhibitors. *Pharmacol. Ther.* **1999,** *84* (2), 157-178.

17. MacMicking, J.; Xie, Q.; Nathan, C., Nitric oxide and macrophage function. *Annu. Rev. Immunol.* **1997,** *15*, 323-350.

18. Lee S -J, Stull J T: Calmodulin-dependent regulation of inducible and neuronal nitric-oxide synthase. *Journal of Biological Chemistry* **1998**, 273, 27430-27437.

19. Hume, D. A. The Biology of Macrophages [An Online Review]. Pubshied Online: May 1, 2012. http://www.macrophages.com/macrophage-review (accessed March 1, 2014)

20. Gordon, S.; Taylor, P. R., Monocyte and macrophage heterogeneity. *Nat. Rev. Immunol.* **2005,** *5* (12), 953-964.

21. Lilly, L. S.; Harvard Medical, S., *Pathophysiology of heart disease : a collaborative project of medical students and faculty*. Wolters Kluwer/Lippincott Williams & Wilkins: Baltimore, MD, 2011.

22. Fukumura, D.; Kashiwagi, S.; Jain, R. K., The role of nitric oxide in tumour progression. *Nat. Rev. Cancer* **2006,** *6* (7), 521-534.

23. Bonavida, B.; Khineche, S.; Huerta-Yepez, S.; Garban, H., Therapeutic potential of nitric oxide in cancer. *Drug Resist. Updates* **2006,** *9* (3), 157-173.

24. Bian, K.; Doursout, M.-F.; Murad, F., Vascular System: Role of Nitric Oxide in Cardiovascular Diseases. *J. Clin. Hypertens.* **2008,** *10* (4), 304-310.

25. Prast, H.; Philippu, A., Nitric oxide as modulator of neuronal function. *Prog. Neurobiol.* **2001,** *64* (1), 51-68.

26. Kroncke, K. D.; Fehsel, K.; Kolb-Bachofen, V., Nitric oxide: cytotoxicity versus cytoprotection-how, why, when, and where? *Nitric Oxide* **1997,** *1* (2), 107-20.

27. Schafer, F. Q.; Buettner, G. R., Redox environment of the cell as viewed through the redox state of the glutathione disulfide/glutathione couple. *Free Radical Biol. Med.* **2001,** *30* (11), 1191-1212.

28. Valko, M.; Leibfritz, D.; Moncol, J.; Cronin, M. T. D.; Mazur, M.; Telser, J., Free radicals and antioxidants in normal physiological functions and human disease. *Int. J. Biochem. Cell Biol.* **2006,** *39* (1), 44-84.

29. Turrens J F: Mitochondrial formation of reactive oxygen species. *The Journal of Physiology* **2003**, 552(2), 335-344.

30. Fang, Y.-Z.; Yang, S.; Wu, G., Free radicals, antioxidants, and nutrition. *Nutrition* **2002,** *18* (10), 872-879.

31. Poljsak, B.; Suput, D.; Milisav, I., Achieving the balance between ROS and antioxidants: when to use the synthetic antioxidants. *Oxid. Med. Cell. Longevity* **2013**, 956792, 11 pp.

32. Kirlin W G, Cai J, Thompson S A, Diaz D, Kavanagh T J, Jones D P; Glutathione redox potential in response to differentiation and enzyme inducers. *Free Radical Biol Med* 1999, **27,**(11/12),1208-1218.

33. Brehm-Stecher, B. F.; Johnson, E. A., Single-cell microbiology: Tools, technologies, and applications. *Microbiol. Mol. Biol. Rev.* **2004,** *68*, 538-559.

34. Wang, D.; Bodovitz, S., Single cell analysis: the new frontier in 'omics'. *Trends Biotechnol.* **2010,** *28*, 281-290.

35. Gordon, S., Alternative activation of macrophages. *Nat. Rev. Immunol.* **2003,** *3*, 23-35.

36. Wilson, H. M., Macrophages heterogeneity in atherosclerosis - implications for therapy. *J. Cell. Mol. Med.* **2010,** *14*, 2055-2065.

37. Wolfs, I. M. J.; Donners, M. M. P. C.; de, W. M. P. J., Differentiation factors and cytokines in the atherosclerotic plaque micro-environment as a trigger for macrophage polarisation. *Thromb. Haemostasis* **2011,** *106*, 763-771.

38. Varin, A.; Gordon, S., Alternative activation of macrophages: immune function and cellular biology. *Immunobiology* **2009,** *214*, 630-641.

39. Mantovani, A.; Garlanda, C.; Locati, M., Macrophage Diversity and Polarization in Atherosclerosis: a question of balance. *Arterioscler., Thromb., Vasc. Biol.* **2009,** 1419-1423.

40. Laskin D. L. Macrophages and inflammatory mediators in chemical toxicity: A battle of forces. *Chem. Res. Toxicol.***2009**, 22(8),1376-1385.

41. Andersson, J.; Libby, P.; Hansson, G. K., Adaptive immunity and atherosclerosis. *Clin. Immunol.* **2010,** *134* (1), 33-46.

42. Botti, H.; Trostchansky, A.; Batthyany, C.; Rubbo, H., Reactivity of Peroxynitrite and Nitric Oxide with LDL. *IUBMB Life* **2005,** *57*, 407-412.

43. Peluffo, G.; Radi, R., Biochemistry of protein tyrosine nitration in cardiovascular pathology. *Cardiovasc. Res.* **2007,** *75*, 291-302.

44. Rajagopalan, S.; Meng, X. P.; Ramasamy, S.; Harrison, D. G.; Galis, Z. S., Reactive oxygen species produced by macrophage-derived foam cells regulate the activity of vascular matrix metalloproteinases in vitro. Implications for atherosclerotic plaque stability. *J. Clin. Invest.* **1996,** *98*, 2572-9.

45. Kockx, M. M.; Herman, A. G., Apoptosis in atherosclerosis: beneficial or detrimental? *Cardiovasc. Res.* **2000,** *45*, 736-46.

46. Upmacis, R. K., Atherosclerosis: a link between lipid intake and protein tyrosine nitration. *Lipid Insights* **2008,** *2*, 75-88.

47. Pacher, P.; Szabo, C., Role of peroxynitrite in the pathogenesis of cardiovascular complications of diabetes. *Curr. Opin. Pharmacol.* **2006,** *6*, 136-141.

48. Halliwell, B., Oxidative stress and neurodegeneration: where are we now? *J. Neurochem.* **2006,** *97* (6), 1634-1658.

49. Mattson, M. P., Apoptosis in neurodegenerative disorders. *Nature Reviews Molecular Cell Biology* **2000,** *1* (2), 120-130.

50. Taylor, J. P.; Hardy, J.; Fischbeck, K. H., Toxic proteins in neurodegenerative disease. *Science* **2002,** *296* (5575), 1991-1995.

51. Barnham, K. J.; Masters, C. L.; Bush, A. I., Neurodegenerative diseases and oxidative stress. *Nat. Rev. Drug Discov.* **2004,** *3* (3), 205-214.

52. Ischiropoulos, H.; Beckman, J. S., Oxidative stress and nitration in neurodegeneration: cause, effect, or association? *J. Clin. Invest.* **2003,** *111* (2), 163-169.

53. Cho, D.-H.; Nakamura, T.; Fang, J.; Cieplak, P.; Godzik, A.; Gu, Z.; Lipton, S. A., S-nitrosylation of Drp1 mediates β-amyloid-related mitochondrial fission and neuronal injury. *Science* **2009,** *324* (5923), 102-105.

54. Brown, G. C.; Neher, J. J., Inflammatory Neurodegeneration and Mechanisms of Microglial Killing of Neurons. *Mol. Neurobiol.* **2010,** *41* (2-3), 242-247.

55. Wink, D. A.; Vodovotz, Y.; Laval, J.; Laval, F.; Dewhirst, M. W.; Mitchell, J. B., The multifaceted roles of nitric oxide in cancer. *Carcinogenesis* **1998,** *19* (5), 711-721.

56. Szabo, C.; Ohshima, H., DNA damage induced by peroxynitrite: subsequent biological effects. *Nitric Oxide* **1997,** *1* (5), 373-385.

57. Niles, J. C.; Wishnok, J. S.; Tannenbaum, S. R., Peroxynitrite-induced oxidation and nitration products of guanine and 8-oxoguanine: Structures and mechanisms of product formation. *Nitric Oxide* **2006,** *14* (2), 109-121.

58. Mocellin, S.; Bronte, V.; Nitti, D., Nitric oxide, a double edged sword in cancer biology: searching for therapeutic opportunities. *Med. Res. Rev.* **2007,** *27* (3), 317-352.

59. Xie, K.; Fidler, I. J., Therapy of cancer metastasis by activation of the inducible nitric oxide synthase. *Cancer Metastasis Rev.* **1998,** *17* (1), 55-75.

60. Huerta, S.; Chilka, S.; Bonavida, B., Nitric oxide donors: novel cancer therapeutics (review). *Int. J. Oncol.* **2008,** *33* (5), 909-927.

61. Mainz, E. R.; Gunasekara, D. B.; Caruso, G.; Jensen, D. T.; Hulvey, M. K.; Fracassi, d. S. J. A.; Metto, E. C.; Culbertson, A. H.; Culbertson, C. T.; Lunte, S. M., Monitoring intracellular nitric oxide production using microchip electrophoresis and laser-induced fluorescence detection. *Anal. Methods* **2012,** *4*, 414-420.

62. Nath, N.; Chattopadhyay, M.; Pospishil, L.; Cieciura, L. Z.; Goswami, S.; Kodela, R.; Saavedra, J. E.; Keefer, L. K.; Kashfi, K., JS-K, a nitric oxide-releasing prodrug, modulates ss-catenin/TCF signaling in leukemic Jurkat cells: evidence of an S-nitrosylated mechanism. *Biochem. Pharmacol.* **2010,** *80* (11), 1641-9.

63. Hetrick, E. M.; Schoenfisch, M. H., Analytical chemistry of nitric oxide. *Annu. Rev. Anal. Chem.* **2009,** *2*, 409-433.

64. Tarpey, M. M.; Fridovich, I., Methods of detection of vascular reactive species. Nitric oxide, superoxide, hydrogen peroxide, and peroxynitrite. *Circ. Res.* **2001,** *89* (3), 224-236.

65. Tsikas, D., A critical review and discussion of analytical methods in the L-arginine/nitric oxide area of basic and clinical research. *Anal. Biochem.* **2008,** *379* (2), 139-163.

66. Amatore, C.; Arbault, S.; Koh, A. C. W., Simultaneous Detection of Reactive Oxygen and Nitrogen Species Released by a Single Macrophage by Triple Potential-Step Chronoamperometry. *Anal. Chem.* **2010,** *82* (4), 1411-1419.

67. Frankenfeld, C. N.; Rosenbaugh, M. R.; Fogarty, B. A.; Lunte, S. M., Separation and detection of peroxynitrite and its metabolites by capillary electrophoresis with UV detection. *J. Chromatogr. A* **2006,** *1111* (2), 147-152.

68. Nagano, T., Practical methods for detection of nitric oxide. *Luminescence* **1999,** *14* (6), 283-290.

69. Gomes, A.; Fernandes, E.; Lima, J. L. F. C., Use of fluorescence probes for detection of reactive nitrogen species: A review. *J. Fluoresc.* **2006,** *16*, 119-139.

70. Xu, X.; Arriaga, E. A., Qualitative determination of superoxide release at both sides of the mitochondrial inner membrane by capillary electrophoretic analysis of the oxidation products of triphenylphosphonium hydroethidine. *Free Radical Biol. Med.* **2009,** *46*, 905-913.

71. Bryan, N. S.; Grisham, M. B., Methods to detect nitric oxide and its metabolites in biological samples. *Free Radical Biol. Med.* **2007,** *43* (5), 645-657.

72. Tonzetich, Z. J.; McQuade, L. E.; Lippard, S. J., Detecting and understanding the roles of nitric oxide in biology. *Inorganic chemistry* **2010,** *49* (14), 6338-6348.

73. Trouillon, R., Biological applications of the electrochemical sensing of nitric oxide: fundamentals and recent developments. *Biol. Chem.* **2013,** *394* (1), 17-33.

74. Bedioui, F.; Griveau, S., Electrochemical Detection of Nitric Oxide: Assessement of Twenty Years of Strategies. *Electroanalysis* **2013,** *25* (3), 587-600.

75. Uppu, R. M.; Pryor, W. A., Synthesis of peroxynitrite in a two-phase system using isoamyl nitrite and hydrogen peroxide. *Anal. Biochem.* **1996,** *236* (2), 242-9.

76. Amatore, C.; Arbault, S.; Bruce, D.; De Oliveira, P.; Erard, M.; Vuillaume, M. Characterization of the electrochemical oxidation of peroxynitrite: relevance to oxidative stress bursts measured at the single cell level. *Chem. Eur. J.* **2001**, *7*(19), 4171-9.

77. Yang, D.; Wang, H.-L.; Sun, Z.-N.; Chung, N.-W.; Shen, J.-G., A Highly Selective Fluorescent Probe for the Detection and Imaging of Peroxynitrite in Living Cells. *J. Am. Chem. Soc.* **2006,** *128* (18), 6004-6005.

78. Peng, T.; Yang, D., HKGreen-3: A Rhodol-Based Fluorescent Probe for Peroxynitrite. *Org. Lett.* **2010,** *12* (21), 4932-4935.

79. Koh, W. C. A.; Son, J. I.; Choe, E. S.; Shim, Y.-B., Electrochemical Detection of Peroxynitrite Using a Biosensor Based on a Conducting Polymer-Manganese Ion Complex. *Anal. Chem.* **2010,** *82* (24), 10075-10082.

80. Peteu, S. F.; Banihani, S.; Gunesekera, M. M.; Peiris, P.; Sicuia, O. A.; Bayachou, M., Peroxynitrite and nitroxidative stress: detection probes and micro-sensors. A case of a nanostructured catalytic film. *ACS Symp. Ser.* **2011,** *1083* (Oxidative Stress), 311-339, 6 plates.

81. Amatore, C.; Arbault, S.; Bouton, C.; Coffi, K.; Drapier, J.-C.; Ghandour, H.; Tong, Y., Monitoring in real time with a microelectrode the release of reactive oxygen and nitrogen species by a single macrophage stimulated by its membrane mechanical depolarization. *Chembiochem.* **2006,** *7* (4), 653-661.

82. Zhang, X.; Kim, W.-S.; Hatcher, N.; Potgieter, K.; Moroz, L. L.; Gillette, R.; Sweedler, J. V., Interfering with nitric oxide measurements. 4,5-diaminofluorescein reacts with dehydroascorbic acid and ascorbic acid. *J. Biol. Chem.* **2002,** *277*, 48472-48478.

83. Ye, X.; Rubakhin, S. S.; Sweedler, J. V., Detection of nitric oxide in single cells. *Analyst.* **2008,** *133* (4), 423-433.

84. Friedberg, M. A.; Hinsdale, M. E.; Shihabi, Z. K., Analysis of nitrate in biological fluids by capillary electrophoresis. *J. Chromatogr. A* **1997,** *781* (1 + 2), 491-496.

85. Morcos, E.; Wiklund, N. P., Nitrite and nitrate measurements in human urine by capillary electrophoresis. *Methods Mol. Biol. (Totowa, NJ, U. S.)* **2004,** *279* (Nitric Oxide Protocols (2nd Edition)), 21-34.

86. Boudko, D. Y., High-resolution capillary electrophoresis on nitrite and nitrate in biological samples. *Methods Mol. Biol. (Totowa, NJ, U. S.)* **2004,** *279* (Nitric Oxide Protocols (2nd Edition)), 9-19.

87. Boudko, D. Y.; Cooper, B. Y.; Harvey, W. R.; Moroz, L. L., High-resolution microanalysis of nitrite and nitrate in neuronal tissues by capillary electrophoresis with conductivity detection. *J. Chromatogr. B: Anal. Technol. Biomed. Life Sci.* **2002,** *774* (1), 97-104.

88. Kim, W.-S.; Ye, X.; Rubakhin, S. S.; Sweedler, J. V., Measuring Nitric Oxide in Single Neurons by Capillary Electrophoresis with Laser-Induced Fluorescence: Use of Ascorbate Oxidase in Diaminofluorescein Measurements. *Anal. Chem.* **2006,** *78* (6), 1859-1865.

89. Govindaraju, K.; Toporsian, M.; Ward, M. E.; Lloyd, D. K.; Cowley, E. A.; Eidelman, D. H., Capillary electrophoresis analysis of nitrite and nitrate in sub-microliter quantities of airway surface liquid. *J. Chromatogr. B: Biomed. Sci. Appl.* **2001,** *762* (2), 147-154.

90. Hunter, R. A.; Privett, B. J.; Henley, W. H.; Breed, E. R.; Liang, Z.; Mittal, R.; Yoseph, B. P.; McDunn, J. E.; Burd, E. M.; Coopersmith, C. M.; Ramsey, J. M.; Schoenfisch, M. H., Microfluidic Amperometric Sensor for Analysis of Nitric Oxide in Whole Blood. *Anal. Chem.* **2013,** *85* (12), 6066-6072.

91. Metto, E. C.; Evans, K.; Barney, P.; Culbertson, A. H.; Gunasekara, D. B.; Caruso, G.; Hulvey, M. K.; Fracassi, d. S. J. A.; Lunte, S. M.; Culbertson, C. T., An Integrated Microfluidic Device for Monitoring Changes in Nitric Oxide Production in Single T-Lymphocyte (Jurkat) Cells. *Anal. Chem.* **2013,** *85* (21), 10188-10195.

92. Vogel, P. A.; Halpin, S. T.; Martin, R. S.; Spence, D. M., Microfluidic Transendothelial Electrical Resistance Measurement Device that Enables Blood Flow and Postgrowth Experiments. *Anal. Chem.* **2011,** *83* (11), 4296-4301.

93. Goto, M.; Sato, K.; Murakami, A.; Tokeshi, M.; Kitamori, T., Development of a microchip-based bioassay system using cultured cells. *Anal. Chem.* **2005,** *77*, 2125-2131.

94. Hulvey, M. K.; Martin, R. S., A microchip-based endothelium mimic utilizing open reservoirs for cell immobilization and integrated carbon ink microelectrodes for detection. *Anal. Bioanal. Chem.* **2009,** *393* (2), 599-605.

95. Halpin, S. T.; Spence, D. M., Direct Plate-Reader Measurement of Nitric Oxide Released from Hypoxic Erythrocytes Flowing through a Microfluidic Device. *Anal. Chem.* **2010,** *82* (17), 7492-7497.

96. Letourneau, S.; Hernandez, L.; Faris, A. N.; Spence, D. M., Evaluating the effects of estradiol on endothelial nitric oxide stimulated by erythrocyte-derived ATP using a microfluidic approach. *Anal. Bioanal. Chem.* **2010,** *397* (8), 3369-3375.

97. Slentz, B. E.; Penner, N. A.; Regnier, F., Sampling BIAS at channel junctions in gated flow injection on chips. *Anal. Chem.* **2002,** *74* (18), 4835-40.

98. Ermakov, S. V.; Jacobson, S. C.; Ramsey, J. M., Computer Simulations of Electrokinetic Injection Techniques in Microfluidic Devices. *Anal. Chem.* **2000,** *72* (15), 3512-3517.

99. Karlinsey, J. M., Sample introduction techniques for microchip electrophoresis: A review. *Anal. Chim. Acta* **2012,** *725*, 1-13.

100. Huynh, B. H.; Fogarty, B. A.; Martin, R. S.; Lunte, S. M., On-line coupling of microdialysis sampling with microchip-based capillary electrophoresis. *Anal. Chem.* **2004,** *76* (21), 6440-7.

101. Backofen, U.; Matysik, F.-M.; Lunte, C. E., A chip-based electrophoresis system with electrochemical detection and hydrodynamic injection. *Anal. Chem.* **2002,** *74* (16), 4054-4059.

102. Chen, C.; Hahn, J. H., Dual-Channel Method for Interference-Free In-Channel Amperometric Detection in Microchip Capillary Electrophoresis. *Anal. Chem.* **2007,** *79*, 7182-7186.

103. Scott, D. E.; Grigsby, R. J.; Lunte, S. M., Microdialysis Sampling Coupled to Microchip Electrophoresis with Integrated Amperometric Detection on an All-Glass Substrate. *Chem. Phys. Chem.* **2013,** *14* (10), 2288-2294.

104. Whatley, H. In *Basic principles and modes of capillary electrophoresis*, Humana Press Inc.: 2001; pp 21-58.

105. Nge, P. N.; Rogers, C. I.; Woolley, A. T., Advances in Microfluidic Materials, Functions, Integration, and Applications. *Chem. Rev.* **2013,** *113* (4), 2550-2583.

106. Mark, J. J. P.; Scholz, R.; Matysik, F.-M., Electrochemical methods in conjunction with capillary and microchip electrophoresis. *J. Chromatogr. A* **2012,** *1267*, 45-64.

107. Gunasekara, D. B.; Hulvey, M. K.; Lunte, S. M., In-channel amperometric detection for microchip electrophoresis using a wireless isolated potentiostat. *Electrophoresis* **2011,** *32* (8), 832-837.

108. Fischer, D. J.; Hulvey, M. K.; Regel, A. R.; Lunte, S. M., Amperometric detection in microchip electrophoresis devices: Effect of electrode material and alignment on analytical performance. *Electrophoresis* **2009,** *30* (19), 3324-3333.

109. Lacher, N. A.; Garrison, K. E.; Martin, R. S.; Lunte, S. M., Microchip capillary electrophoresis/electrochemistry. *Electrophoresis* **2001,** *22* (12), 2526-2536.

110. Lacher, N. A.; Lunte, S. M.; Martin, R. S., Development of a microfabricated palladium decoupler/electrochemical detector for microchip capillary electrophoresis using a hybrid glass/poly(dimethylsiloxane) device. *Anal. Chem.* **2004,** *76* (9), 2482-2491.

111. Osbourn, D. M.; Lunte, C. E., Cellulose acetate decoupler for on-column electrochemical detection in capillary electrophoresis. *Anal. Chem.* **2001,** *73* (24), 5961-5964.

112. Park, S.; Lunte, S. M.; Lunte, C. E., A perfluorosulfonated ionomer joint for capillary electrophoresis with on-column electrochemical detection. *Anal. Chem.* **1995,** *67* (5), 911-18.

113. O'Shea, T. J.; Greenhagen, R. D.; Lunte, S. M.; Lunte, C. E.; Smyth, M. R.; Radzik, D. M.; Watanabe, N., Capillary electrophoresis with electrochemical detection employing an on-column Nafion joint. *J. Chromatogr.* **1992,** *593* (1-2), 305-12.

114. Osbourn, D. M.; Lunte, C. E., Cellulose Acetate Decoupler for On-Column Electrochemical Detection in Capillary Electrophoresis. *Anal. Chem.* **2001,** *73* (24), 5961-5964.

115. Martin, R. S.; Ratzlaff, K. L.; Huynh, B. H.; Lunte, S. M., In-channel electrochemical detection for microchip capillary electrophoresis using an electrically isolated potentiostat. *Anal. Chem.* **2002,** *74* (5), 1136-1143.

116. Chen, C.-P.; Teng, W.; Hahn, J.-H., Nanoband electrode for high-performance in-channel amperometric detection in dual-channel microchip capillary electrophoresis. *Electrophoresis* **2011,** *32*, 838-843.

117. Gunasekara, D. B.; Hulvey, M. K.; Lunte, S. M.; Fracassi, d. S. J. A., Microchip electrophoresis with amperometric detection for the study of the generation of nitric oxide by NONOate salts. *Anal. Bioanal. Chem.* **2012,** 403, 2377-2384.

118. Hulvey, M. K.; Frankenfeld, C. N.; Lunte, S. M., Separation and Detection of Peroxynitrite Using Microchip Electrophoresis with Amperometric Detection. *Anal. Chem.* **2010,** *82*, 1608-1611.

119. Kikura-Hanajiri, R.; Martin, R. S.; Lunte, S. M., Indirect Measurement of Nitric Oxide Production by Monitoring Nitrate and Nitrite Using Microchip Electrophoresis with Electrochemical Detection. *Anal. Chem.* **2002,** *74* (24), 6370-6377.

120. Vazquez, M.; Frankenfeld, C.; Coltro, W. K. T.; Carrilho, E.; Diamond, D.; Lunte, S. M., Dual contactless conductivity and amperometric detection on hybrid PDMS/glass electrophoresis microchips. *Analyst* **2010,** *135* (1), 96-103.

121. Shiddiky, M. J. A.; Lee, K.-S.; Son, J.; Park, D.-S.; Shim, Y.-B., Development of Extraction and Analytical Methods of Nitrite Ion from Food Samples: Microchip Electrophoresis with a Modified Electrode. *J. Agric. Food Chem.* **2009,** *57* (10), 4051-4057.

122. Troska, P.; Chudoba, R.; Danc, L.; Bodor, R.; Horciciak, M.; Tesarova, E.; Masar, M., Determination of nitrite and nitrate in cerebrospinal fluid by microchip electrophoresis with microsolid phase extraction pre-treatment. *J. Chromatogr. B: Anal. Technol. Biomed. Life Sci.* **2013,** *930*, 41-47.

123. Noblitt, S. D.; Schwandner, F. M.; Hering, S. V.; Collett, J. L., Jr.; Henry, C. S., High-sensitivity microchip electrophoresis determination of inorganic anions and oxalate in atmospheric aerosols with adjustable selectivity and conductivity detection. *J. Chromatogr. A* **2009,** *1216* (9), 1503-1510.

124. Zhong, M.; Lunte, S. M., Tubular-Wire Dual Electrode for Detection of Thiols and Disulfides by Capillary Electrophoresis/Electrochemistry. *Anal. Chem.* **1999,** *71* (1), 251-255.

125. Zhong, M.; Zhou, J.; Lunte, S. M.; Zhao, G.; Giolando, D. M.; Kirchhoff, J. R., Dual-electrode detection for capillary electrophoresis/electrochemistry. *Anal. Chem.* **1996,** *68* (1), 203-7.

126. Zhou, J.; O'Shea, T. J.; Lunte, S. M., Simultaneous detection of thiols and disulfides by capillary electrophoresis-electrochemical detection using a mixed-valence ruthenium cyanide-modified microelectrode. *J. Chromatogr., A* **1994,** *680* (1), 271-7.

127. Pasas, S. A.; Lacher, N. A.; Davies, M. I.; Lunte, S. M., Detection of homocysteine by conventional and microchip capillary electrophoresis/electrochemistry. *Electrophoresis* **2002,** *23* (5), 759-766.

128. Lin, B. L.; Colon, L. A.; Zare, R. N., Dual electrochemical detection of cysteine and cystine in capillary zone electrophoresis. *J. Chromatogr., A* **1994,** *680* (1), 263-70.

129. Amatore, C.; Arbault, S.; Ferreira, D. C. M.; Tapsoba, I.; Verchier, Y., Vitamin C stimulates or attenuates reactive oxygen and nitrogen species (ROS, RNS) production depending on cell state: Quantitative amperometric measurements of oxidative bursts at PLB-985 and RAW 264.7 cells at the single cell level. *J. Electroanal. Chem.* **2008,** *615* (1), 34-44.

130. Lodge, J. K., Molecular actions of ascorbic acid. *Curr. Top. Nutraceutical Res.* **2008,** *6* (1), 1-13.

Chapter 2

Microchip electrophoresis coupled with in-channel electrochemical detection for the separation and detection of nitrosative and oxidative stress markers

This work has been published in the following journal publication:

D. B. Gunasekara, M. K. Hulvey, S. M. Lunte, "In-channel amperometric detection for microchip electrophoresis using a wireless isolated potentiostat," *Electrophoresis*, **2011**, 32, 832-837 (Feature article)

2.1 Introduction

Amperometry is a popular detection method for lab-on-a-chip devices due to its low detection limits and selectivity as well as the fact that electrodes can be fabricated using the same photolithographic techniques employed to create the microfluidic device [1-3]. Microchip electrophoresis is a technique that is able to generate very fast, highly efficient separations in a small and potentially portable format [3-6]. The combination of amperometric detection with microchip electrophoresis (ME) provides a powerful approach for the determination of a variety of biologically important compounds including reactive oxygen species (ROS) [7], reactive nitrogen species (RNS) [8], catecholamines [9,10], thiols [11,12], and carbohydrates [13-15].

Coupling amperometric detection with electrophoresis however can be challenging. The high voltages used to perform electrophoretic separations create a large amount of noise at the detector and can irreversibly damage the electronic circuitry of conventional potentiostats. To avoid these issues, three approaches have been employed to isolate the detector electrode from the high voltage field. These methods include aligning the electrode outside of the separation channel in what is referred to as an "end-channel" configuration [16,17] (Figure 2.1A), using a decoupler to shunt the high voltage to ground just prior to the detector (off-channel) [9,18,19], and using specialized electrically isolated potentiostats that allow the electrode to be placed directly in the separation channel (in-channel) [16,20,21] (Figure 2.1B). Each of these approaches posses their own advantages and disadvantages. End-channel alignment is the easiest to implement but can suffer from band broadening due to dispersion of the analyte plug once it exits the separation channel prior to detection. This can greatly reduce separation efficiency and make it more difficult to resolve closely migrating peaks. Also the band broadening can lead to a reduction in sensitivity. Using a decoupler in the off-channel configuration leads to higher separation efficiencies since the electrode is in the channel [16]. In the positive polarity separation mode, a Pd decoupler can be employed in order to adsorb the H_2 gas generated by the cathode. Unfortunately, a Pd decoupler cannot be used in a reverse polarity separation because the anode (decoupler) generates O_2 not H_2 from water.

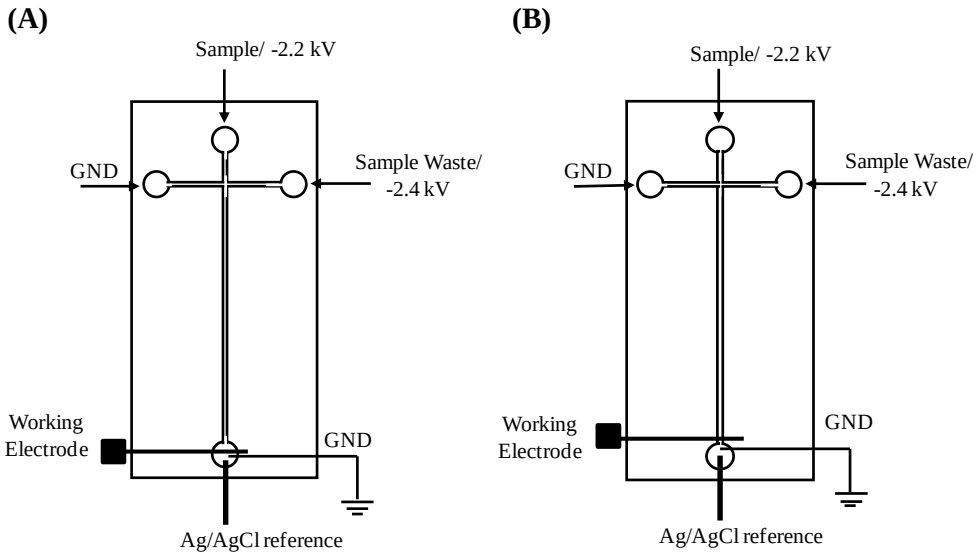

Figure 2.1: Schematic of (A) End-channel and (B) In-channel detection

The third approach requires the use of an electrically isolated potentiostat. This makes it possible to place the working electrode directly in the separation channel without a decoupler. The benefit of this approach is that it reduces band broadening while maintaining detector sensitivity. It is also possible to perform separations in reverse polarity without developing a decoupler that will adsorb oxygen. While a few reports have demonstrated the use of electrically isolated potentiostats to perform amperometric detection in microfluidic devices [20,21], none have focused on applications using negative polarity separation for small electroactive anions. One application reported the indirect detection of non-electroactive anions using reverse polarity with an in-channel electrode alignment [22]. This chapter focuses on the characterization and application of a microchip electrophoresis device employing a wireless isolated potentiostat to perform the separation and in-channel amperometric detection of small electroactive anionic species using negative polarity separation voltages and a cationic surfactant for modification of the electroosmotic flow. The effect of the separation voltage on the observed half-wave potentials, as well as a comparison of separation efficiencies, limits of detection (LOD), and sensitivity to that of end-channel alignment are presented.

2.2 Materials and methods

2.2.1 Materials and reagents

The following chemicals and materials were used as received: SU-8 10 photoresist and SU-8 developer (MicroChem Corp., Newton, MA, USA); AZ 1518 photoresist and 300 MIF developer (Mays Chemical Co., Indianapolis, IN, USA); photolithography film mask (50,000 dpi; Infinite Graphics Inc., Minneapolis, MN, USA); N(100) 100 mm (4") silicon (Si) wafers (Silicon, Inc., Boise, ID, USA); borosilicate float glass (4"× 1.1 mm.; Precision Glass and Optics, Santa Ana, CA, USA); Pt film coated glass substrates (2000 Å Pt layer over 200 Å Ti), The Stanford Nanofabrication Facility, Stanford, CA, USA; Sylgard 184 Silicone Elastomer Kit: Polydimethysiloxane (Ellsworth Adhesives, Germantown, WI, USA); Titanium (Ti) etchant (TFTN; Transene Co., Danvers, MA, USA); epoxy and Cu wire (22 gauge; Westlake Hardware, Lawrence, KS, USA); silver colloidal paste (Ted Pella, Inc., Redding, CA,

USA); acetone, 2-propanol (isopropyl alcohol, IPA), 30% H_2O_2, H_2SO_4, HNO_3, NaOH and HCl (Fisher Scientific, Fair Lawn, NJ, USA); sodium nitrite, boric acid, tetradecyltrimethylammonium bromide (TTAB), ascorbic acid (AA), tyrosine (Tyr) and reduced glutathione (GSH) (Sigma, St. Louis, MO, USA); peroxynitrite (Cayman Chemicals, Ann Arbor, MI, USA). All water used was ultrapure (18.3 MΩ·cm) (Millipore, Kansas City, MO, USA).

2.2.2 PDMS fabrication

The fabrication of PDMS-based microfluidic devices has been described previously [8]. Briefly, SU-8 10 negative photoresist (for electrophoresis channels) was spin coated on a 100 mm Si wafer to a thickness of 15 ± 1 μm using a Cee 100 spincoater (Brewer Science Inc., Rolla, MO, USA). The wafer was then transferred to a programmable hotplate (Thermo Scientific, Asheville, NC, USA) for a soft bake at 65^{o}C for 2 minutes and then 95 ^{o}C for five minutes. Microfluidic channel designs were created using AutoCad LT 2004 (Autodesk, Inc., San Rafael, CA, USA) and printed on to a transparency film at a resolution of 50,000 dpi (Infinite Graphics Inc., Minneapolis MN, USA). The coated wafer was covered with the transparency film mask and exposed to UV light (344 mJ/cm^2 for 16 s) using an i-line UV flood source (ABM Inc., San Jose, CA, USA). Following the UV exposure, the wafer was post-baked at 65^{o}C for 2 minutes and 95^{o}C for 10 minutes. The wafer was then developed in SU-8 developer, rinsed with IPA, and dried under nitrogen. A final "hard-bake" was performed at 175°C for 2hr. The thickness of the raised photoresist, which corresponds to the depth of the PDMS channels, was measured with a surface profiler (Alpha Step-200, Tencor Instruments, Mountain View, CA, USA). PDMS microstructures were made by casting a 10:1 mixture of PDMS elastomer and curing agent, respectively, against the patterned Si master. A simple "T" device containing a 5 cm separation channel (from the T intersection to the end of the separation channel) and 0.75 cm side arms was used for these studies. The width and depth of the electrophoresis microchannels were 50 μm and 14 μm, respectively. Holes for the reservoirs were created in the polymer using a 4 mm biopsy punch (Harris Uni-core, Ted Pella Inc., Redding, CA, USA).

2.2.3 Platinum electrode fabrication

The platinum (Pt) electrodes used for EC detection consisted of a 200 Å Ti adhesion layer followed by a 2000 Å Pt electrode layer deposited on a glass substrate by the Stanford Nanofabrication Facility. Positive photoresist (AZ 1518) was dynamically applied to the Pt coated glass plate at 100 rpm for 5 s. The spin coater was then ramped to a final speed of 3500 rpm and held for 30 s to yield a photoresist thickness of 2.0-2.2 μm. The photoresist was soft baked at 100°C for 2 min and then exposed to 86 mJ/cm^2 using an i-line UV flood source and the appropriate transparency mask. After exposure, the plate was developed for ~30 s in 300 MIF developer and then rinsed thoroughly with 18.2 MΩ cm H_2O and blown dry with N_2. A final hard bake was performed at 100°C for 10 min.

The remaining photoresist on the plate served to protect the underlying metal from the subsequent acid-etch procedure. Pt metal was removed by immersion in 85°C aqua regia (3:1:6 $H_2O/HCl/HNO_3$) for ~30 s or until no Pt metal could be seen. Ti metal was removed by immersing the plate in Ti etchant held at 95°C for ~ 45 s or until no remaining metal could be seen. After completion of the metal etching procedure, remaining photoresist was removed by rinsing the plate with acetone, followed by IPA, and drying with N_2. Wire leads for the electrodes were made by fixing bare Cu wire on the plate with quick-set epoxy. Bonding between the copper wire and the Pt electrodes was accomplished using Ag colloidal paste.

2.2.4 Chip construction

The layer of PDMS containing the separation channel was aligned and reversibly sealed to the glass plate containing the Pt electrode. For end-channel detection, the working electrode was placed 10-20 μm outside of the separation channel, in the ground reservoir. For in-channel detection, the electrode was placed 1-5 μm upstream from the end of the separation channel. The exception was for the hydrodynamic voltammetry (HDV) experiments, where the electrode was placed 10 μm upstream and downstream from the end of the channel for in-channel and end-channel configurations, respectively.

2.2.5 Solution preparation

The nitrite (NO_2^-, 10 mM) stock solutions were prepared weekly by dissolving $NaNO_2$ in ultrapure water. Stock solutions of hydrogen peroxide (H_2O_2, 10 mM), tyrosine (Tyr, 10 mM), GSH (10 mM) and AA (10mM) were all prepared in ultrapure water and stored at 4 °C. Subsequent dilutions of each stock solution for use in the microchip system were made in the appropriate run buffer at the time of analysis. Peroxynitrite standards were stored at –80 °C for no longer than two months and thawed on ice before use. Once thawed, the $ONOO^-$ was diluted fourfold in cold (4 ^oC) 0.3 M NaOH (per the vendor's instructions) to yield a solution of approximately 10 mM. 100 µl of 10 mM peroxynitrite solution was further diluted into 900 µl of run buffer for analysis. Verification of this concentration was established by measuring the absorbance of the ~10 mM solution at 302 nm using an extinction coefficient (ε) of 1670 $cm^{-1}M^{-1}$ (ε information is provided by the vendor).

2.2.6 Electrophoresis procedure

Electrophoretic separations were carried out on the device using a gated injection method. Two negative high voltage leads were placed in the sample and buffer reservoirs, while two earth ground leads were placed in the sample waste and buffer waste reservoirs. Gated injections were carried out by floating the high voltage at the buffer reservoir, which allowed the high voltage in the sample reservoir to deliver sample into the channel intersection of the microchip. To stop an injection, the high voltage in the buffer reservoir was reestablished. All data were collected using 1 s injections. The separation buffer consisted of 10 mM boric acid with 2 mM TTAB at pH 11.

2.2.7 Electrochemical detection

EC detection was accomplished using a modified model 8151BP 2-channel wireless, electrically isolated potentiostat (Pinnacle Technology Inc., Lawrence, KS, USA) operating in a two-electrode format (Pt working; Ag/AgCl reference (Bioanalytical Systems, W. Lafayette, IN, USA)) at 5 Hz sampling rate (Gain = 5,000,000 V/A, Resolution = 30 fA). Pinnacle Acquisition Laboratory (PAL) software was used for all data acquisition. The data acquisition is performed by wireless data transmission from potentiostat.

2.3 Results and discussion

2.3.1 In-channel amperometric detection

The use of an electrically isolated potentiostat for ME-EC makes it possible to place the working electrode directly in the separation channel in the presence of a high voltage without generation of excessive noise and/or damaging the potentiostat electronics. However, with the in-channel configuration the separation potential has a significant effect on the observed half-wave potentials. Previous reports have shown that the high voltages used for separations in both capillary [17,23] and microchip electrophoresis [21] create a negative bias that shifts the apparent half-wave potential several hundred millivolts when performing amperometric detection in the oxidative mode. These reports all employed conventional separations where the high voltages used for separation were positive polarity. In these cases, a positive shift in the apparent half-wave potential occurred, requiring higher potentials to be applied to the working electrode in order to oxidize analytes.

It can be expected that when using negative polarity to perform separations a positive bias will be imposed on the working electrode, creating an opposite shift in the half-wave potentials. Xu *et al.* reported this phenomena using ME-EC with indirect detection of anions [22]. Also, the C. lunte group observed a negative shift of $E_{1/2}$ for an analyte when the electrode is placed in end channel configuration due to negative polarity compared to flow injection [24]. Figures 2.2 A and B depict the effect of electrode placement on the observed half-wave potential for the oxidation of NO_2^- and H_2O_2 respectively using reversed polarity separation. As the working electrode potential is increased, we see an increase in response of each analyte peak until a maximum current (peak height) is obtained. In the end channel configuration (Figure 2.2 A and B) the working electrode is almost completely decoupled from the separation voltage and the species exhibit a half-wave potential similar to that obtained by cyclic voltammetry in a conventional electrochemical cell. The $E_{½}$ values for NO_2^- and H_2O_2 were found to be

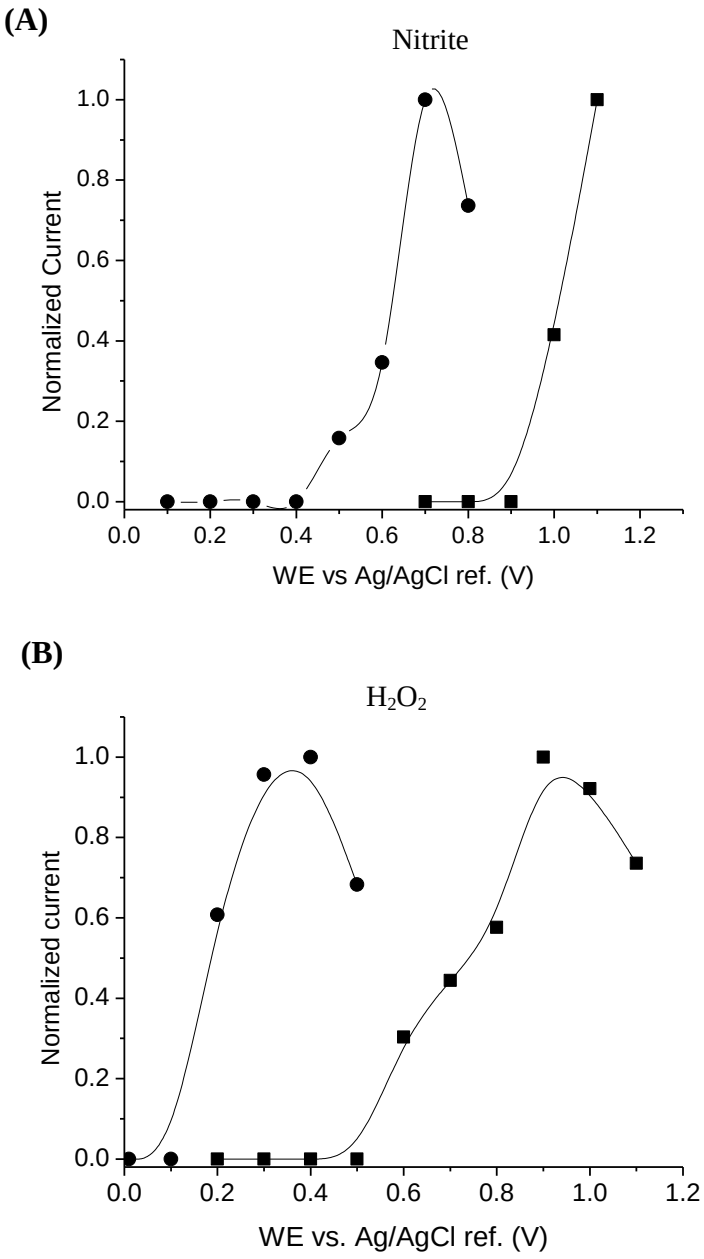

Figure 2.2: HDVs for in-channel and end-channel detection of (A) NO_2^- (100 µM) and (B) H_2O_2 (100 µM). Separation voltages were -1400 V and -1200 V for both in-channel and end-channel configurations. ● - in-channel, ■-end-channel

approximately +1050 mV and +600 mV vs. Ag/AgCl, respectively, for end channel configuration. However, when the working electrode is placed in the in-channel configuration, the observed half-wave potentials are shifted negative by approximately +500 mV for both NO_2^- and H_2O_2 (Figure 2.2 A and B). As was expected, the use of the negative polarity separation potentials creates a positive bias on the working electrode, reducing the apparent potential required to produce an oxidative current. Electrochemical detection was performed using two electrode configuration; however, measured currents were in low nA level. Therefore, the Ag/AgCl reference electrode can behave as a good thermodynamic reference.

2.3.2 Evaluation of separation performance

A major benefit of the in-channel electrode alignment is the increased separation efficiencies that are obtained. When employing an end-channel electrode configuration, band broadening can be a significant problem leading to a loss of resolution between analyte peaks, as well as a reduction in detector response. To demonstrate the improvement in resolution afforded by in-channel alignment, a separation of two analytes (GSH and AA) that migrate very close to one another under our separation conditions was performed using both end-channel and in-channel detection method. As can be seen in Figure 2.3A, using an end-channel alignment, GSH and AA migrate as a single, wide peak. However, using the in-channel alignment, the two peaks are nearly resolved (R = 1.3), allowing proper identification and quantitation to be performed. Figure 2.3B shows another separation of two closely migrating peaks. As can be seen in the electropherogram, Tyr and AA are barely resolved using end-channel (R=0.9). However, using in-channel, the two peaks were almost baseline resolved (R=1.2).

To evaluate the separation performance of in-channel electrode alignment for its eventual application to cellular analysis, the separation and detection of five electroactive analytes that are markers for oxidative stress and/or possible interfering analytes present in cells was performed. In these experiments, the WE was placed in channel, but as close as possible to the exit to minimize the influence of the separation field on the WE. For end-channel detection, the electrode was placed 10-20 μm away

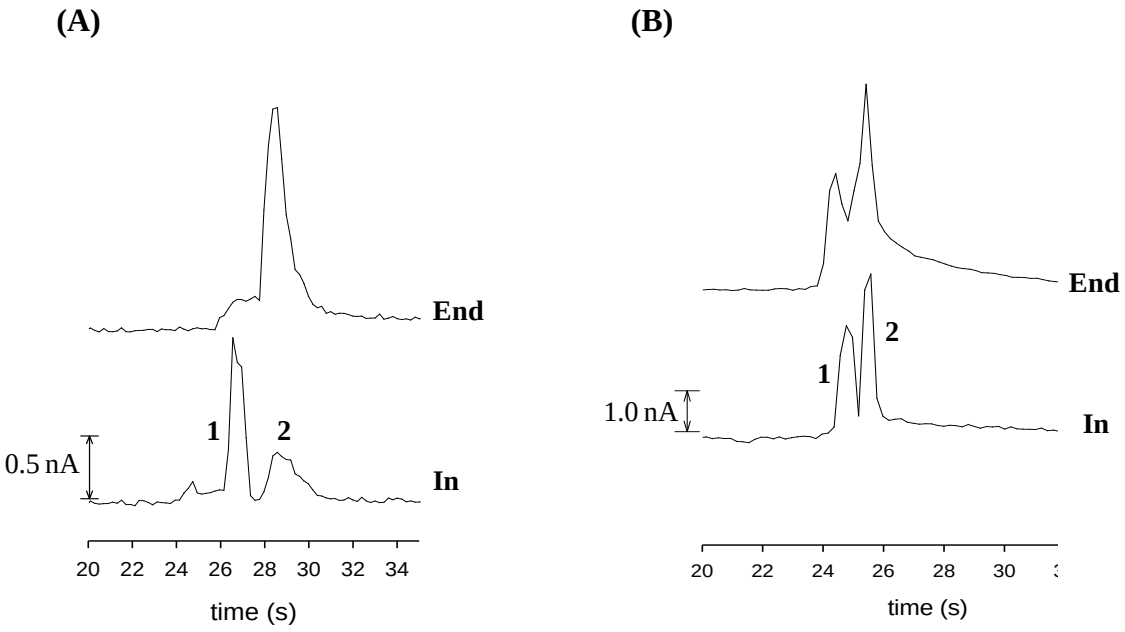

Figure 2.3: In-channel and end-channel detection of closely migrating species. (A) separation of AA (50 μM, peak 1) and GSH (50 μM, peak 2); (B) separation of Tyr (50 μM, peak 1) and AA (50 μM, peak 2). Separation voltages were -2400 V and -2200 V for both in-channel and end-channel configurations. A WE potential of +750 mV for in-channel and +1100 mV for end-channel vs. Ag/AgCl was applied.

from the channel exit. Figure 2.4 shows electropherograms obtained for a mixture of NO_2^- (100 µM), Tyr (30 µM), AA (40 µM), GSH 100 (µM), and H_2O_2 (100 µM) using ME-EC in the end-channel (2.4 A) and in-channel (2.4 B) configurations. With the end-channel configuration, AA and GSH are not resolved and there is a noticeable reduction in peak height for all of the species (Figure 2.4 A). Figure 2.4 B shows the same sample separated using the in-channel configuration. In this case AA and GSH are completely resolved and the peak heights for both NO_2^- (Figure 2.4 B peak 1), and H_2O_2 (Figure 2.4 B peak 5) are higher.

Another observation was that the background currents for the two methods were very similar. The background currents shown for the separations in Figure 2.4 A and B are actual experimentally observed values. For in-channel detection the background was 3.5 nA while 1.5 nA was observed for end-channel alignment. This is evidence that the background for the in-channel alignment is not significantly increased due to high voltage separation field.

The resolution for the separation using end-channel detection can be improved by moving the electrode closer (less than 5 µm) to the end of channel. This can be accomplished by the isolated potentiostat employed in these studies, but would destroy the electronics of a conventional potentiostat. Fisher *et al.* investigated the effect of electrode placement with end-channel detection and a conventional potentiostat [16]. They observed a significant increase in separation efficiency when the electrode was placed 10 µm from the end compared to 20 µm [16].

2.3.3 Comparison of separation parameters in end and in-channel amperometric detection

The LODs for NO_2^- (Figure 2.4 peak 1), and H_2O_2 (Figure 2.4 peak 5) were determined using both in-channel and end channel alignment (Table 1). As shown in Table 1, the peak-to-peak noise and LODs for in-channel and end-channel channel alignments were similar. However, the sensitivity was approximately 2-fold higher for in-channel alignment. Separation efficiencies of approximately 81,000 plates/m for NO_2^- and 155,000 plates/m for H_2O_2 were obtained using in-channel detection. The N values

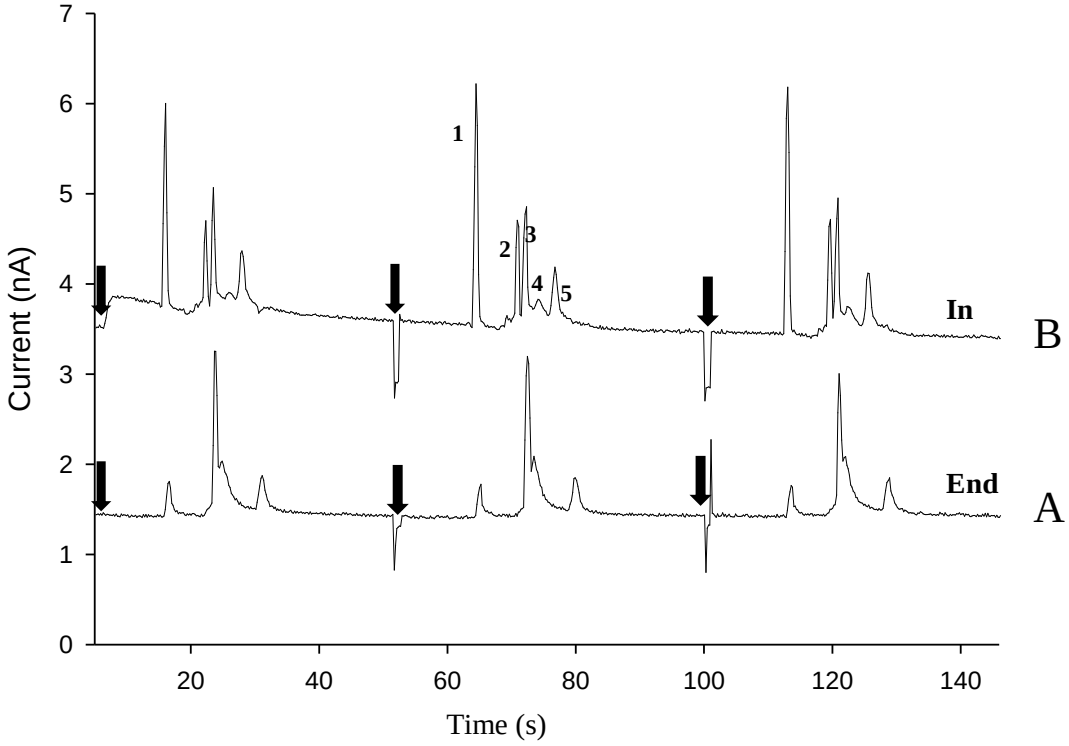

Figure 2.4: Comparison of (A) end-channel and (B) in-channel separation of NO_2^- (100 μM, peak 1), Tyr (30 μM, peak 2), AA (40 μM, peak 3), GSH (100 μM, peak 4), H_2O_2 (100 nM, peak 5). Separation voltages were -2400 V and -2200 V for both in-channel and end-channel configurations. A WE potential of +1100 mV vs. Ag/AgCl was used in both in-channel and end-channel detection. (⬇ -new injection)

observed for end-channel detection were significanly lower with N values of 54,000 plates/m for NO_2^- and 126,000 plates/m for H_2O_2.

2.3.4 Peroxynitrite detection

Hulvey *et al.* previously reported using microchip electrophoresis with end-channel amperometric detection as a method to monitor the transient reactive nitrogen species peroxynitrite ($ONOO^-$) [8]. Figure 2.5 shows the separation of a $ONOO^-$ standard using in-channel alignment. The in-channel detection exhibited better resolution and higher separation efficiencies compared to the previous report by Hulvey *et al.* [8]. The use of in-channel alignment will allow a more accurate quantitation of $ONOO^-$ in complicated matrices.

An additional useful feature of the electrically isolated potentiostat used in these studies is that it employs wireless data transmission. This attribute will be especially useful in applications where the analytical device is in a different location than the analyst. Examples include remote sensing of hazardous substances [5,6], point of care testing in third world countries and separation based sensors for on-animal monitoring of neurotransmitters [4,6].

2.4 Conclusions

This chapter demonstrates the advantages of employing an electrically isolated wireless potentiostat in order to perform in-channel amperometric detection on a microchip electrophoresis device. In particular, it is possible to place the working electrode in the separation channel without increased noise or damage to the potentiostat. This makes it possible to take advantage of the full potential of both the highly efficient method of electrophoretic separation and the high sensitivity of amperometric detection. The potentiostat was employed for the detection of small anions under reverse polarity separation conditions. These conditions are not compatible with off-channel detection using a Pd decoupler due to the formation of oxygen gas at the anode. The effect of the separation field on the observed half-wave potentials of two electroactive species was investigated. The results showed that the optimal working electrode potential for any application involving in-channel detection will have to be

Table 2.1. Comparison of peak-to-peak noise, LOD, sensitivity, and number of theoretical plates (N) for in-channel and end-channel configurations using NO_2^- (100 µM) and H_2O_2 (100 µM).

Species	Alignment	Peak-to-peak noise (pA)	LOD[b] at S/N = 3 (µM)	Sensitivity[b] (pA/µM)	N[a] (Plates/m)
NO_2^-	In	25	2.6 ± 0.1	30 ± 1	80,000
	End	30	6.2 ± 0.5	18 ± 1	50,000
H_2O_2	In	60	23 ± 1	15 ± 2	160,000
	End	50	27 ± 1	7.3 ± 0.3	130,000

a) Calculated from Figure 4
b) Standard deviation was calculated for 3 consecutive injections in a same microchip (n = 3)

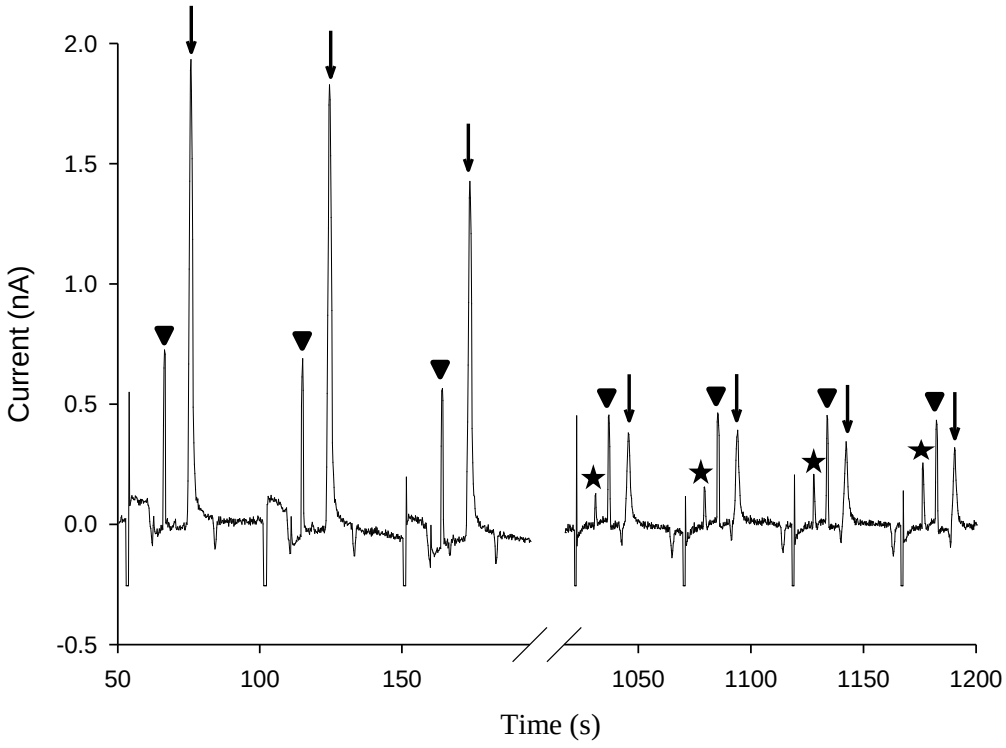

Figure 2.5: In-channel separation of $ONOO^-$ (100 μM) standards (↓- $ONOO^-$, ▼ - NO_2^- and ★-unknown). Other conditions as in Figure 4.

experimentally determined in order to compensate for the bias placed on the working electrode. The high separation efficiencies and sensitivity of the in-channel detection method will be exploited for the determination of electroactive RNS and ROS in cellular analysis. The wireless capabilities of the potentiostat also make it useful for remote sensing applications and on-animal analysis.

2.5 References

1. Hulvey, M. K.; Lunte, S. M.; Fischer, D. J.; Kuhnline, C. D., In Electrochemical Detection Methods Following Liquid Chromatography, Capillary Electrophoresis, and Microchip Electrophoresis Separations. Meyer, R. A., (Ed.), *Encyclopedia of Analytical Chemistry*, Wiley, Weinheim **2010**.

2. Xu, J. J.; Wang, A. J.; Chen, H. Y., Electrochemical detection modes for microchip capillary electrophoresis. *Trac-Trend. Anal. Chem.* **2007,** *26* (2), 125-132.

3. Kuban, P.; Hauser, P. C., Fundamentals of electrochemical detection techniques for CE and MCE. *Electrophoresis* **2009,** *30* (19), 3305-3314.

4. Lunte, S.; Nandi, P.; Regel, A.; Grigsby, R.; Hulvey, M.; Scott, D.; Naylor, E.; Gabbert, S.; Johnson, D., Development of a Miniaturized Wireless Microdialysis-Microchip Electrophoresis System for In Vivo Monitoring of Drugs and Neurotransmitters in Freely Roaming Sheep. *Micro TAS abstract paper* **2010**, Topic No: 1.4 Paper ID No: 0844.

5. Berg, C.; Valdez, D. C.; Bergeron, P.; Mora, M. F.; Garcia, C. D.; Ayon, A., Lab-on-a-robot: Integrated microchip CE, power supply, electrochemical detector, wireless unit, and mobile platform. *Electrophoresis* **2008,** *29* (24), 4914-4921.

6. Arora, A.; Simone, G.; Salieb-Beugelaar, G. B.; Kim, J. T.; Manz, A., Latest Developments in Micro Total Analysis Systems. *Anal. Chem.* **2010,** *82* (12), 4830-4847.

7. Amatore, C.; Arbault, S.; Bouton, C.; Drapier, J.-C.; Ghandour, H.; Koh, A. C. W., Real-time amperometric analysis of reactive oxygen and nitrogen species released by single immunostimulated macrophages. *Chem. Bio. Chem.* **2008,** *9* (9), 1472-1480.

8. Hulvey, M. K.; Frankenfeld, C. N.; Lunte, S. M., Separation and Detection of Peroxynitrite Using Microchip Electrophoresis with Amperometric Detection. *Anal. Chem.* **2010,** *82*, 1608 -1611.

9. Lacher, N. A.; Lunte, S. M.; Martin, R. S., Development of a microfabricated palladium decoupler/electrochemical detector for microchip capillary electrophoresis using a hybrid glass/poly(dimethylsiloxane) device. *Anal. Chem.* **2004,** *76* (9), 2482-2491.

10. Mecker, L. C.; Martin, R. S., Use of micromolded carbon dual electrodes with a palladium decoupler for amperometric detection in microchip electrophoresis. *Electrophoresis* **2006,** *27* (24), 5032-5042.

11. Kuhnline, C. D.; Gangel, M. G.; Hulvey, M. K.; Martin, R. S., Detecting thiols in a microchip device using micromolded carbon ink electrodes modified with cobalt phthalocyanine. *Analyst* **2006,** *131* (2), 202-207.

12. Pasas, S. A.; Lacher, N. A.; Davies, M. I.; Lunte, S. M., Detection of homocysteine by conventional and microchip capillary electrophoresis/electrochemistry. *Electrophoresis* **2002,** *23*, 759-766.

13. Fanguy, J. C.; Henry, C. S., Pulsed amperometric detection of carbohydrates on an electrophoretic microchip. *Analyst* **2002,** *127* (8), 1021-1023.

14. Garcia, C. D.; Henry, C. S., Direct determination of carbohydrates, amino acids, and antibiotics by microchip electrophoresis with pulsed amperometric detection. *Anal. Chem.* **2003,** *75* (18), 4778-4783.

15. Garcia, C. D.; Henry, C. S., Enhanced determination of glucose by microchip electrophoresis with pulsed amperometric detection. *Anal. Chim. Acta* **2004,** *508* (1), 1-9.

16. Fischer, D. J.; Hulvey, M. K.; Regel, A. R.; Lunte, S. M., Amperometric detection in microchip electrophoresis devices: Effect of electrode material and alignment on analytical performance. *Electrophoresis* **2009,** *30* (19), 3324-3333.

17. Matysik, F.-M., Improved end-column amperometric detection for capillary electrophoresis. *J. Chromatogr. A* **1996,** *742*, 229 - 234.

18. Chen, D. C.; Hsu, F. L.; Zhan, D. Z.; Chen, C. H., Palladium Film Decoupler for Amperometric Detection in Electrophoresis Chips. *Anal. Chem.* **2001,** *73*, 758-762.

19. Osbourn, D. M.; Lunte, C. E., On-column Electrochemical Detection for Microchip Capillary Electrophoresis. *Anal. Chem.* **2003,** *75*, 2710-2714.

20. Chen, C.; Hahn, J. H., Dual-Channel Method for Interference-Free In-Channel Amperometric Detection in Microchip Capillary Electrophoresis. *Anal. Chem.* **2007,** *79* (18), 7182-7186.

21. Martin, R. S.; Ratzlaff, K. L.; Huynh, B. H.; Lunte, S. M., In-channel electrochemical detection for microchip capillary electrophoresis using an electrically isolated potentiostat. *Anal. Chem.* **2002,** *74* (5), 1136-1143.

22. Xu, J. J.; Peng, Y.; Bao, N.; Xia, X. H.; Chen, H. Y., In-channel indirect amperometric detection of nonelectroactive anions for electrophoresis on a poly(dimethylsiloxane) microchip. *Electrophoresis* **2005,** *26* (19), 3615-3621.

23. Wallenborg, S. R.; Nyholm, L.; Lunte, C. E., End-Column Amperometric Detection in Capillary Electrophoresis: Influence of Separation-Related Parameters on the Observed Half-Wave Potential for Dopamine and Catechol. *Anal. Chem.* **1999,** *71* (3), 544-549.

24. Wallenborg, S. R.; Dorholt, S. M.; Faibushevich, A.; Lunte, C. E., Determination of Chlorite in Drinking Water Using Capillary Electrophoresis with Amperometric Detection. *Electroanalysis* **1999,** *11* (5), 362-366.

Chapter 3

Microchip electrophoresis with amperometric detection for the study of the generation of nitric oxide by NONOate salts

This work has been published in the following journal publication:

D. B. Gunasekara, M. K. Hulvey, S. M. Lunte, J. A. F. da Silva, "Microchip electrophoresis with amperometric detection for the study of generation of nitric oxide by NONOate salts," *Anal. Bioanal. Chem.*, **2012**, 403, 2377-2384

3.1 Introduction

The short half-life of NO *in vivo* makes its detection and quantification an analytical challenge. NO can directly or indirectly react with amino acids, proteins, metal ions, molecular oxygen, radical species, and DNA, which makes the half-life of NO relatively short in biological media [1]. Many approaches for the detection of NO *in vivo* have been reported in the literature. These include the reaction of NO with fluorescent probes [2-8], direct amperometric detection [9-11], chemiluminescence [12], electron paramagnetic resonance [8,11], voltammetry [13], and indirect detection of its degradation products nitrite and nitrate [14-17].

NO has been detected directly using amperometric biosensors [10,11]. For example, Schoenfisch's group developed NO-specific biosensors using xerogel membranes and platinum black and platinum electrodeposited tungsten substrates [9,10]. These biosensors have detection limits in the pM range, and the xerogel membrane shows high selectivity and permeability for NO [9]. However, interference due to other electroactive compounds is a challenge for some amperometric biosensors [11]. As described earlier in introduction chapter, indirect measurements of NO degradation products such as nitrate and nitrite or the reaction of NO with fluorescent probes have also been employed for NO detection. Although these methods are effective, there can be problems with specificity, cross-reactivity of the probes, and efficiency or kinetics of reactions. An alternative approach to improve selectivity of these techniques is to separate NO or NO reacted fluorescence probes from interferences prior to the detection [18,19].

Among the existing separation techniques, capillary electrophoresis (CE) presents many advantages, including low consumption of sample and reagents, high efficiency and resolution, reduced analysis time, easy method development, and several modes of separation. When CE is accomplished in microchannels (ME), it has the additional advantage of faster analyses, even lower reagents and samples volume consumption, and the possibility of parallel processing and integration of analytical steps [20].

Another feature of ME is the ability to perform sequential injections, making it possible to monitor the progress of a reaction. Among the detectors available for ME, LIF and electrochemical (EC) detection schemes are preferred, mainly due to their high sensitivity and ease of application. With EC detection, it is possible to integrate the electrodes into the chip during the fabrication process, leading to a fully integrated microfluidic systems [21-24]. Electrode materials such as carbon (carbon fiber, ink and screen printed) and metal (Au, Pt and Pd) have been widely used in ME-EC devices [25-28]. Nanomaterials have also been employed to enhance electrochemical performance [29].

ME coupled to LIF has already been used for the detection of NO in human blood and leukemia-type cells [18,30]. To the best of our knowledge, ME coupled to electrochemical detection (ME-EC) for the measurement of NO has not been achieved; however, ME-EC of peroxynitrite and the metabolites (nitrite and nitrate) of NO and peroxynitrite has been reported previously [27,31,25,32]. One of the advantages of ME-EC is the possibility of detecting several compounds simultaneously in a single sample. Many biologically important compounds involved in oxidative stress such as ascorbic acid, glutathione, hydrogen peroxide, and nitrite are electroactive and can be measured along with NO by ME-EC.

Due to the important role of NO in vasodilatation and immune signaling, there have been many drugs developed to deliver NO or enhance its production *in vivo* [33]. In particular, several diazeniumdiolates have been developed as NO donors [34], and several compounds of this class are now commercially available. These same compounds have also been employed as NO standards for *in vivo* and *in vitro* studies. For example, we have employed the diethylamine adduct of NO for calibration purposes in laser-induced fluorescence (LIF) detection of NO [18]. Spence's and Martin's groups have also used these compounds for quantitation of NO release from platelets, endothelial cells, and erythrocytes in microfluidic studies [35-40]. NONOates offer an efficient way to generate known

quantities of NO. NO generation occurs via acid hydrolysis, and NONOates with half-lives varying from few seconds to several minutes are available.

In this chapter, microchip electrophoresis with electrochemical detection was used to monitor the generation of nitric oxide from NONOate salts with a temporal resolution of 60 s. Since both the salt and NO are electroactive, it is possible to simultaneously monitor the disappearance of the NONOate and the appearance of the NO. Nitrite was also well resolved from the two compounds. The method described here will be employed in the future to investigate the reaction products of NO with biomolecules in a microfluidic-based system.

3.2 Experimental

3.2.1 Reagents and solutions

All reagents were of analytical grade and used as received. Sodium nitrite ($NaNO_2$), boric acid, tetradecyltrimethylammonium bromide (TTAB), and sodium phosphate monobasic and dibasic were from Sigma (St. Louis, MO, USA). Sodium hydroxide and hydrochloric acid were from Fisher Scientific (Fair Lawn, NJ, USA). Diethylammonium (Z)-1-(N,N-diethylamino)diazen-1-ium-1,2-diolate (diethylamine NONOate, DEA/NO) and 1-(hydroxyl-NNO-azoxy)-L-proline disodium salt (PROLI/NO) were purchased from Cayman Chemical (Ann Arbor, MI, USA). All solutions were prepared using deionized (DI) water with resistivity greater than 18.3 MΩ cm (Millipore, Kansas City, MO, USA). Phosphate-buffered saline (PBS) dry powder in foil pouches was purchased from Sigma and dissolved in 1 L of deionized water to prepare 10 mM PBS pH 7.4 solution (salt concentrations were 140 mM NaCl and 3 mM KCl). The 10 mM phosphate buffer at pH 7 was prepared by mixing appropriate amounts of sodium monobasic and dibasic in DI water. Nitrite and hydrogen peroxide stock standard solutions were prepared in DI water at a concentration of 10 mM and diluted in the run buffer to the desired concentration. Diluted standards were prepared daily. Stable stock solutions were kept for a week at 4 °C, while unstable solutions such as DEA/NO and PROLI/NO were prepared immediately before use. The

background electrolyte (BGE) employed for the electrophoresis experiments consisted of 10.0 mM boric acid and 2.0 mM TTAB. The pH was adjusted to 11 with sodium hydroxide.

3.2.2 Microchip fabrication and instrumentation

Fabrication of the PDMS-based microchips for ME-EC has been fully described elsewhere [27,31]. Briefly, the masters for replication were fabricated from a 4-inch wafer coated with SU-8 10 photoresist (Silicon, Inc., Boise, ID, USA) using soft lithography. The width and depth of the microchannels were 50 and 14 µm, respectively. PDMS microstructures were made by casting a 10:1 mixture of PDMS elastomer:curing agent against the silicon master using Sylgard 184 Silicone Elastomer Kit (Ellsworth Adhesives, Germantown, WI, USA). Following fabrication of the PDMS layer containing the electrophoresis channels, 4-mm holes for the sample and waste reservoirs were produced using a biopsy punch (Harris Uni-core, Ted Pella, Redding, CA, USA). The PDMS substrate containing the electrophoresis channel was then reversibly sealed against a flat borosilicate glass (Precision Glass and Optics, Santa Ana, CA, USA) that contained a 15µm Pt band working electrode. Fabrication of Pt band electrodes were reported previously [27]. The separation channel and Pt electrode were carefully aligned to place the electrode exactly at the edge of the channel outlet (in-channel detection) [27]. The microchip design for all experiments was a simple-T design with a 5-cm separation channel and 0.75-cm side arms (Figure 3.1)

A dual channel high voltage power supply (HV Rack, Ultravolt Inc., Ronkonkoma, NY, USA) controlled by software written in Labview (National Instruments, Austin, TX, USA) was employed in these experiments. Gated injection [41] and electrophoretic separation were accomplished through the application of –2400 and –2200 V to the BGE and sample reservoirs, respectively. The injection time was 1 s, and the separation lasted 60 s. Sequential injections could be easily conducted using gated injection, which allows continuous monitoring of the reactions.

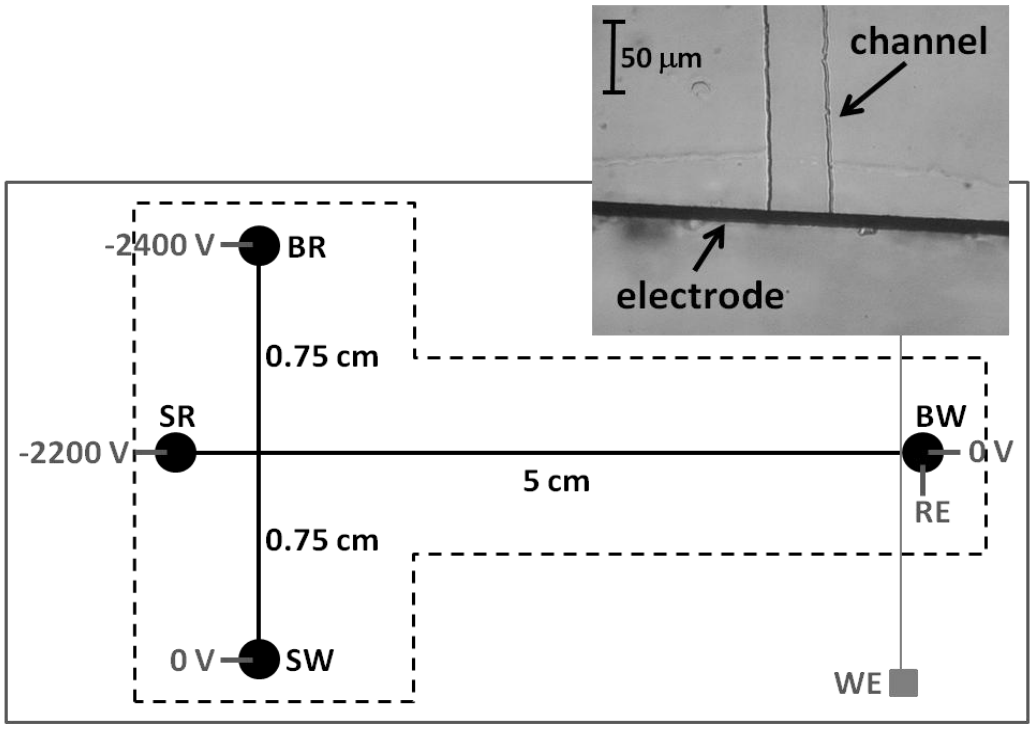

Figure 3.1: Microchip setup. BR, SR, BW and SW indicate BGE, sample, BGE waste, and sample waste reservoirs, respectively. WE and RE are working (Pt band) and reference (Ag/AgCl) electrodes, respectively. The dotted line represents the limits of the PDMS microchip. The inset shows a picture of the electrode/channel alignment.

Electrochemical detection was achieved using a wireless isolated potentiostat (Pinnacle Technology, Lawrence, KS, USA) in a two-electrode configuration [27]. Working and reference electrodes were 15 µm Pt band and Ag/AgCl (RE-5B, Bioanalytical Systems, Inc., West Lafayette, IN, USA), respectively. To facilitate the electrode-channel alignment, the microchip was set up on an inverted microscope (Nikon Ti-U, Melville, NY, USA).

3.2.3 Procedures

3.2.3.1 DEA/NO and PROLI/NO sample preparation

The general procedure for preparation of the NONOate salts is as follows: The NONOate salt was dissolved in 1 mL 0.01 M NaOH to obtain a stable 10 mg/mL NONOate standard solution. This solution was then diluted five times in phosphate or PBS in order to initiate the hydrolysis reaction and production of NO. The sample was again diluted tenfold in run buffer or water prior to introduction into the chip. The pH of the phosphate or PBS was selected such that the final pH was around pH 7 after addition of NONOate dissolved NaOH solution. The reaction for the generation of NO using the two types of NONOate salts is depicted in Figure 3.2.

First, DEA/NO was investigated with two different sets of acidic solutions to initiate the acid hydrolysis—10 mM phosphate with pH 2–3 and 10 mM PBS with pH 2–3 (the pH of the phosphate and PBS was adjusted to 2–3 by acidifying stock buffer solutions using concentrated HCl). DEA/NO was diluted five times in this acidified solution (phosphate or PBS). When phosphate buffer was employed for hydrolysis, the sample was diluted ten times in run buffer (10 mM boric acid with 2 mM TTAB at pH 11) prior to analysis. When PBS was used, the sample was diluted ten times in deionized water.

PROLI/NO sample preparation was straightforward after optimizing the acid hydrolysis conditions with DEA/NO. To prepare a PROLI/NO standard, 10 mg of PROLI/NO was dissolved in 0.01 M NaOH (800 µL). Then 250 µL of PROLI/NO NaOH solution was diluted into 750 µL of 10 mM PBS with 2 mM TTAB at pH 2. This solution was further diluted 10 times in degassed water and analyzed.

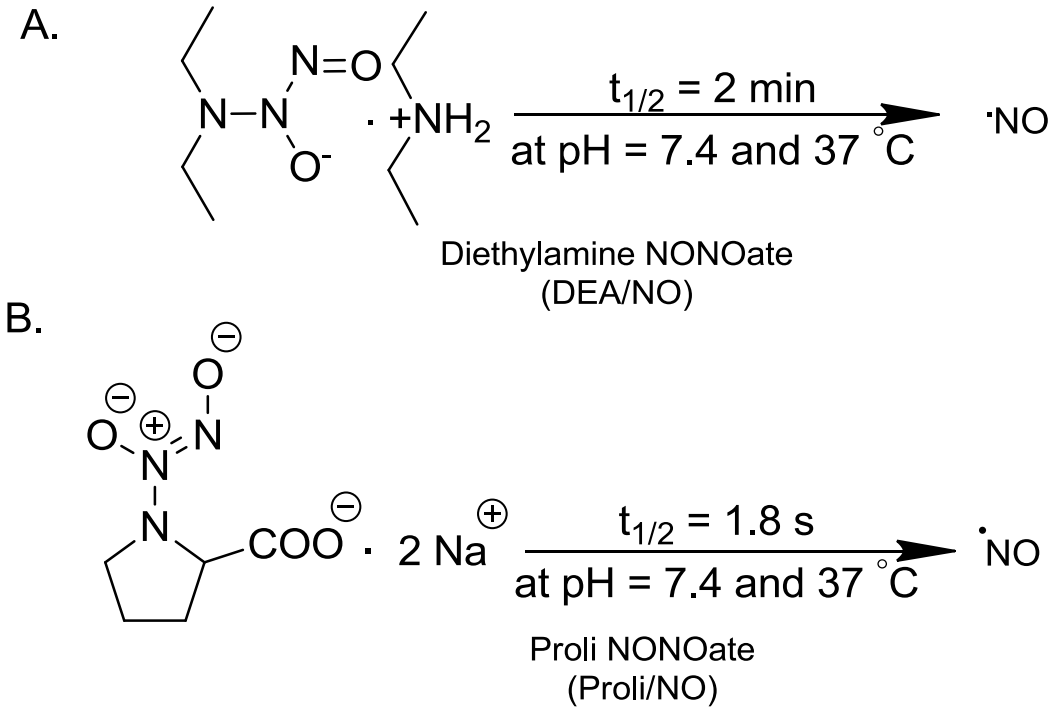

Figure 3.2: Generation of NO using (A) DEA/NO and (B) PROLI/NO (The reaction schemes were adapted from www.caymanchem.com).

3.2.3.2 Microchip operation

Freshly prepared PDMS microchips were conditioned with 0.1 M NaOH solution followed by run buffer. For ME-based analysis, the potentials were applied to the reservoirs, as indicated in Figure 3.1. At this point, the currents registered would be approximately 11–12 μA and 8–9 μA for the buffer reservoir (BR) and sample reservoir (SR), respectively. The high voltage was turned off for sample introduction. Next, the BGE was replaced by the sample at SR, the potentiostat was turned on for data acquisition, and the gated injection program was run. The acquired data were processed using Microcal Origin 8.0.

3.3. Results and discussion

3.3.1 Advantages of ME-EC for study NO generation from NONOate

The main advantage of using a separation method is the possibility of detection and quantification of several related species in complexes matrices, which improves the selectivity of the method. We previously reported ME-based methods for the detection of nitrate, nitrite, peroxynitrite, and RNS related species [27,31,32]. The present study was focused on detection of NO using ME-EC, and this goal was accomplished by employing NO-donor NONOate salts. The dynamic behavior of NONOates during acid hydrolysis can be used to investigate the electrophoretic behavior of NO. That is, one can observe nitrite generation, NONOate decomposition, and NO generation and/or decomposition with ME-EC during the acid hydrolysis of NONOates. The migration times for the NONOate anions can be determined by diluting NONOate stock solution in high pH run buffer and ME-EC analysis. This makes it possible to identify the NO peak (that is produce upon hydrolysis) based on migration order and its appearance using low pH reaction buffer. Also, ME-EC is an alternative way to investigate NO generation from NONOate as a function of pH. Since NONOates are commonly employed for biological investigations as a NO delivery system, ME-EC will yield a better understanding of the mechanism of NO delivery under different pH and solvent conditions.

3.3.2 Considerations with in-channel detection

NO and NO donors are electroactive and can be directly oxidized at Pt electrodes. For these studies, in-channel amperometric detection was employed. With this configuration, the exact potential needed for the oxidation is dependent on the position of the working electrode in the separation field [27,42]. When the electrode was placed fully inside the channel (10 µm from the channel end) for amperometric detection with reverse polarity conditions (negative polarity at sample reservoir), there was an approximately 500 mV negative shift in half-wave potential for nitrite and H_2O_2 standards in comparison to the half-wave potentials observed for end channel detection (electrode placed 10 µm outside of the channel, chapter 2) [27]. Hence, a lower potential must be applied to the working electrode for oxidation of analytes since the voltage bias is additive under reverse polarity separation conditions. Therefore, hydrodynamic voltammetric experiment must be performed with each new microchip to determine the voltage bias. As shown in chapter 2 the voltage bias produced by the separation field can be minimized by placing the working electrode at the very end of the separation channel but still in the channel (0–5 µm). This approach also preserves the high separation efficiencies characteristic of in-channel detection, making it possible to resolve closely migrating species [27].

Optimization of the detection potential was necessary to assure good sensitivity with this electrochemical detection scheme. In these experiments, the potential was set at +1.0 to +1.1 V vs. the Ag/AgCl reference, which is sufficiently positive for the oxidation of NO, nitrite, and the NO donors. Another useful approach consists of injecting a 100 µM nitrite solution and checking the peak height, which should be higher than 2.5 nA.

3.3.3 NONOate sample preparation

Both 10 mM phosphate and 10 mM PBS at pH 2–3 were evaluated for the hydrolysis studies. Following ME-EC analysis, three peaks corresponding to DEA/NO, NO, and nitrite were obtained. It was found that PBS appeared to be the better reaction medium. It was also determined that the desired final

pH of the NONOate buffer mix was approximately 7. Since the hydrolysis reaction is highly dependent on the pH of the solution, one must be aware that below pH 5 the reaction is so fast that only the nitrite peak is observed. At final pH values above 8, NO cannot be detected.

3.3.4 NO generation from DEA NONOate

Figure 3.3 shows typical results obtained for the acid hydrolysis of DEA/NO in PBS. The electropherogram shows sequential injections of the DEA/NO sample. The migration times for nitrite, DEA/NO, and NO were 22.0 ± 0.3, 33.5 ± 0.4, and 37.6 ± 0.2 s, respectively. This migration order can be expected because nitrite is smaller than DEA/NO, although both species have one negative charge. Since NO is neutral, it moves with the electroosmotic flow (EOF). The efficiencies given in plates per meter were $2.5 \pm 0.4 \times 10^4$, $1.0 \pm 0.5 \times 10^5$, and $1.1 \pm 0.4 \times 10^5$ for nitrite, DEA/NO, and NO, respectively. Although the nitrite peak presented a slow decrease in height (about 44 % after 10 injections) over time, the decrease in response for the DEA/NO peak was more dramatic. The observed decay for nitrite could be due to electrokinetic injection irreproducibility and stacking effects due to saline used with phosphate.

The DEA/NO peak could be identified by measuring the kinetics of the DEA/NO hydrolysis reaction. The peak corresponding to DEA/NO exhibited peak currents that were fitted into zero-, first-, and second-order rate law. The best correlation ($R^2 = 0.97$) was obtained for a first-order reaction (versus 0.90 and 0.76 for zero- and second-order, respectively) (Figure 3.4A). This agrees with the vendor product information for the reaction of DEA/NO (www.caymanchem.com). After the tenth injection (10 min), there was an appearance of a shoulder at the DEA/NO peak that became a clear third peak upon subsequent injections. This new peak indicates NO production. This NO peak is not visible in the first injections because of the high intensity of the DEA/NO peak. When the DEA/NO peak becomes smaller, the resolution is adequate for identification of NO.

Figure 3.4B shows the peak heights for DEA/NO and NO as a function of time. In the case of NO, only the last six injections were taken into account. From this figure, it is also possible to see the

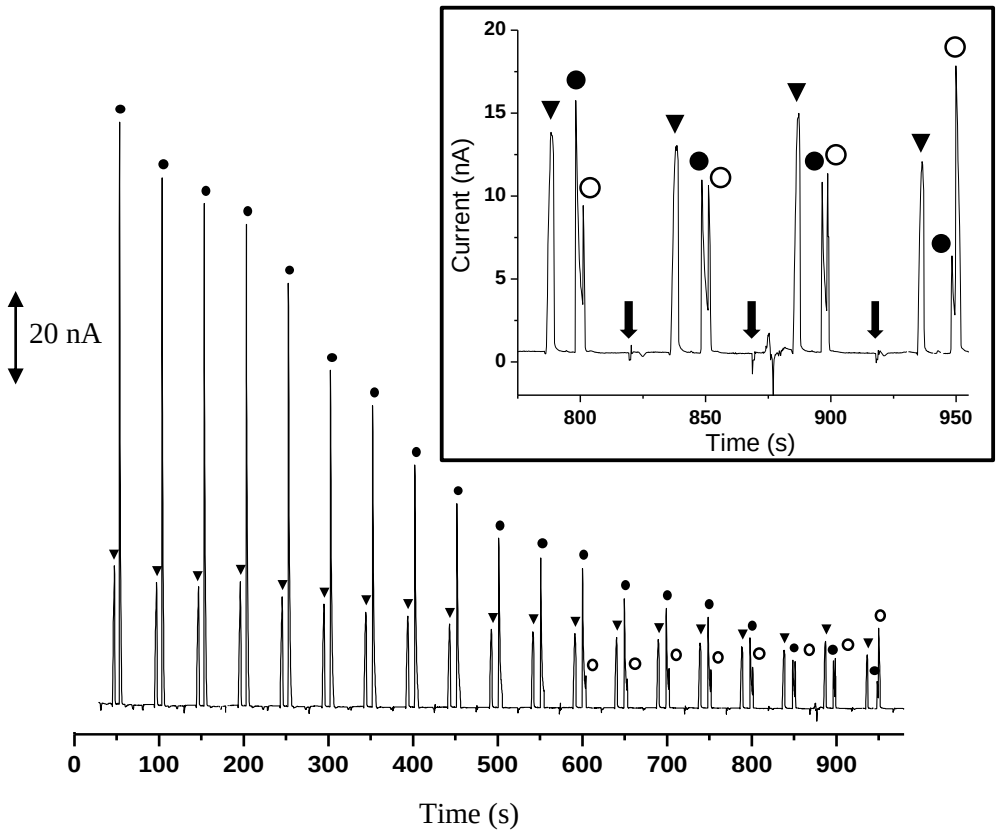

Figure 3.3: Monitoring the acid hydrolysis of DEA/NO at pH 7. Conditions: BGE: 10 mM boric acid, 2 mM TTAB, pH 11. Triangle – nitrite; solid circle – DEA/NO; open circle – NO. Gated injection: –2200 V at SR, –2400 V at BR, 1 s injection, 60 s run. The inset shows the magnification of the electropherogram from 750 to 950 s. The arrows indicate the sample injection. Baseline subtraction was accomplished using Origin

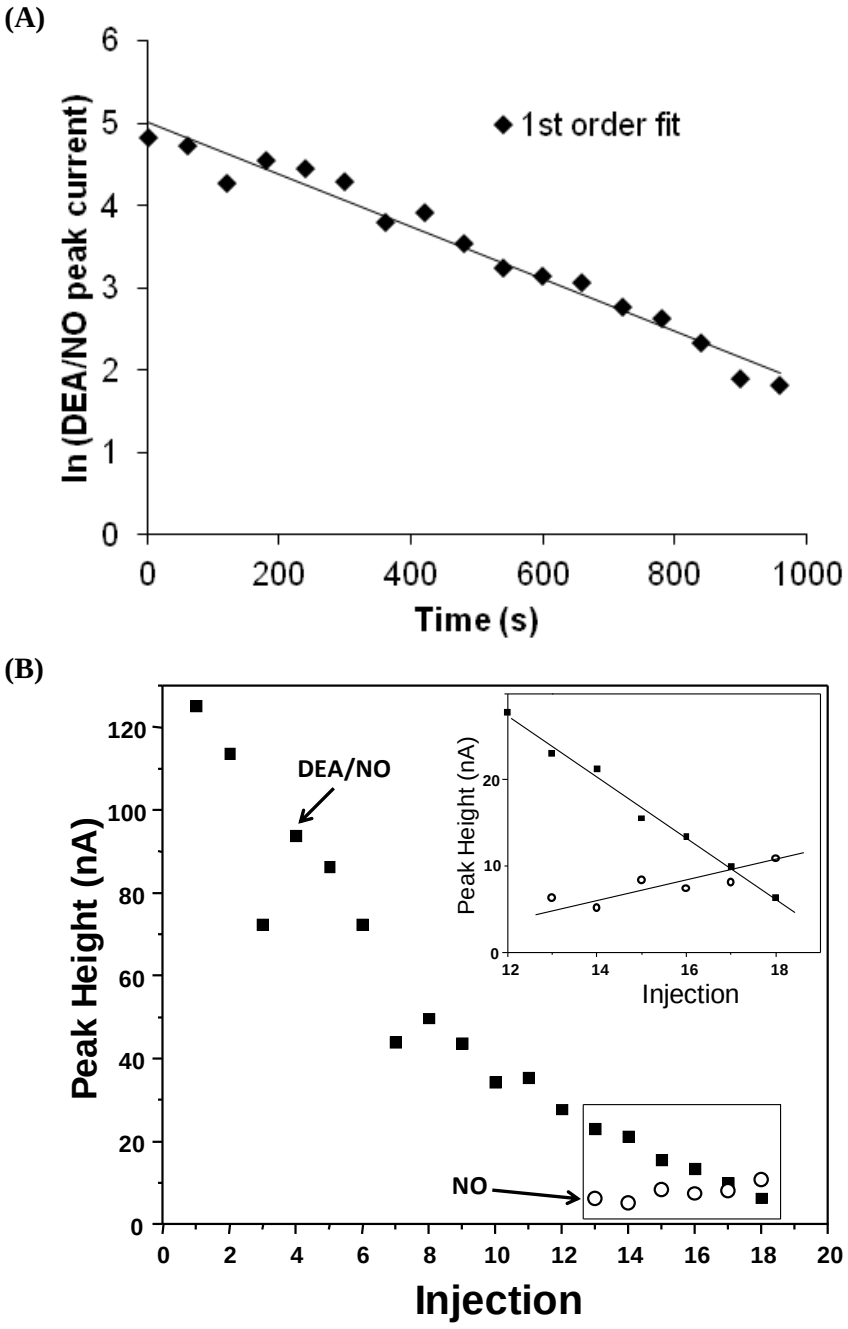

Figure 3.4: (A) DEA/NO peak decay fit into first-order rate law. (B) Peak heights obtained during DEA/NO acid hydrolysis as a function of sequential injections. (The data represented here obtain from the electropherogram in Figure 3.3)

exponential decay of the DEA/NO peak. The inset in Figure 3.4B shows that the rate of increase of the NO peak that corresponds with the decrease for the response of the DEA/NO. It was also observed after several injections that the NO peak height was reduced (after 18^{th} injection in the electropherogram in the Figure 3.3), probably due to volatilization from the sample reservoir or reactions with oxygen. These experiments were not performed under an inert atmosphere, except that the solutions were degassed by bubbling nitrogen at the start of the experiment.

3.3.5 NO generation from Proline NONOate

Under the experimental conditions described above, the resolution between DEA/NO and NO peaks was low (R = 1.0 ± 0.2), and NO migrated with DEA/NO when the concentration of the NONOate salt was higher. Therefore, a different NONOate salt was selected in an attempt to improve resolution based on the structure of the NONOate. As shown in Figure 3.2 B, the net negative charge of the PROLI/NO molecule is 2. DEA/NO has only one negative charge (Figure 3.2 A). Therefore, the electrophoretic mobility of PROLI/NO should be higher than that of DEA/NO, leading to improved resolution of PROLI/NO and NO. Figure 3.5 A shows electropherograms obtained for sequential injections of PROLI/NO. As expected, PROLI/NO and NO were fully separated. Although PROLI/NO migrates closer to nitrite, good resolution between nitrite and PROLI/NO was also observed (R = 2.4 ± 0.2). The migration times obtained for nitrite, PROLI/NO, and NO were 16.4 ± 0.2, 20.1 ± 0.4, and 34.5 ± 0.7 s. The efficiencies given in plates per meter were 6.3 ± $1.1x10^4$, 7.7 ± $1.3x10^4$ and 3.1 ±$0.3x10^5$ for nitrite, PROLI/NO, and NO, respectively. As shown in Figure 3.5 B the PROLI/NO, NO, and nitrite peaks height changed over time due to PROLI/NO hydrolysis. Injection of 100 µM nitrite standard confirmed the peak assignment for nitrite (Figure 3.6). First peak in the electropherogram of PROLI/NO acid hydrolysis matches with nitrite standard. We have determined that at pH 11 hydrogen peroxide has a residual negative charge and consequently migrates faster than the EOF (Figure 3.6). We can conclude

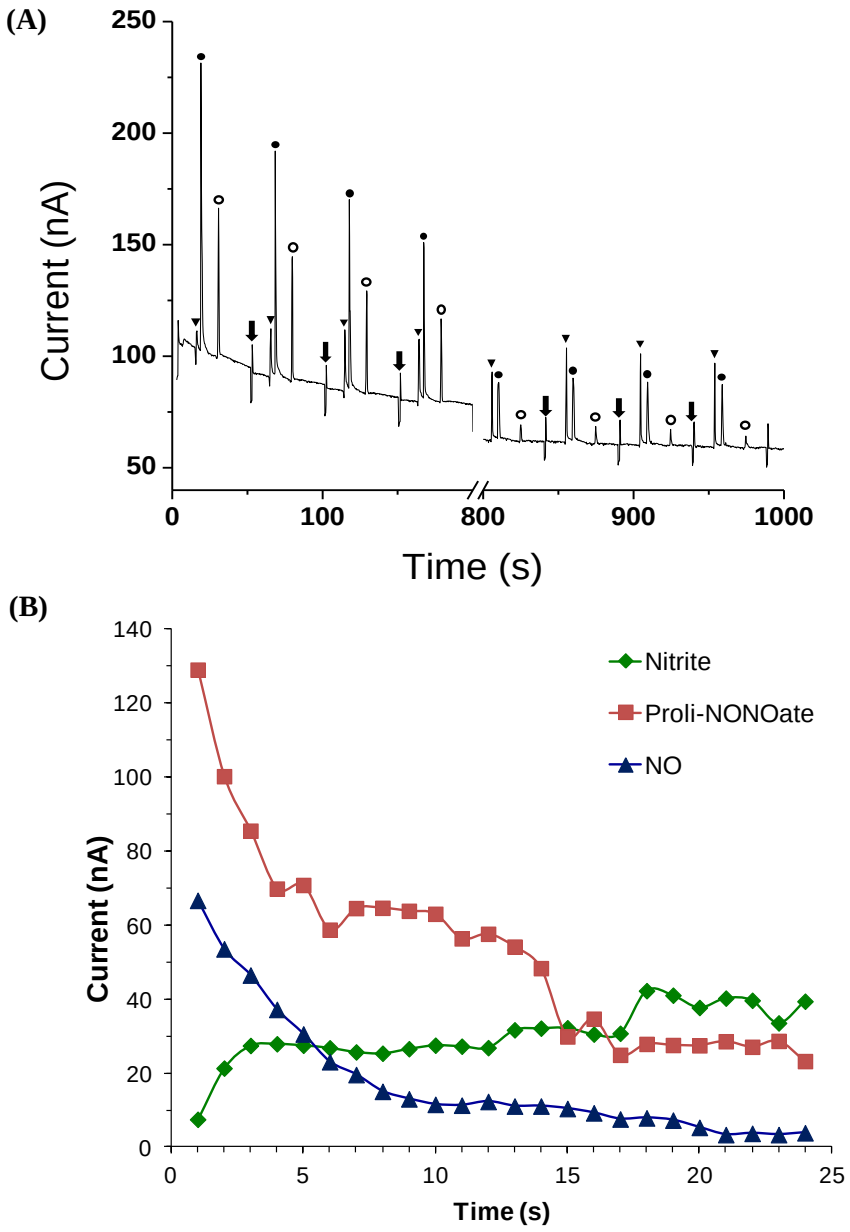

Figure 3.5: (A) Monitoring the acid hydrolysis of PROLI/NO at pH 7.2–7.4. Triangle – nitrite; solid circle – PROLI/NO; open circle – NO. The arrows indicate sample injections. Other conditions as in (B) Peak heights in the part A as function of sequential injections. The *x*-axis can be converted to time by using the total separation time.

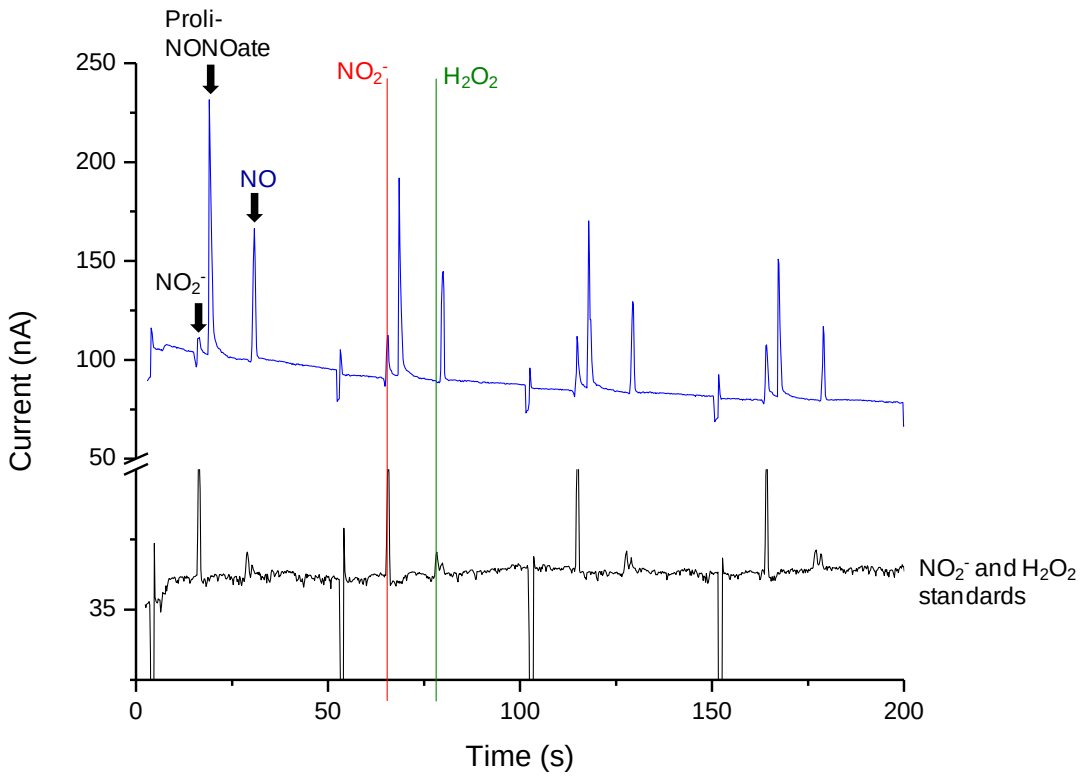

Figure 3.6: Comparison of the nitrite and NO migration times with a 100 µM nitrite and hydrogen peroxide standard solution

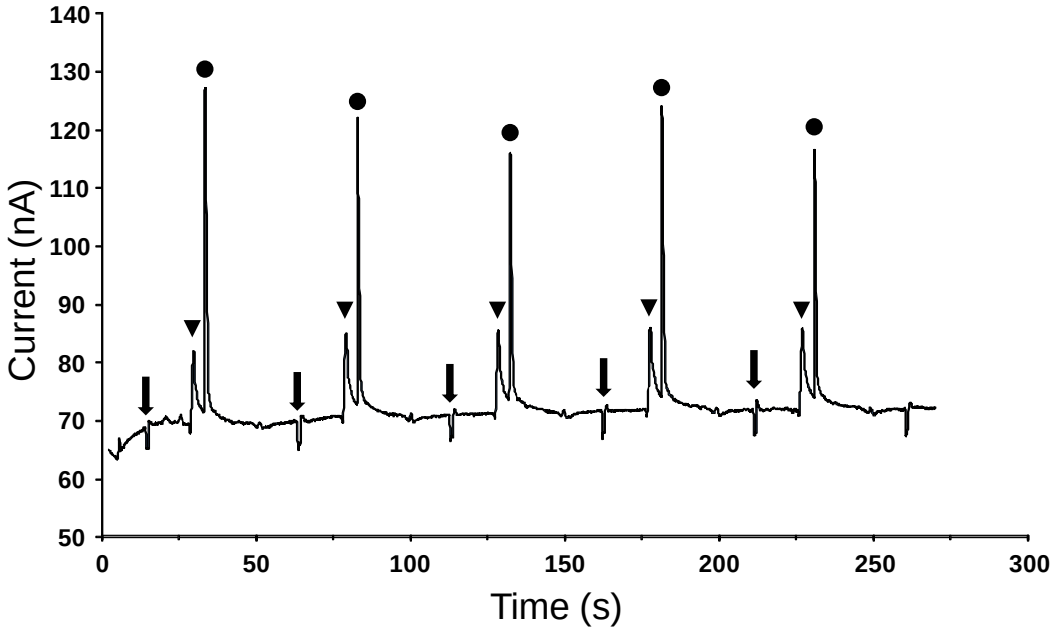

Figure 3.7: Monitoring the acid hydrolysis of PROLI/NO at pH 9.0. ▼– nitrite; ●– PROLI/NO. The arrows indicate sample injections. Other conditions as in Figure 3.3.

that the NO peak moving with the EOF will present a migration time slightly higher than that of hydrogen peroxide, which agrees with the present data.

Similar to that for DEA/NO, the pH of PROLI/NO in the final buffer should be around pH 7 to facilitate the hydrolysis reaction. Also in PROLI/NO experiments, it was still found that whenever the pH of the final hydrolysis solution was above 8, only two peaks were observed, those of parent PROLI/NO and nitrite. At pH=9, we observed two stable peaks in the electropherograms for nitrite (13.5 ± 0.7 nA) and PROLI/NO (43.0 ± 9.6 nA), respectively over period of approximately 5 min as shown in Figure 3.7.

This means that the conditions for the reaction can be adjusted on-chip for advanced applications, for example, a confluence of NO donor delivery and reaction.

3.4 Conclusions

In this paper, a method for monitoring NO generation by NONOate salts using microchip electrophoresis with electrochemical detection is presented. The hydrolysis reaction was initiated by NONOate NaOH mixing with an acidic buffer to obtain the desired reaction pH. For DEA/NO and PROLI/NO, we observed that pH around 7 was suitable to promote the hydrolysis, while no degradation occurred above pH 8. The progress of the reaction could be monitored through sequential injections from the sample reservoir followed by electrophoretic separation. Nitrite was present in all the NONOate standards investigated; however, it did not interfere with the separation, as it has a higher negative electrophoretic mobility than the NO donors. NO migrated with the velocity of the EOF. The total separation was performed in less than 40 s with satisfactory resolution and good efficiency.

3.5 References

1. Pacher, P.; Beckman, J. S.; Liaudet, L., Nitric oxide and peroxynitrite in health and disease. *Physiol. Rev.* **2007,** *87* (1), 315-424.

2. Wu, C.-M.; Chen, Y.-H.; Dayananda, K.; Shiue, T.-W.; Hung, C.-H.; Liaw, W.-F.; Chen, P.-Y.; Wang, Y.-M., Sensitivity evaluation of rhodamine B hydrazide towards nitric oxide and its application for macrophage cells imaging. *Anal. Chim. Acta* **2011,** *708* (1–2), 141-148.

3. Olasehinde, E. F.; Takeda, K.; Sakugawa, H., Development of an Analytical Method for Nitric Oxide Radical Determination in Natural Waters. *Anal. Chem.* **2009,** *81* (16), 6843-6850.

4. Kim, W.-S.; Ye, X.; Rubakhin, S. S.; Sweedler, J. V., Measuring Nitric Oxide in Single Neurons by Capillary Electrophoresis with Laser-Induced Fluorescence: Use of Ascorbate Oxidase in Diaminofluorescein Measurements. *Anal. Chem.* **2006,** *78* (6), 1859-1865.

5. Gabe, Y.; Urano, Y.; Kikuchi, K.; Kojima, H.; Nagano, T., Highly Sensitive Fluorescence Probes for Nitric Oxide Based on Boron Dipyrromethene ChromophoreRational Design of Potentially Useful Bioimaging Fluorescence Probe. *J. Am. Chem. Soc.* **2004,** *126* (10), 3357-3367.

6. Kojima, H.; Hirotani, M.; Nakatsubo, N.; Kikuchi, K.; Urano, Y.; Higuchi, T.; Hirata, Y.; Nagano, T., Bioimaging of Nitric Oxide with Fluorescent Indicators Based on the Rhodamine Chromophore. *Anal. Chem.* **2001,** *73* (9), 1967-1973.

7. Kojima, H.; Nakatsubo, N.; Kikuchi, K.; Kawahara, S.; Kirino, Y.; Nagoshi, H.; Hirata, Y.; Nagano, T., Detection and Imaging of Nitric Oxide with Novel Fluorescent Indicators: Diaminofluoresceins. *Anal. Chem.* **1998,** *70* (13), 2446-2453.

8. Nagano, T.; Yoshimura, T., Bioimaging of Nitric Oxide. *Chem. Rev.* **2002,** *102* (4), 1235-1270.

9. Shin, J. H.; Privett, B. J.; Kita, J. M.; Wightman, R. M.; Schoenfisch, M. H., Fluorinated Xerogel-Derived Microelectrodes for Amperometric Nitric Oxide Sensing. *Anal. Chem.* **2008,** *80* (18), 6850-6859.

10. Privett, B. J.; Shin, J. H.; Schoenfisch, M. H., Electrochemical nitric oxide sensors for physiological measurements. *Chem. Soc. Rev.* **2010,** *39* (6), 1925-1935.

11. Hetrick, E. M.; Schoenfisch, M. H., Analytical chemistry of nitric oxide. *Annu. Rev. Anal. Chem.* **2009,** *2*, 409-433.

12. Huang, J.; Sommers, E. M.; Kim-Shapiro, D. B.; King, S. B., Horseradish Peroxidase Catalyzed Nitric Oxide Formation from Hydroxyurea. *J. Am. Chem. Soc.* **2002,** *124* (13), 3473-3480.

13. Vitecek, J.; Petrlova, J.; Petrek, J.; Adam, V.; Potesil, D.; Havel, L.; Mikelova, R.; Trnkova, L.; Kizek, R., Electrochemical study of S–nitrosoglutathione and nitric oxide by carbon fibre NO sensor and cyclic voltammetry – possible way of monitoring of nitric oxide. *Electrochim. Acta* **2006,** *51* (24), 5087-5094.

14. Kikura-Hanajiri, R.; Martin, R. S.; Lunte, S. M., Indirect Measurement of Nitric Oxide Production by Monitoring Nitrate and Nitrite Using Microchip Electrophoresis with Electrochemical Detection. *Anal. Chem.* **2002,** *74* (24), 6370-6377.

15. Kang, S.-M.; Kim, K.-N.; Lee, S.-H.; Ahn, G.; Cha, S.-H.; Kim, A.-D.; Yang, X.-D.; Kang, M.-C.; Jeon, Y.-J., Anti-inflammatory activity of polysaccharide purified from AMG-assistant extract of Ecklonia cava in LPS-stimulated RAW 264.7 macrophages. *Carbohydrate Polymers* **2011,** *85* (1), 80-85.

16. Grau, M.; Hendgen-Cotta, U. B.; Brouzos, P.; Drexhage, C.; Rassaf, T.; Lauer, T.; Dejam, A.; Kelm, M.; Kleinbongard, P., Recent methodological advances in the analysis of nitrite in the human circulation: Nitrite as a biochemical parameter of the l-arginine/NO pathway. *J. Chromatogr. B* **2007,** *851* (1–2), 106-123.

17. Andrade, R.; Viana, C. O.; Guadagnin, S. G.; Reyes, F. G. R.; Rath, S., A flow-injection spectrophotometric method for nitrate and nitrite determination through nitric oxide generation. *Food Chem.* **2003,** *80* (4), 597-602.

18. Mainz, E. R.; Gunasekara, D. B.; Caruso, G.; Jensen, D. T.; Hulvey, M. K.; Fracassi, d. S. J. A.; Metto, E. C.; Culbertson, A. H.; Culbertson, C. T.; Lunte, S. M., Monitoring intracellular nitric oxide production using microchip electrophoresis and laser-induced fluorescence detection. *Anal. Methods* **2012,** *4* (2), 414-420.

19. Lunte, S. M.; Gunakesera, D. B.; Metto, E. C.; Hulvey, M. K.; Mainz, E. R.; Caruso, G.; da Silva, J. A. F.; Jensen, D. T.; Culbertson, A. H.; Grigsby, R. J.; Culbertson, C. T., Microchip electrophoresis devices for the detection of nitric oxide: comparison of bulk cell and single cell analysis, In *microTAS*, proceedings of the 15th International Conference on Miniaturized Systems for Chemistry and Life Sciences October 2-6, 2011, Seattle, Washington, **2011**, 1728-1730.

20. Arora, A.; Simone, G.; Salieb-Beugelaar, G. B.; Kim, J. T.; Manz, A., Latest Developments in Micro Total Analysis Systems. *Anal. Chem.* **2010,** *82* (12), 4830-4847.

21. Martin, R. S., Interfacing amperometric detection with microchip capillary electrophoresis. *Methods Mo.l Biol.* **2006,** *339*, 85-112.

22. Kubáň, P.; Hauser, P. C., Fundamentals of electrochemical detection techniques for CE and MCE. *Electrophoresis* **2009,** *30* (19), 3305-3314.

23. Pumera, M.; Merkoçi, A.; Alegret, S., New materials for electrochemical sensing VII. Microfluidic chip platforms. *TrAC, Trends in Anal. Chem.* **2006,** *25* (3), 219-235.

24. Garcia, C. D.; Henry, C. S., *Coupling electrochemical detection with microchip capillary electrophoresis*, CRC Press; LLC, 2007; pp 265-297.

25. Fischer, D. J.; Hulvey, M. K.; Regel, A. R.; Lunte, S. M., Amperometric detection in microchip electrophoresis devices: Effect of electrode material and alignment on analytical performance. *Electrophoresis* **2009,** *30* (19), 3324-3333.

26. Wang, J.; Pumera, M.; Prakash Chatrathi, M.; Rodriguez, A.; Spillman, S.; Martin, R. S.; Lunte, S. M., Thick-Film Electrochemical Detectors for Poly(dimethylsiloxane)-based Microchip Capillary Electrophoresis. *Electroanalysis* **2002,** *14* (18), 1251-1255.

27. Gunasekara, D. B.; Hulvey, M. K.; Lunte, S. M., In-channel amperometric detection for microchip electrophoresis using a wireless isolated potentiostat. *Electrophoresis* **2011,** *32* (8), 832-837.

28. Holcomb, R. E.; Kraly, J. R.; Henry, C. S., Electrode array detector for microchip capillary electrophoresis. *Analyst* **2009,** *134* (3), 486-492.

29. Pumera, M.; Escarpa, A., Nanomaterials as electrochemical detectors in microfluidics and CE: Fundamentals, designs, and applications. *Electrophoresis* **2009,** *30* (19), 3315-3323.

30. Wang, Y.; Yin, M., Sensitive and rapid determination of nitric oxide in human serum using microchip capillary electrophoresis with laser-induced fluorescence detection. *Microchim. Acta* **2009,** *166*, 243-249.

31. Hulvey, M. K.; Frankenfeld, C. N.; Lunte, S. M., Separation and Detection of Peroxynitrite Using Microchip Electrophoresis with Amperometric Detection. *Anal. Chem.* **2010,** *82* (5), 1608-1611.

32. Vazquez, M.; Frankenfeld, C.; Coltro, W. K. T.; Carrilho, E.; Diamond, D.; Lunte, S. M., Dual contactless conductivity and amperometric detection on hybrid PDMS/glass electrophoresis microchips. *Analyst* **2010,** *135* (1), 96-103.

33. Wang, P. G.; Xian, M.; Tang, X.; Wu, X.; Wen, Z.; Cai, T.; Janczuk, A. J., Nitric Oxide Donors: Chemical Activities and Biological Applications. *Chem. Rev.* **2002,** *102* (4), 1091-1134.

34. Hrabie, J. A.; Keefer, L. K., Chemistry of the Nitric Oxide-Releasing Diazeniumdiolate ("Nitrosohydroxylamine") Functional Group and Its Oxygen-Substituted Derivatives. *Chem. Rev.* **2002,** *102* (4), 1135-1154.

35. Carroll, J. S.; Ku, C.-J.; Karunarathne, W.; Spence, D. M., Red Blood Cell Stimulation of Platelet Nitric Oxide Production Indicated by Quantitative Monitoring of the Communication between Cells in the Bloodstream. *Anal. Chem.* **2007,** *79* (14), 5133-5138.

36. Halpin, S. T.; Spence, D. M., Direct Plate-Reader Measurement of Nitric Oxide Released from Hypoxic Erythrocytes Flowing through a Microfluidic Device. *Anal. Chem.* **2010,** *82* (17), 7492-7497.

37. Letourneau, S.; Hernandez, L.; Faris, A. N.; Spence, D. M., Evaluating the effects of estradiol on endothelial nitric oxide stimulated by erythrocyte-derived ATP using a microfluidic approach. *Anal. Bioanal. Chem.* **2010,** *397*, 3369-3375.

38. Genes, L. I.; Tolan, N. V.; Hulvey, M. K.; Martin, R. S.; Spence, D. M., Addressing a vascular endothelium array with blood components using underlying microfluidic channels. *Lab Chip* **2007,** *7*, 1256-1259.

39. Hulvey, M.; Martin, R. S., A microchip-based endothelium mimic utilizing open reservoirs for cell immobilization and integrated carbon ink microelectrodes for detection. *Anal. Bioanal. Chem.* **2009,** *393* (2), 599-605.

40. Spence, D. M.; Torrence, N. J.; Kovarik, M. L.; Martin, R. S., Amperometric determination of nitric oxide derived from pulmonary artery endothelial cells immobilized in a microchip channel. *Analyst* **2004,** *129* (11), 995-1000.

41. Zhang, G.; Du, W.; Liu, B.-F.; Hisamoto, H.; Terabe, S., Characterization of electrokinetic gating valve in microfluidic channels. *Anal. Chim. Acta* **2007,** *584* (1), 129-135.

42. Martin, R. S.; Ratzlaff, K. L.; Huynh, B. H.; Lunte, S. M., In-Channel Electrochemical Detection for Microchip Capillary Electrophoresis Using an Electrically Isolated Potentiostat. *Anal. Chem.* **2002,** *74* (5), 1136-1143.

Chapter 4

Evaluation of microchip electrophoresis with dual-series and dual-parallel electrode configurations for identification of chemically labile species

4.1 Introduction

Amperometric detection is the main electrochemical method used with capillary or microchip electrophoresis. This is because amperometry provides better detection limits than other electrochemical methods (especially voltammetric methods) due to the lack of charging current, and selectivity can be enhanced by carefully choosing the working electrode potential. ME with amperometric detection has been used for the separation and detection of various electrochemically active species including catechols, phenolic acids, reactive nitrogen and oxygen species and their metabolites, inorganic ions and various other organic molecules [1-4]. However, amperometric detection at a single electrode (Figure 4.1 A) does not allow for the exploitation of all features of electrochemical detection. Some of these features include investigating the reversibility of the redox process and identification of analytes using voltammetry. A common way to exploit these features is to employ two working electrodes [5-14].

There are two main dual electrode configurations in liquid chromatography (LC), CE and ME. These are the dual-series and dual-parallel electrode configurations, as shown in Figure 4.1 B and C for ME. Both of these configurations have been widely employed in LC with electrochemical detection for the identification of analytes [15-17]. Dual-series electrodes are mainly employed in the generation-collection mode and analytes identified based on chemically reversible redox processes [5,7,9,12,13]. In the generation-collection mode, the first electrode is utilized for generation of a product, which is commonly an oxidized species. Then the product is reduced back to the oxidizable species and detected at the second electrode. Catecholamine detection is the most common use of the generator-collector mode [5,9,13]. Catechols oxidize in the first electrode and generate o-quinones. These quinones can then be reduced back to the catechols at the second electrode.

The series configuration can be used for chemically reversible redox processes even if they are not electrochemically reversible. Also, chemically reversible redox species can be identified using dual-series configuration. In this case, the first electrode is held at a potential which oxidizes the analytes of

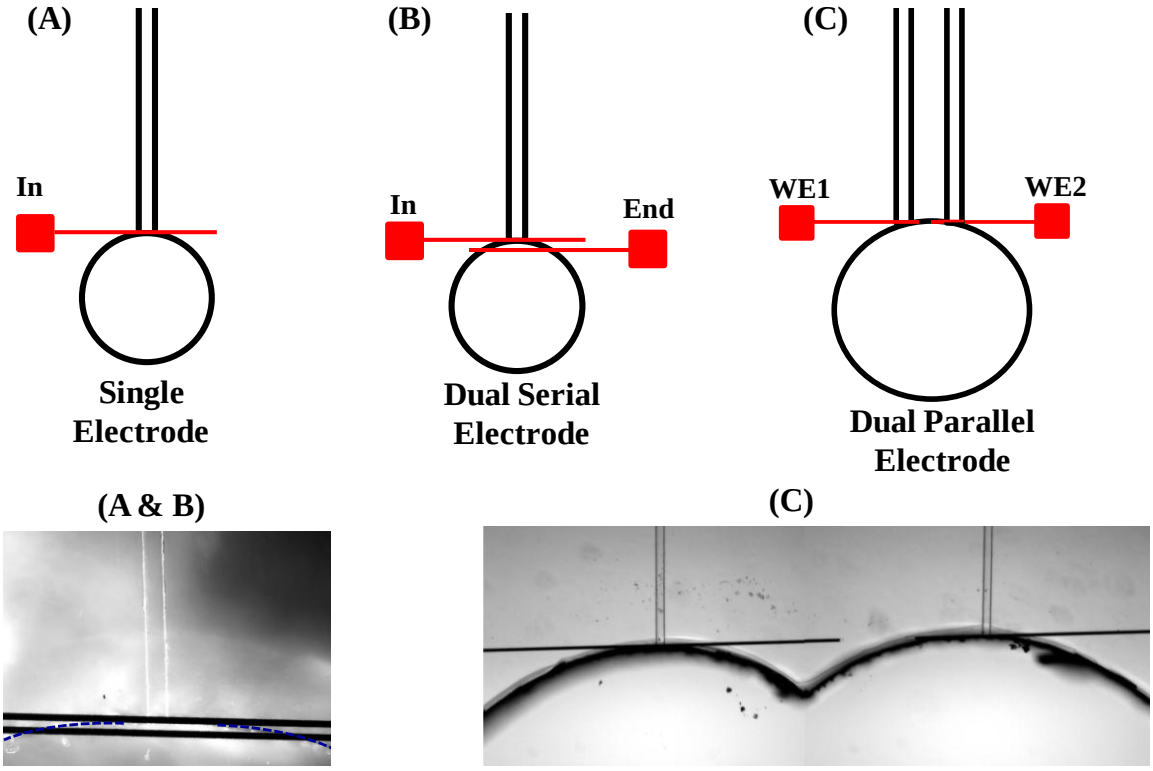

Figure 4.1: (A) Single (B) Dual-series and (C) Dual-parallel electrode configuration and pictures of these electrode alignments

interest and the second electrode is held at a low or negative potential where the oxidized species is reduced. Only chemically reversible species produce a current in the second electrode. Collection efficiency, the percentage of species reduced at the second electrode compared to the amount of species oxidized at the first electrode can also be used for identification of analyte. This is due to the fact that the collection efficiency is different for species and dependent on the mass transport and the redox reversibility. The dual-series configuration has been extensively used for the identification of phenolic acids and catechols in both ME and CE [5,9,12,13]. A ring-disk electrode is another way to integrate electrodes in the series configuration [6,11]. In this case, the disk is the generator and the ring serves as the collector.

Electrogeneration of bromine by oxidizing bromide present in the run buffer at the first electrode has also been reported as an indirect detection method for thiols [18]. In this method bromine is electrogenerated in the run buffer at a high positive potential (+1 V) at the first electrode. The second electrode is held at a low potential (0 V) where only bromine reduces, producing a baseline current. When an analyte plug reaches the second electrode there will be a reduction in the baseline current due to the loss of bromine in the analyte plug and it produces a vacancy response [18].

The dual-parallel electrode configuration (or parallel opposed) is used for obtaining a higher response by redox cycling or identification of analytes by generating a current ratio at different working electrode potentials. To obtain redox cycling, two cylindrical electrodes have been used in CE in a parallel configuration [11,14]. To perform redox cycling, one electrode is held at a negative potential and the second electrode is at a positive potential. When a reversible redox species is oxidized at the anode it will diffuse to the cathode and be reduced. These reduced species diffuse back again to the anode and are reoxidized, beginning the cycling process again [14]. In addition to redox cycling, an integration of Hg/Au and carbon fiber disk parallel electrodes for multi-analyte detection was also reported [6].

Voltammetry is key for the identification of species in electrochemistry. Voltammetry is accomplished by scanning the potential as a function of time over a potential window in order to obtain a

voltammogram. This voltammogram is characteristic for each analyte and can be used for identification of compounds in classical electrochemistry. However, there are challenges when a scanning technique is integrated with CE or ME. Some challenges include high background noise that results from the voltage scanning due to capacitance (charging current), low temporal resolution of slow scanning techniques, high LODs, and reduced sensitivity [19-21]. However, some voltammetric techniques have been reported as detectors for CE [19,21-25]. An alternative approach to classical voltammetry is to obtain voltammetric data using two electrodes held at different electrode potentials. The dual-parallel configuration has been used in CE for obtaining current ratios that can be used for voltammetric identification [6,14]. For analytes with different hydrodynamic voltammograms, this current ratio will be different (Figure 4.2).

Current ratios can be generated by either the dual-series and dual-parallel configuration. The dual-series configuration can be easily integrated into a simple-T device [5]. However, in this case analyte depletion at the first electrode and the position of the electrodes relative to each other need to taken into consideration. Alternatively, the dual-parallel configuration has been used for voltammetric identification of analytes in CE [14]. This configuration uses two cylindrical electrodes in a glass sheath. The analyte plug passes over both electrodes simultaneously. In the parallel configuration, analyte depletion or difference in position of two electrodes does not influence the results [14].

Thus far the dual-series configuration has been predominantly employed for identification of reversible species and in the generation-collection mode with ME because it is easy to implement. However, the parallel electrode configuration has not been widely used for ME. In this study we compare dual-series and dual-parallel electrode configurations for generation of current ratios in microchip electrophoresis for identification of chemically labile species. Correction factors that are necessary to obtain a more realistic current ratio in the dual-series configuration is also discussed. For the dual-parallel configuration a dual-channel microchip was used that made it possible to perform injection of the same sample and sample volume into two separation channels each with an electrode. Both configurations were then employed for the analysis of commercially available $ONOO^-$ standards.

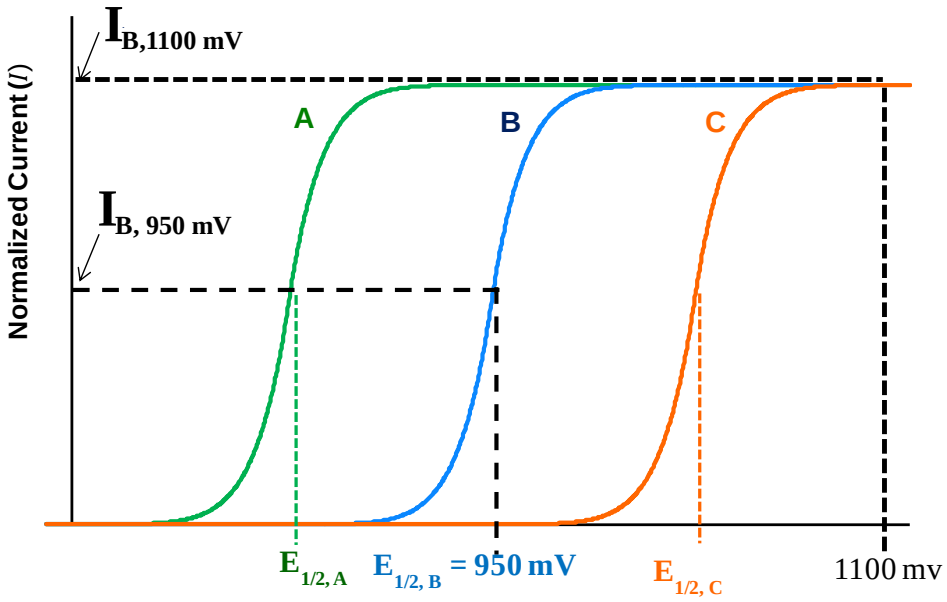

Figure 4.2: The basis of generation of current ratios by hydrodynamic voltammetry

Table 4.1: Current ratios for species A, B and C generated using +950 mV and +1100 mV

Species	I_{950}/I_{1100}
A	**1.0**
B	**0.5**
C	**0.0**

4.2 Materials and methods

4.2.1 Materials and reagents

The following chemicals and materials were used as received: SU-8 10 photoresist and SU-8 developer (MicroChem Corp., Newton, MA, USA); AZ 1518 photoresist and 300 MIF developer (Mays Chemical Co., Indianapolis, IN, USA); photolithography film masks (50,000 dpi; Infinite Graphics Inc., Minneapolis, MN, USA); N(100) 100 mm (4") silicon (Si) wafers (Silicon, Inc., Boise, ID, USA); chrome and AZ1518 positive photoresist coated soda lime glass substrates (4" × 4" × 0.090", Nanofilm, Westlake, CA, USA); Sylgard 184 Silicone Elastomer Kit: Polydimethylsiloxane (Ellsworth Adhesives, Germantown, WI, USA); Titanium (Ti) etchant (TFTN; Transene Co., Danvers, MA, USA); epoxy and 22 gauge Cu wire (Westlake Hardware, Lawrence, KS, USA); silver colloidal paste (Ted Pella, Inc., Redding, CA, USA); acetone, 2-propanol (isopropyl alcohol, IPA), 30% H_2O_2, H_2SO_4, HNO_3, NaOH and HCl (Fisher Scientific, Fair Lawn, NJ, USA); sodium nitrite, boric acid, tetradecyltrimethylammonium bromide (TTAB), tetradecyltrimethylammonium chloride (TTAC), tyrosine (Tyr), sodium azide, potassium iodide, NaCl, (Sigma, St. Louis, MO, USA); buffered oxide etchant (JT Baker, Austin, TX, USA) and $ONOO^-$ (Cayman Chemicals, Ann Arbor, MI, USA or EMD Millipore, Billerica, MA, USA). All water used was ultrapure (18.3 MΩ·cm, Milli-Q Synthesis A10, Millipore, Burlington, MA, USA).

4.2.2 PDMS fabrication

The fabrication of PDMS-based microfluidic devices has been described previously [26]. Microfluidic channel designs were created using AutoCad LT 2004 (Autodesk, Inc., San Rafael, CA, USA) and printed onto a transparency film at a resolution of 50,000 dpi (Infinite Graphics Inc., Minneapolis, MN, USA). A simple-T device containing a 5 cm separation channel (from the T intersection to the end of the separation channel) and 0.75 cm side arms was used for dual-series configuration. For dual-parallel electrode configuration dual channel microchip design in Figure 4.3 was used. The two separation channels were 5 cm long and sampling and buffer side arm length were as

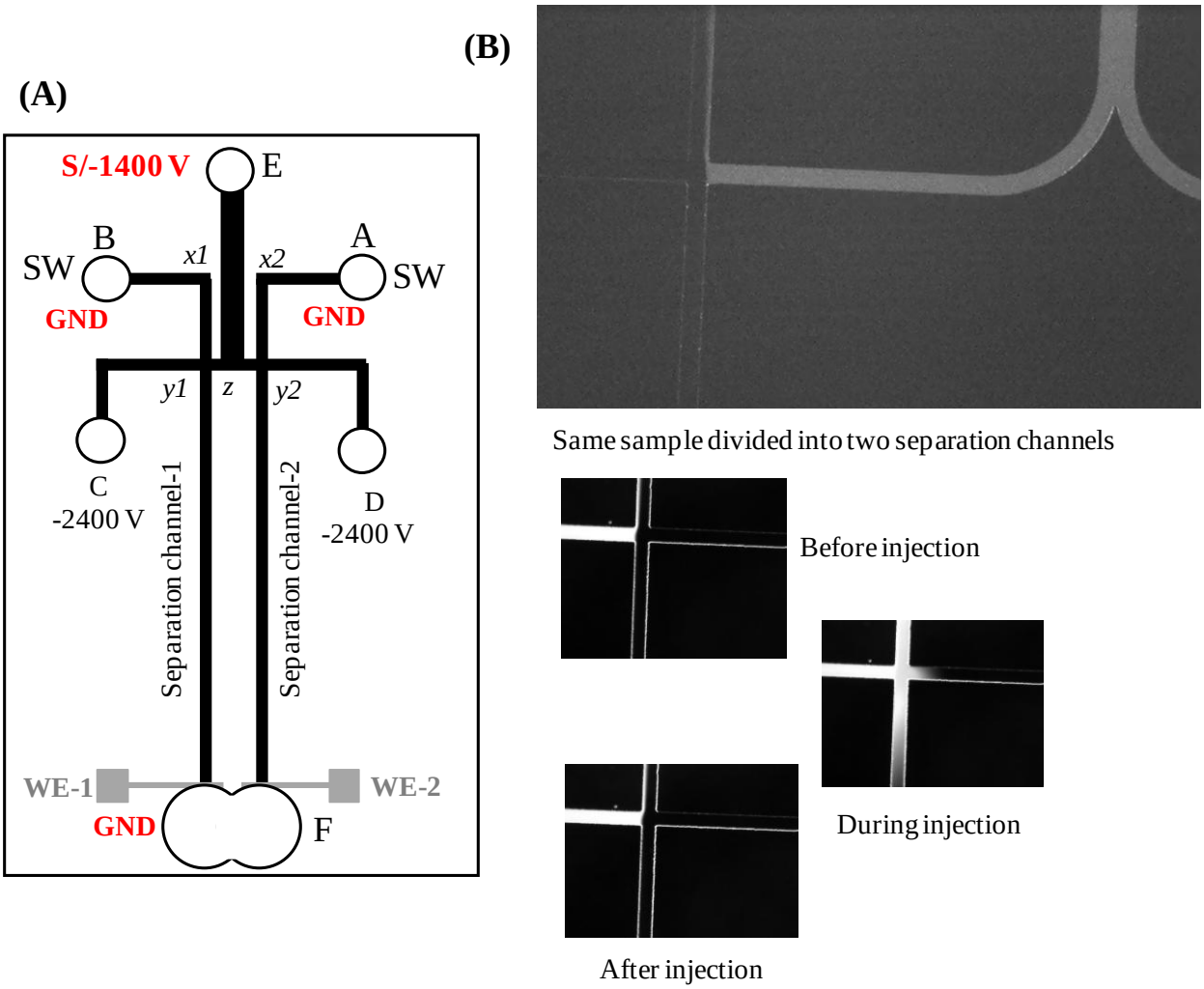

Figure 4.3: (A) Dual channel microchip design used for dual-parallel electrode configuration (Adapted from ref. 29) (B) An injection of a same sample into the two separation channels using normal polarity

follows: Ax2, Bx1, x1y1 and x2y2 are all equal to 0.75 cm; Cy1, Dy2 and EZ equal to 1.5 cm and y1z and y2z are equal to 0.25 cm. For both configurations, the width and depth of the electrophoresis microchannels were 40 μm and 14 μm, respectively. All PDMS microstructures were made by casting a 10:1 mixture of PDMS elastomer and curing agent respectively, against the patterned Si master and cured at 70 ºC overnight. Holes for the reservoirs were created in the polymer using a 4 mm biopsy punch (Harris Uni-core, Ted Pella Inc., Redding, CA, USA).

4.2.3 Platinum electrode fabrication

All electrochemical measurements were obtained using 15 μm Pt working electrodes. Electrodes were fabricated using an in-house magnetron sputtering system (AXXIS DC magnetron sputtering system, Kurt J. Lesker Co., Jefferson Hills, PA, USA). The electrode fabrication protocol was reported earlier by our group [27]. For the dual-serial electrode configuration, two 15 μm electrodes placed 15 μm apart them were used. For the dual-parallel configuration, 15 μm electrodes with a 100 μm spacing between the two electrodes was used (Figure 4.3 A). These designs were created using AutoCad LT 2004 (Autodesk, San Rafael, CA, USA) and printed onto a transparency film at a resolution of 50,000 dpi (Infinite Graphics, Minneapolis MN, USA). The width and height of the resulting Pt electrodes were measured using an Alpha-step 200 profilometer after the electrode preparation (Alpha Step-200, Tencor Instruments, Mountain View, CA, USA).

4.2.4 Solution preparation

All solutions were made using 18 MΩ ultrapure water from a Millipore A10 system. Stock solutions of nitrite (NO_2^-, 10 mM), hydrogen peroxide (H_2O_2, 10 mM), KI (5 mM), and NaN_3 (5 mM) were all prepared in ultrapure water and stored at 4°C. To dissolve tyrosine (Tyr, 10 mM), the solution was acidified using 1–1.5 M HCl. Subsequent dilutions of each stock solution were made into the run buffer at the time of analysis. For separation buffer, a boric acid (50 mM) stock solution was prepared and diluted five-fold to obtain 10 mM boric acid solution. The buffer pH was then adjusted to 11 using 10

mM or 1 M NaOH solution. The required amount of TTAB was added from a 200 mM TTAB stock solution to obtain a final concentration of TTAB of 2 mM.

Peroxynitrite standards were purchased from two commercial sources (Cayman and CalBioChem) and were stored in a -80 ºC freezer. For $ONOO^-$ standard analysis, the standards were diluted twice to obtain a final concentration of 100-200 µM. First, 100 or 200 µL of $ONOO^-$ standards were diluted in 800 or 900 µL of 0.03 M NaOH and then 10 or 20 µL of diluted $ONOO^-$ solution was further diluted in 990 or 980 µL of run buffer. Finally, 20 µL from this solution was placed in the microchip. The $ONOO^-$ sample preparation was achieved less than 1 min.

4.2.5 Chip construction and electrophoresis procedure

PDMS microchips were used for all studies. Amperometric signals were recorded using 15 µm Pt working electrode with a Ag/AgCl reference electrode that was placed in the buffer waste reservoir after the separation ground lead when 5 cm simple T microchips were used (Figure 4.4). However, the reference electrode was kept before the separation ground lead in the dual-channel design. This was done because there was a difference in migration times and band broadening between channels when the ground electrode was placed before the reference. This was probably due to the shape of the PDMS cut in the waste reservoir (Figure 4.1 C). For both configurations, a microchip containing the separation channel was aligned and reversibly sealed to the glass plate containing the Pt electrode. For in-channel detection, the electrode was placed exactly at the end of the separation channel as shown in Figure 4.1 B.

Electrophoretic separations were carried out using reverse polarity with TTAB as the cationic surfactant to modify the channel walls. For simple-T microchips, two negative high voltage Pt leads (Pt wire) were placed in the sample and buffer reservoirs, while two earth ground Pt leads were placed in the sample waste and buffer waste reservoirs. To establish a gate between the sample and run buffer, -2200 V was applied to the sample reservoir and -2400 V was applied to the buffer reservoir. For dual-channel microchips the sample was placed in the reservoir E (Figure 4.3) and -1400 V was applied. The sample traveled to both the A and B reservoirs by keeping both A and B reservoirs at ground. Additionally, -2400

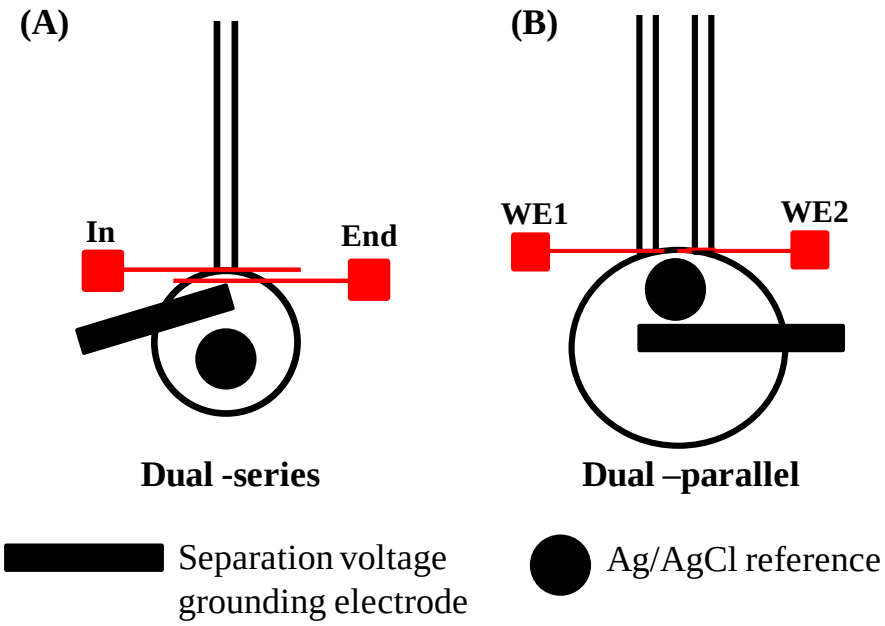

Figure 4.4: The separation ground and Ag/AgCl reference electrode placement in (A) Dual-series and (B) Dual-parallel configuration

V was applied to the C and D reservoirs while keeping the F reservoir at ground. A gated injection was used for injection of the sample in both cases, with an injection time of 1 s.

4.2.6 Electrochemical detection

EC detection was accomplished using a modified model of an 8151BP, 8100-K6, or 9051 single- or dual-channel wireless, electrically isolated potentiostats (Pinnacle Technology Inc., Lawrence, KS, USA) operating in a two-electrode format (Pt working; Ag/AgCl reference: Bioanalytical Systems, West Lafayette, IN, USA). The model 8151P, 8100-K6, and 9051 potentiostats have a sampling rate of 5 Hz (Gain = 5,000,000 V/A, Resolution = 30 fA), 10 Hz (Gain = 5,000,000 V/A, Resolution = 27 fA), and 6.5 to 13 Hz (Gain = 5,000,000 V/A, Resolution = 47 fA), respectively. Pinnacle Acquisition Laboratory (PAL or Sirenia) software was used for all data acquisition. The data acquisition is performed via wireless data transmission or Bluetooth from the potentiostat to a computer. A working electrode potential of +1100 mV versus Ag/AgCl reference was used for all experiments.

4.3 Results and discussion

Both dual-series and dual-parallel electrode configurations can be used to obtain current ratios for analyte identification. To obtain current ratios in ME or CE, two electropherograms are recorded at two different working electrode potentials where one of selected potentials is in the current limiting plateau and the second potential is in the vicinity of the half-wave potential of the analytes. The resultant peak currents are then divided in order to generate the current ratio. The basis of this method is shown in Figure 4.2, which shows hypothetical voltammograms obtained for three different analytes using a microelectrode. As shown in Figure 4.2 and Table 4.1 a different current ratio is generated for each species exhibiting a different half-wave potential. The relative ease or difficulty in oxidizing the species is described by this current ratio. A current ratio of zero is obtained at working electrode potentials of +950 mV and +1100 mV for species C in Figure 4.2, indicating that species C is difficult to oxidize. On the other hand, species A in Figure 4.2 generates a current ratio of one under similar conditions and this indicates that species A is very easy to oxidize. Species B describes a case between the maximum and

minimum current ratio. That is, analytes of interest can be categorized on a zero to one scale where zero is a difficult to oxidize species and one is an easy to oxidize species. This voltammetric information can then be combined with migration time for a more complete identification of analytes. Due to the fact that the current ratio is a relative measurement, nitrite was chosen as a difficult to oxidize species in these studies and the two working electrode potentials were selected based on its hydrodynamic voltamogram. Nitrite does not reach its current limiting plateau at +1100 mV; however, +1100 mV is the maximum potential that can applied to our microfabricated Pt electrode without damaging to the electrode (due to water oxidation at potentials higher than +1100 mV). Therefore, +1100 mV and +950 mV were chosen for determining the current ratio.

4.3.1 Comparison of dual-series and dual-parallel electrode configurations with ME

The current ratio of a compound can be obtained using a single electrode; however, the same sample must be analyzed twice while changing working electrode potential between each injection. For chemically labile species such as $ONOO^-$ this approach can lead to large experimental errors due to degradation of the analyte between runs. A dual electrode set up automates the sample characterization by voltammetry making it possible to obtain both electropherograms in a single run (Figure 4.1 B and C). Therefore, dual-series and dual-parallel electrode configurations were investigated for identification of contaminants in $ONOO^-$ standards.

4.3.1.1 Dual-series configuration

For the dual-series electrode configuration, a 5 cm single channel simple-T microchip was used with two 15 μm Pt electrodes. These two electrodes were fabricated with a spacing of 15 μm between them. There are two main draw backs when the dual-series configuration is employed for obtaining the current ratios. Oxidation of analytes at the first electrode causes depletion of analyte molecules in the diffusive layer of the analyte plug. Therefore, the number of analyte molecules in the diffusive layer reaching the second electrode is less than the original amount injected into the chip. This problem can be

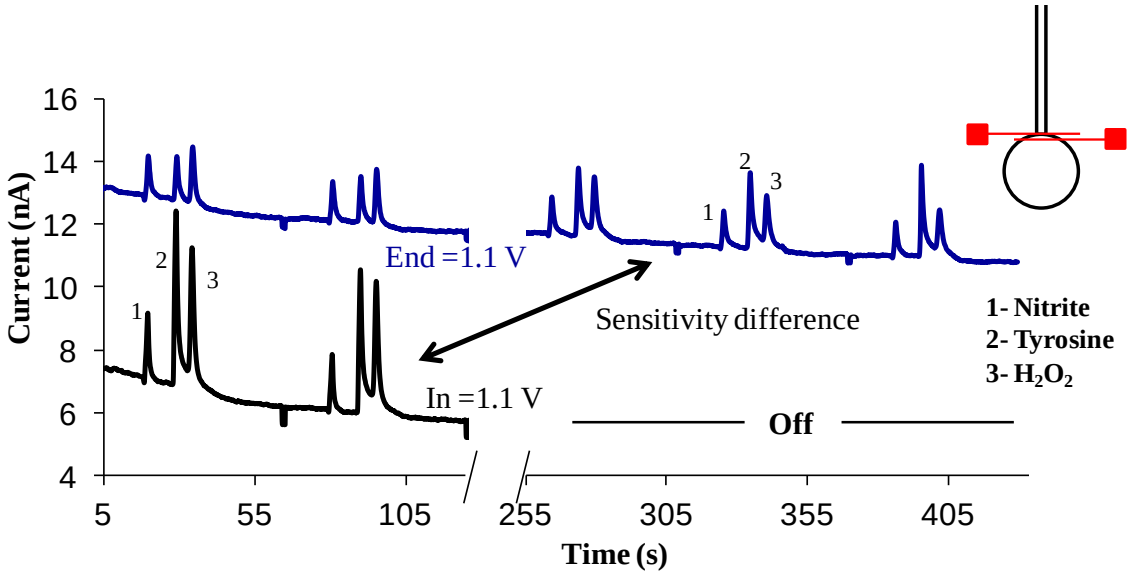

Figure 4.5: An example for characterization of dual-series configuration using nitrite, tyrosine and H_2O_2 standards. The sample was prepared in 10 mM boric and 2 mM TTAB buffer at pH 11 and the separation was also achieved using the same buffer. +1100 mV versus Ag/AgCl reference electrode was used for both end and in-channel electrodes.

Table 4.2: Oxidation, sensitivity and corrected current ratios by dual-series configuration for nitrite, tyrosine and H_2O_2. The standard deviation was calculated using the same sample and three consecutive injections in the same microchip (n = 3)

Species	I_{950}/I_{1100}	Oxidation ratio[a] I_{950}/I_{1100}	Sensitivity ratio[b] I_{950}/I_{1100}	Corrected[c] I_{950}/I_{1100}
Nitrite	0.25 ± 0.02	-0.16 ± 0.03	1.65 ± 0.17	0.15 ± 0.01
Tyr	2.27 ± 0.04	1.33 ± 0.12	2.03 ± 0.57	1.12 ± 0.02
H_2O_2	2.29 ± 0.04	-0.04 ± 0.26	2.57 ± 0.16	0.89 ± 0.01

[a]The oxidation ratio is the difference between sensitivity ratio (at both electrodes 1100 mV) and the current ratio when both in- and end-channel electrodes were switched on (at both electrodes 1100 mV)

[b]The sensitivity ratio is the peak height ratio between the section of the end-channel electropherogram after the in-channel electrode disconnected from the potentiostat and in-channel electrode

[c]Corrected for sensitivity differences between electrodes

Standard deviation was calculated for three consecutive injections in a same microchip (n = 3)

avoided by increasing the distance between two electrodes so that the reduced molecules can diffuse away from the diffusion layer, however this approach can lead to band broadening and low resolution. The second drawback is that there is a sensitivity difference between two electrodes due to the difference of positions of two electrodes relative to channel-end. In these experiments the first electrode of dual-series configuration is placed with an in-channel configuration (at exact end of the channel) leaving second electrode in the end-channel configuration. Sensitivity differences between in- and end-channel configurations has been reported previously and it has been observed that there is a two fold increase in sensitivity with the in-channel configuration compared to end-channel configuration [28]. Therefore, the current ratios must be corrected, taking into account the oxidation difference and the sensitivity difference between the two electrodes. To perform this correction, standards were analyzed with both electrodes set to +1100 mV versus the Ag/AgCl reference. After three injections, the in-channel electrode was switched-off. Three more injections were then recorded for the end-channel electrode (Figure 4.5). There was no significant difference observed in the nitrite peak height at the end-channel electrode when the potentiostat connected to the in-channel electrode was switched-on versus in-channel electrode switched-off (Figure 4.5 and oxidation ratio in Table 4.2). However, there was a difference in peak heights for tyrosine and hydrogen peroxide under these same conditions (Figure 4.5 and oxidation ratio in Table 4.2).

The sensitivity difference between in- and end-channel electrodes was the most important parameter to be considered between the two correction factors (sensitivity ratio in Table 4.2). It was found that the error due to oxidation at the first electrode was much lower than the sensitivity difference in this case (except tyrosine) and therefore, only the sensitivity difference was corrected in subsequent experiments. The current ratios obtained before and after correction are also shown in the Table 4.2. The current ratio of tyrosine decreased from 2.27 to 1.12 with the correction. Tyrosine exhibits a current ratio slightly higher than 1 due to the oxidation at the first electrode. If tyrosine current ratios are corrected for the oxidation at first electrode the final current ratio of tyrosine is 0.85. Nitrite current ratio slightly decreased and corrected current ratio matched with the HDV of nitrite. The current ratio value for the

hydrogen peroxide was 0.89. However, hydrogen peroxide current ratio higher than 1 can be expected (it has been observed in other experiments) because the hydrogen peroxide oxidation current decreases at working electrode potentials after +950 mV under these conditions.

4.3.1.2 Dual-parallel configuration

For the dual-parallel configuration, a microchip with two separation channels was utilized. This was based on a design that was first reported by Hahn's group as a noise subtraction method in ME-EC (Figure 4.3) [29,30]. In these reports, two dual-parallel electrodes were placed inside two channels and one electrode was used as the working electrode while second electrode was used as the reference electrode. The separation buffer was always injected into both channels (from reservoir C and D in Figure 4.3); however, the sample was only injected into the channel containing the working electrode (Figure 4.3). Run buffer was injected into the channel containing the reference electrode in place of sample. In this configuration, two separate reservoirs (Figure 4.3 reservoir A and B) were utilized for the injection of sample and run buffer. In our studies, the sample (from reservoir E in Figure 4.3) was divided and injected into two separation channels using conditions mentioned previously (Figure 4.3). Electrophoresis voltages were optimized to obtain a proper gating using normal polarity and fluorescein, and an injection of a similar portion of sample into the two separation channels (The run buffer is 10 mM boric with 2 mM SDS at pH 11, and sampling and separation voltages were +1400 V and +2400 V respectively) was observed. The optimized gating and injection voltages are shown in Figure 4.3 B. Then negative polarity conditions were applied as shown in the Figure 4.3 A (The run buffer is 10 mM boric with 2 mM TTAB at pH 11, and sampling and separation voltages were -1400 V and -2400 V respectively)

In the dual-parallel configuration, both electrodes were placed in an in-channel configuration (Figure 4.3 A). As can be seen in Figure 4.6A and Table 4.3 a similar response is obtained for each analyte when the two electrodes are held at the potential of +1100 mV. Figure 4.6 B shows the difference

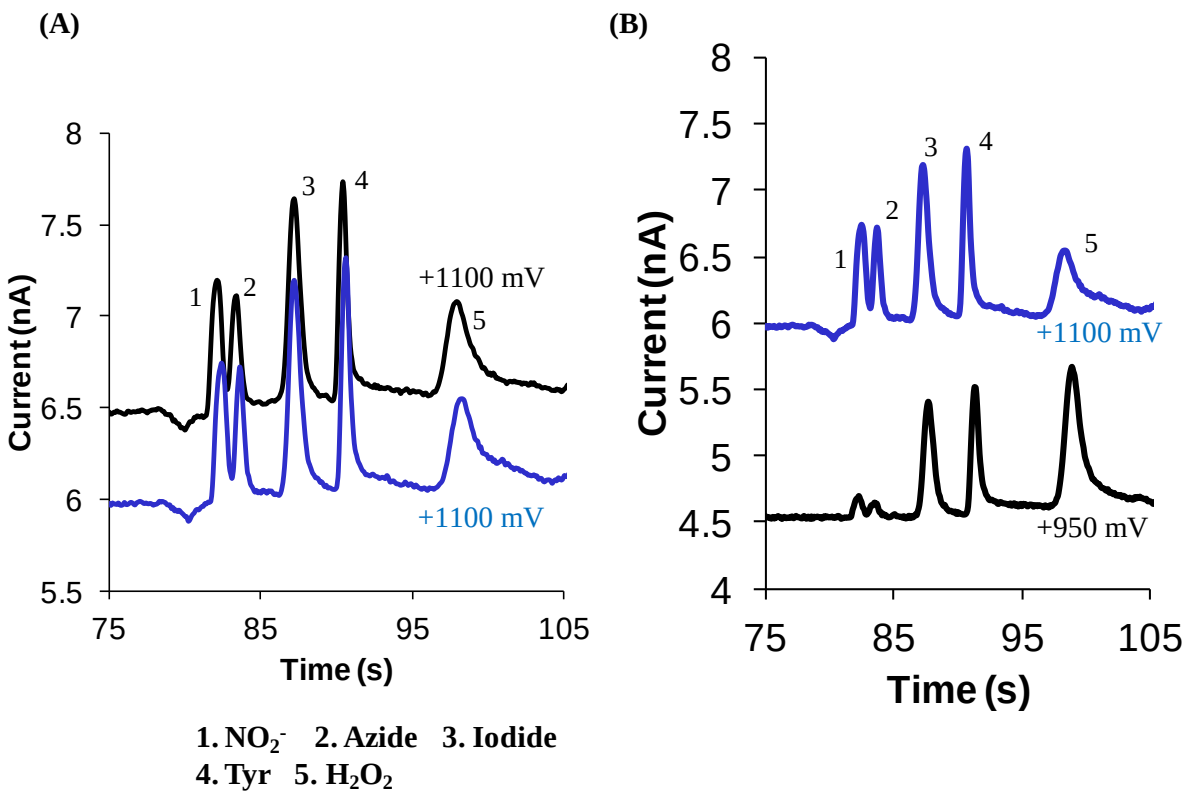

Figure 4.6: An example for characterization of dual-parallel configuration using nitrite, tyrosine and H_2O_2 standards. The sample was prepared in 10 mM boric and 2 mM TTAB buffer at pH 11 and the separation was also achieved using the same buffer. (A) WE-1 = WE-2 = +1100 mV (B) WE-1 = +1100 and WE -2 = +950 mV versus Ag/AgCl reference electrode were used.

in analyte responses when one of electrodes is lowered to +950 mV. The current ratios for each analyte were then calculated without performing any corrections and are shown in Table 4.3. A comparison of corrected current ratios obtained for dual-series with the dual-parallel configuration was made and there was a slight variation of these ratios between the two configurations. This is mostly likely due to the interaction of the separation voltage on in-channel electrodes in both configurations. Also, a response difference between the two electrodes was observed from time to time even with the dual-parallel electrode configuration due to microfabrication variables. When this occurred, the response difference could be corrected. The surface area of two channels was assumed to be same. However, if the surface of one channel was modified due to adsorption, it could lead to change in peak current and affect the current ratio. Therefore, both dual-serial and dual-parallel configurations were characterized using standards on each chip.

4.3.2 Identification of hydrogen peroxide contamination in peroxynitrite standards

Peroxynitrite is a reactive nitrogen species produced by the reaction between NO and superoxide. The half-life of $ONOO^-$ at physiological pH is less than 1 s [31]. However, it has been shown that $ONOO^-$ can be stabilized in its anionic form under high pH conditions [26,32,33]. Therefore, ME and CE have been used for detection of $ONOO^-$ standards using high pH run buffers [26,32]. Previously, current ratios have been used for identification of $ONOO^-$ peaks, but these current ratios were obtained using a ME-EC set up with a single electrode [26]. Sample degradation can have a huge influence on voltammetric identification by ME-EC using a single electrode, thus the dual-serial and dual-parallel configurations were evaluated for the analysis of commercially available $ONOO^-$ samples in this work.

The standard reduction potential for $ONOO^-$ has been studied previously by Amatore's group and they obtained $E_{1/2}$ of 0.43 V versus NHE (0.23 V versus Ag/AgCl electrode) using a platinum disk microelectrode at pH 10.5 [33]. That is, $ONOO^-$ should be easily oxidized at our platinum microband electrodes. In contrast, Hulvey *el. al* observed current ratios of 0.46 and 0.14 at +900 mV and +1100 mV

Table 4.3: Current ratios generated by dual-parallel configuration for nitrite, azide, iodide, tyrosine and H_2O_2. The standard deviation was calculated using the same sample and three consecutive injections in the same microchip (n = 3)

Species	I_{1100}/I_{1100}	I_{950}/I_{1100}
Nitrite	1.04 ± 0.06	0.21 ± 0.03
Azide	0.87 ± 0.05	0.17 ± 0.01
Iodide	0.98 ± 0.03	0.74 ± 0.03
Tyrosine	0.92 ± 0.04	0.76 ± 0.02
H_2O_2	1.04 ± 0.06	1.98 ± 0.06

Standard deviation was calculated for three consecutive injections in a same microchip (n = 3)

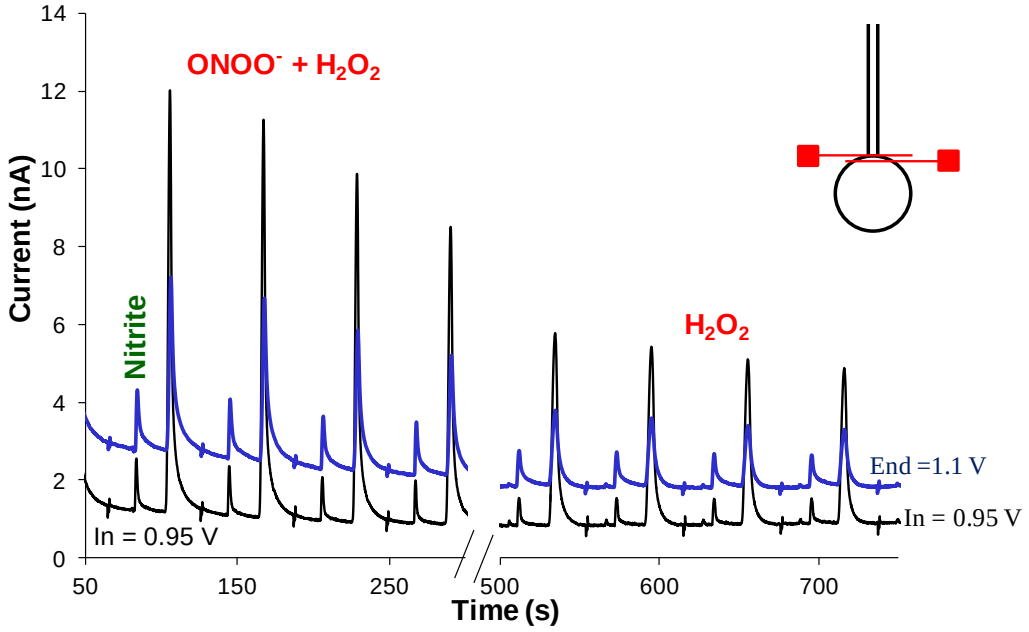

Figure 4.7: The degradation of contaminated $ONOO^-$ standards over several injections using the dual-series configuration. The sample was prepared in 10 mM boric and 2 mM TTAB buffer at pH 11 and the separation was also achieved using the same buffer. +1100 mV and +950 mV versus Ag/AgCl reference electrode was used for end and in-channel electrodes respectively.

for $ONOO^-$ and nitrite standards, respectively, using a ME-EC set up with a single 10 µm platinum band electrode and pH 11 [26]. These results indicated that $ONOO^-$ is not easily oxidized under our ME-EC conditions. Amatore's group also observed a $E_{1/2}$ of 0.7 V versus saturated sodium calomel electrode for nitrite [33]. However, an $E_{1/2}$ for nitrite of around +1.05 V versus Ag/AgCl was observed under our conditions. That is, there is a positive shift in potential in our system. This is likely due to larger oxide layer on platinum electrodes at the high pH (11) was used for these studies. Also, the microfabricated electrodes were difficult to clean by polishing and an oxide layer is produced on electrode surface can change the electrode response. Therefore, +0.95 V and +1.1 V were employed for identification of $ONOO^-$ samples. At the same time, there is a current decrease for H_2O_2 above +0.95 V versus Ag/AgCl in our system and this feature can be used for the identification H_2O_2.

4.3.2.1 Dual-series configuration

Figure 4.7 shows degradation of $ONOO^-$ standards over several injections using the dual-series configuration. Two peaks were observed in this $ONOO^-$ standard. In previous studies these peaks were identified as nitrite and $ONOO^-$ by their migration time, kinetics and current ratios [26,28]. The $ONOO^-$ peak decay observed in Figure 4.7 was expected. Unexpectedly, this decay reached a steady state condition, implying a contamination of the $ONOO^-$ standards with a stable analyte.

One of the disadvantages of dual-serial configuration is sensitivity ratio for each analytes needs to known prior to an unknown analysis for correction. The sensitivity ratio of nitrite (harder to oxidize compound) was 2.5 while tyrosine (easy to oxidize compound) showed a sensitivity ratio of 2.7. However, the tyrosine peak can also be affected by oxidation when both electrodes were switched on. In contrast, the H_2O_2 sensitivity difference was not used since H_2O_2 oxidation is affected by the catalytic properties of the Pt surface. Therefore, sensitivity ratio of nitrite was used for obtaining a more realistic $ONOO^-$ current ratio in this case.

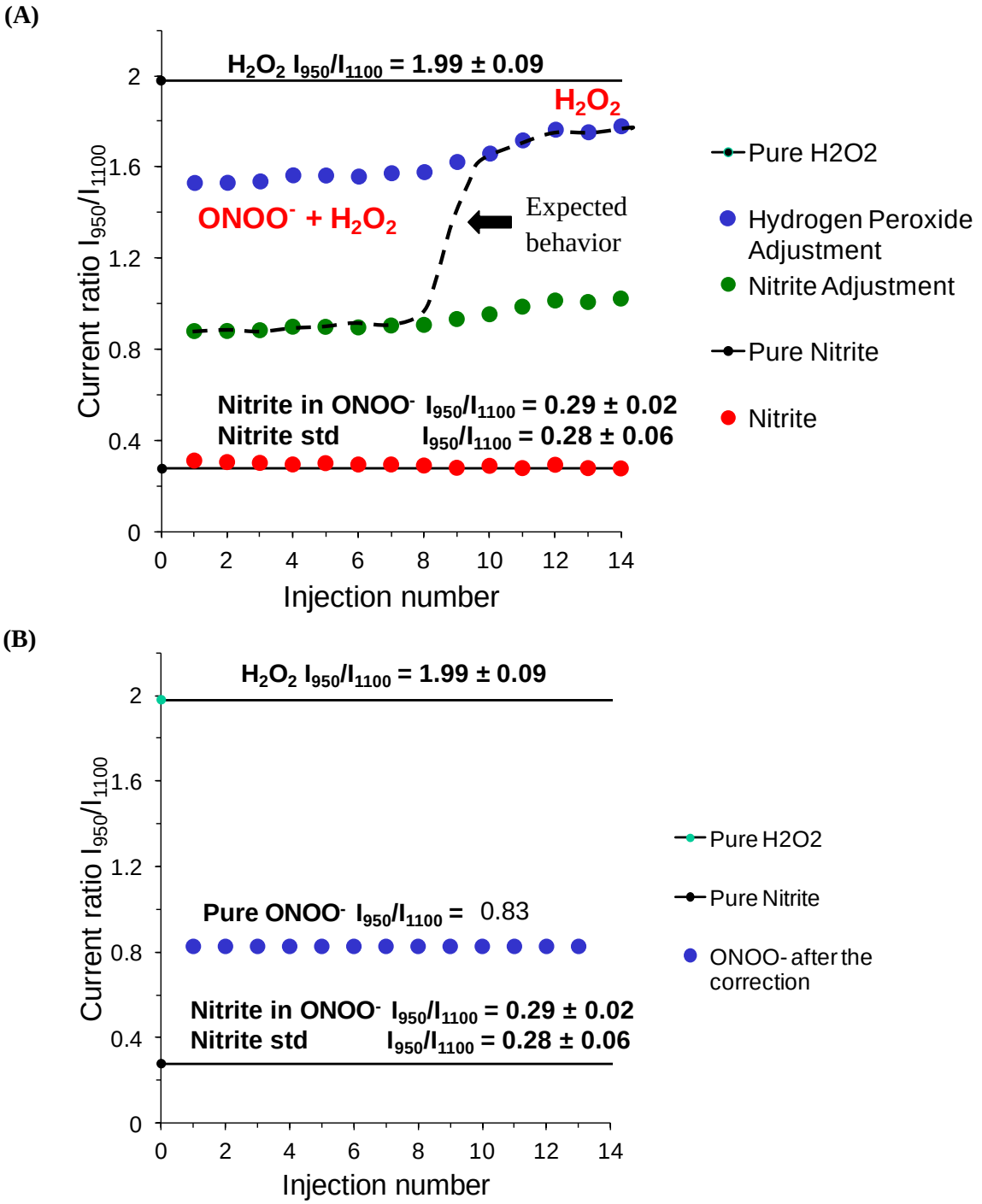

Figure 4.8: (A) The corrected current ratios of the contaminated $ONOO^-$, and nitrite peak change over several injections (B) Current ratio for pure $ONOO^-$ peak after removing H_2O_2 peak heights throughout injections in dual-series configuration

The corrected current ratios of $ONOO^-$ peak (using two types of corrections) were plotted against migration time and it was observed that the corrected current ratio of the $ONOO^-$ peak changed throughout injections as shown in Figure 4.8 A. The current ratio of $ONOO^-$ peak (after correcting using the sensitivity ratio of nitrite) change from 0.9 to 1.2 over the 11 injections and remained steady at 1.2 for the remaining 3 injections. The expected current ratio (not calculated) is also shown in the Figure 4.8 A. To obtain the real change in the current ratio of $ONOO^-$ peak, the peak is needed to be corrected using a combination of nitrite and H_2O_2 correction factors and taking into account the concentrations. The corrected current ratio of nitrite and H_2O_2 standards were 0.29 and 1.8, respectively. Hulvey *el. al* observed current ratios of 0.46 and 0.14 at +900 mV and +1100 mV for $ONOO^-$ and nitrite standards, respectively, using a ME-EC set up with a single electrode [26]. Therefore, the final current ratio of 1.2 in the $ONOO^-$ standard analyzed here is most likely due to contamination of the peak with a species with a higher current ratio, as the expected current ratio was only around 0.5. $ONOO^-$ can be synthesized using isomyl nitrite and hydrogen peroxide under high pH conditions and this procedure is widely used for commercial $ONOO^-$ synthesis [34]. The leftover hydrogen peroxide is supposed to be removed using a MnO_2 column to catalytically degrade hydrogen peroxide into water [34]. However, if this remaining hydrogen peroxide is not properly removed, it will be present in the $ONOO^-$ samples. Therefore, the higher initial current ratio is probably due to hydrogen peroxide contamination of the commercially available $ONOO^-$ samples. When the current ratio reaches a steady state, the sample contains only hydrogen peroxide.

The current ratio of $ONOO^-$ peak does not reach the expected H_2O_2 current ratio in Figure 4.8 A. This is because the $ONOO^-$ peak was corrected using the nitrite sensitivity ratio and the H_2O_2 sensitivity ratio is not similar to nitrite. Therefore, the $ONOO^-$ peak was also corrected using the sensitivity difference between hydrogen peroxide standards at two electrodes, considering the large amounts of hydrogen peroxide contamination (Figure 4.8 A). Now the current ratios reached into 1.8, which is close to the expected current ratio for H_2O_2. However, the amount of both hydrogen peroxide and $ONOO^-$

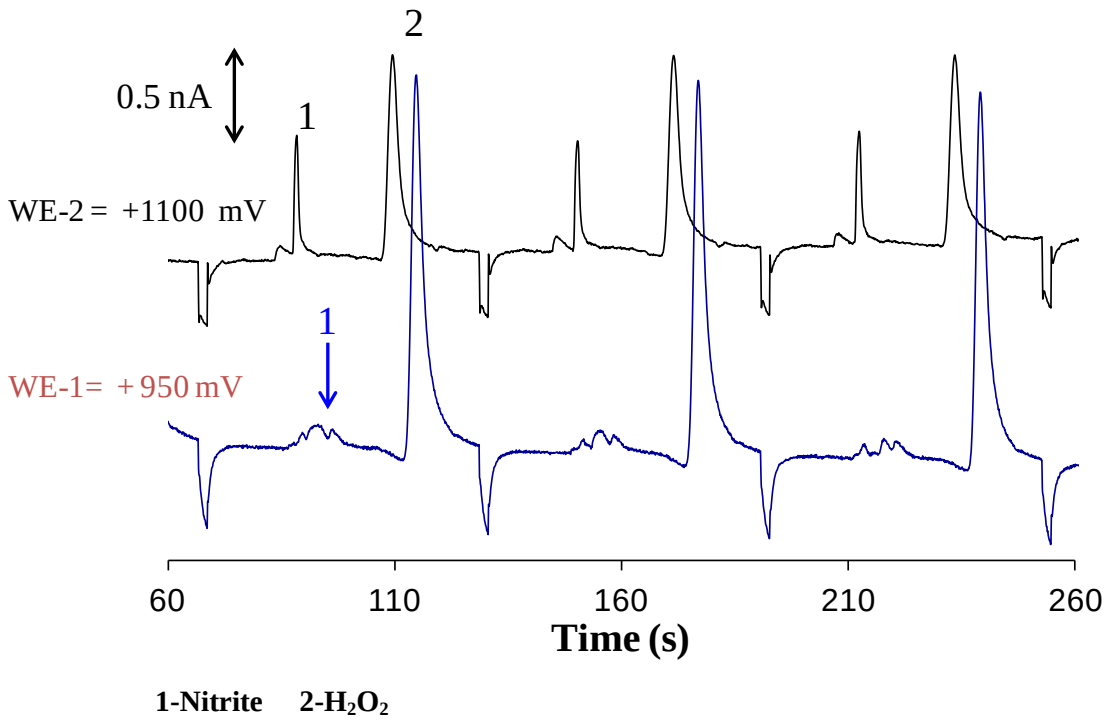

Figure 4.9: The contaminated $ONOO^-$ standards over three injections using the dual-parallel configuration. The sample was prepared in 10 mM boric and 2 mM TTAB buffer at pH 11 and the separation was also achieved using the same buffer. +1100 mV and +950 mV versus Ag/AgCl reference electrode was used for both WE-1 and WE-2.

Table 4.4: Comparison of peaks in contaminated $ONOO^-$ standards with nitrite and H_2O_2 current ratios

Species	I_{950}/I_{1100}
Nitrite standards	0.12 ± 0.02
1st Peak	0.18 ± 0.03
H_2O_2 standards	1.10 ± 0.01
2nd Peak	0.95 ± 0.03

in the sample needs to be taken into account to obtain a more realistic change of current ratios through injections.

It can be assumed that the decaying peak is due to $ONOO^-$ (during first 11 injections) and the remaining steady peaks after the decay is due solely to hydrogen peroxide. The amount of $ONOO^-$ in each peak can then be estimated by subtracting the hydrogen peroxide peak height (steady state peaks) from the total peak height (from the peaks before peaks reached into steady state). Then hydrogen peroxide subtracted $ONOO^-$ peaks can be used for calculation of current ratios. If the decaying peak is solely due to $ONOO^-$ the current ratio should be much lower than hydrogen peroxide but higher than the nitrite. Figure 4.8 B shows a steady ratio of the $ONOO^-$ peak over multiple injections. This ratio is 0.83 and it is in between hydrogen peroxide ratio and nitrite ratio.

4.3.1.2 Dual-parallel configuration

For further investigation of commercially available $ONOO^-$ samples, dual channel microchips with dual-parallel electrodes were employed. In this case, the $ONOO^-$ sample was purchased from another commercial source. Figure 4.9 shows two stable peaks for these $ONOO^-$ standards and respective current ratios were shown in Table 4.4. The current ratio and migration time of the first and second peak is very close to the current ratio and migration time of nitrite and hydrogen peroxide standards. The first peak can be positively identified as nitrite. However, the second peak does not exhibit the decay characteristics of $ONOO^-$, and therefore can be solely attributed to hydrogen peroxide. Therefore, this $ONOO^-$ sample contains nitrite and hydrogen peroxide, and no $ONOO^-$.

4.4 Conclusions

Two electrode arrangements were developed and compared which can be employed for the generation of a current ratio for identification of species. Current ratios can be obtained using a single electrode, but the sample needs to be analyzed twice. Dual-series configuration automates the sample analysis but corrections need to be performed in order to obtain a correct current ratio. On the other hand, dual-parallel arrangement avoids such corrections. These two systems were used for the analysis of

commercially available $ONOO^-$ standards and it was found that these standards were heavily contaminated with hydrogen peroxide.

Commercially available peroxynitrite standards are commonly used for different types of biological assays for studying nitrosative stress. Therefore, care must be taken in those studies regarding interpretation of results since they can be influenced by the presence of hydrogen peroxide. In the future, a dual electrode setup will be employed for identification of $ONOO^-$ and NO in a macrophage cell lysate.

4.5 References

1. Lacher, N. A.; Garrison, K. E.; Martin, R. S.; Lunte, S. M., Microchip capillary electrophoresis/electrochemistry. *Electrophoresis* **2001,** *22* (12), 2526-2536.

2. Martin, A.; Vilela, D.; Escarpa, A., Food analysis on microchip electrophoresis: An updated review. *Electrophoresis* **2012,** *33* (15), 2212-2227.

3. Chen, G.; Lin, Y.; Wang, J., Microchip capillary electrophoresis with electrochemical detection for monitoring environmental pollutants. *Curr. Anal. Chem.* **2006,** *2* (1), 43-50.

4. Vandaveer, W. R. I. V.; Pasas-Farmer, S. A.; Fischer, D. J.; Frankenfeld, C. N.; Lunte, S. M., Recent developments in electrochemical detection for microchip capillary electrophoresis. *Electrophoresis* **2004,** *25* (21-22), 3528-3549.

5. Martin, R. S.; Gawron, A. J.; Lunte, S. M.; Henry, C. S., Dual-Electrode Electrochemical Detection for Poly(dimethylsiloxane)-Fabricated Capillary Electrophoresis Microchips. *Anal. Chem.* **2000,** *72* (14), 3196-3202.

6. Zhong, M.; Zhou, J.; Lunte, S. M.; Zhao, G.; Giolando, D. M.; Kirchhoff, J. R., Dual-electrode detection for capillary electrophoresis/electrochemistry. *Anal. Chem.* **1996,** *68* (1), 203-207.

7. Zhong, M.; Lunte, S. M., Tubular-Wire Dual Electrode for Detection of Thiols and Disulfides by Capillary Electrophoresis/Electrochemistry. *Anal. Chem.* **1999,** *71* (1), 251-255.

8. Voegel, P. D.; Baldwin, R. P., Electrochemical detection in capillary electrophoresis with dual-parallel on-capillary electrodes. *Electrophoresis* **1998,** *19* (12), 2226-2232.

9. Mecker, L. C.; Martin, R. S., Use of micromolded carbon dual electrodes with a palladium decoupler for amperometric detection in microchip electrophoresis. *Electrophoresis* **2006,** *27* (24), 5032-5042.

10. Lin, B. L.; Colon, L. A.; Zare, R. N., Dual electrochemical detection of cysteine and cystine in capillary zone electrophoresis. *J. Chromatogr. A* **1994,** *680* (1), 263-270.

11. Jin, W.; Li, X.; Gao, N., Simultaneous Determination of Tryptophan and Glutathione in Individual Rat Hepatocytes by Capillary Zone Electrophoresis with Electrochemical Detection at a Carbon Fiber Bundle-Au/Hg Dual Electrode. *Anal. Chem.* **2003,** *75* (15), 3859-3864.

12. Holland, L. A.; Harmony, N. M.; Lunte, S. M., Characterization of an integrated on-capillary dual electrode for capillary electrophoresis-electrochemistry. *Electroanalysis* **1999,** *11* (5), 327-330.

13. Fischer, D. J.; Vandaveer, W. R. I. V.; Grigsby, R. J.; Lunte, S. M., Pyrolyzed photoresist carbon electrodes for microchip electrophoresis with dual-electrode amperometric detection. *Electroanalysis* **2005,** *17* (13), 1153-1159.

14. Dorris, M. K.; Crick, E. W.; Lunte, C. E., A parallel dual-electrode detector for capillary electrophoresis. *Electrophoresis* **2012,** *33* (17), 2725-2732.

15. Lunte, C. E.; Ridgway, T. H.; Heineman, W. R., Voltammetric-amperometric dual-electrode detection for flow injection analysis and liquid chromatography. *Anal. Chem.* **1987,** *59* (5), 761-766.

16. Lunte, C. E.; Kissinger, P. T.; Shoup, R. E., Difference mode detection with thin-layer dual-electrode liquid chromatography/electrochemistry. *Anal. Chem.* **1985,** *57* (8), 1541-1546.

17. Roston, D. A.; Shoup, R. E.; Kissinger, P. T., Liquid chromatography/electrochemistry: thin-layer multiple electrode detection. *Anal. Chem.* **1982,** *54* (13), 1417A-1434A.

18. Holland, L. A.; Lunte, S. M., Postcolumn Reaction Detection with Dual-Electrode Capillary Electrophoresis-Electrochemistry and Electrogenerated Bromine. *Anal. Chem.* **1999,** *71* (2), 407-412.

19. Ferris, S. S.; Lou, G.; Ewing, A. G., Scanning electrochemical detection in capillary electrophoresis. *J. Microcolumn Sep.* **1994,** *6*, 263-268.

20. Swanek, F. D.; Chen, G.; Ewing, A. G., Identification of Multiple Compartments of Dopamine in a Single Cell by Scanning Electrochemical Detection. *Anal. Chem.* **1996,** *68*, 3912-3916.

21. Fang, H.; Vickrey, T. L.; Venton, B. J., Analysis of Biogenic Amines in a Single Drosophila Larva Brain by Capillary Electrophoresis with Fast-Scan Cyclic Voltammetry Detection. *Anal. Chem.* **2011,** *83*, 2258-2264.

22. Gerhardt, G. C.; Cassidy, R. M.; Baranski, A. S., Square-Wave Voltammetry Detection for Capillary Electrophoresis. *Anal. Chem.* **1998,** *70*, 2167-2173.

23. Hebert, N. E.; Kuhr, W. G.; Brazill, S. A., Microchip capillary electrophoresis coupled to sinusoidal voltammetry for the detection of native carbohydrates. *Electrophoresis* **2002,** *23*, 3750-3759.

24. Park, S.; McGrath, M. J.; Smyth, M. R.; Diamond, D.; Lunte, C. E., Voltammetric Detection for Capillary Electrophoresis. *Anal. Chem.* **1997,** *69*, 2994-3001.

25. Wen, J.; Baranski, A.; Cassidy, R., Cyclic Voltammetric Detection in Capillary Electrophoresis with Application to Metal Ions. *Anal. Chem.* **1998,** *70*, 2504-2509.

26. Hulvey, M. K.; Frankenfeld, C. N.; Lunte, S. M., Separation and Detection of Peroxynitrite Using Microchip Electrophoresis with Amperometric Detection. *Anal. Chem.* **2010,** *82* (5), 1608-1611.

27. Scott, D. E.; Grigsby, R. J.; Lunte, S. M., Microdialysis Sampling Coupled to Microchip Electrophoresis with Integrated Amperometric Detection on an All-Glass Substrate. *Chem. Phys. Chem.* **2013,** *14* (10), 2288-2294.

28. Gunasekara, D. B.; Hulvey, M. K.; Lunte, S. M., In-channel amperometric detection for microchip electrophoresis using a wireless isolated potentiostat. *Electrophoresis* **2011,** *32* (8), 832-837.

29. Chen, C.; Hahn, J. H., Dual-Channel Method for Interference-Free In-Channel Amperometric Detection in Microchip Capillary Electrophoresis. *Anal. Chem.* **2007,** *79*, 7182-7186.

30. Chen, C.-P.; Teng, W.; Hahn, J.-H., Nanoband electrode for high-performance in-channel amperometric detection in dual-channel microchip capillary electrophoresis. *Electrophoresis* **2011,** *32*, 838-843.

31. Pacher, P.; Beckman, J. S.; Liaudet, L., Nitric oxide and peroxynitrite in health and disease. *Physiol. Rev.* **2007,** *87* (1), 315-424.

32. Frankenfeld, C. N.; Rosenbaugh, M. R.; Fogarty, B. A.; Lunte, S. M., Separation and detection of peroxynitrite and its metabolites by capillary electrophoresis with UV detection. *J. Chromatogr. A* **2006,** *1111* (2), 147-152.

33. Amatore, C.; Arbault, S.; Bruce, D.; De Oliveira, P.; Erard, M.; Vuillaume, M., Characterization of the electrochemical oxidation of peroxynitrite: relevance to oxidative stress bursts measured at the single cell level. *Chem. Eur. J.* **2001,** *7* (19), 4171-4179.

34. Uppu, R. M.; Pryor, W. A., Synthesis of peroxynitrite in a two-phase system using isoamyl nitrite and hydrogen peroxide. *Anal. Biochem.* **1996,** *236* (2), 242-249.

Chapter 5

Comparison of cellular nitric oxide production in single and bulk cell lysates using microchip electrophoresis with laser induced fluorescence detection

This work has been reported in the following journal publications and conference proceeding, and some of parts of this chapter were taken from those publications

E. R. Mainz, **D. B. Gunasekara**, G. Caruso, D. Jensen, M. K. Hulvey, J. A. F. da Silva, E. C. Metto, A. H. Culbertson, C. T. Culbertson, S. M. Lunte, "Monitoring of intracellular nitric oxide production by microchip electrophoresis and laser induced fluorescence detection," *Anal. Methods*, **2012**, 4, 414-420

E. C. Metto, K. Evans, K. Barney, A. H. Culbertson, **D. B. Gunasekara**, G. Caruso, M. K. Hulvey, J. A. F. da Silva, S. M. Lunte, C. T. Culbertson, "Integrated microfluidic device for monitoring nitric oxide production in single cells," *Anal. Chem.*, **2013**, 85, 10188–10195

S. M. Lunte, **D. B. Gunasekara**, E. C. Metto, M. K. Hulvey, E. R. Mainz, G. Caruso, J. A. F. da Silva, D. T. Jensen, A. H. Culbertson, R. J. Grigsby, C. T. Culbertson, "Microchip electrophoresis devices for the detection of nitric oxide: Comparison of bulk cell and single cell analysis," *Proceedings of μTAS*, Seattle, USA, **2011**, 0536.

5.1 Introduction

NO is present in many biological samples including blood and tissue, and is most commonly estimated through measurement of its stable oxidation products, nitrite and nitrate due to its transient nature [1,2]. There are several methods for the direct detection of NO and these have been highlighted in a recent review by Hetrick *et al.* [3]. Another popular method for indirect detection of NO is the use of fluorescent probes. There are several commercially available probes that react with the partially oxidized form of NO (N_2O_3) to produce fluorescent triazole derivatives [4-6]. The most popular probes are based on diaminofluorofluorescein (DAF) and these have been widely employed for imaging NO production in live cells using microscopic techniques [7].

There are several different DAF probes available; however, 4-amino-5-methylamino-2',7'-difluorofluorescein diacetate (DAF-FM) is most widely used. Most of these probes react not only with NO but also with other intracellular species to produce fluorescent species. DAF-FM probe can be contaminated by the formation of fluorescent products due to photo-oxidation of the probe, the formation of DAF-FM T due to presence of NO in air (DAF-FM T is the product of NO and DAF-FM) and the formation of interfering products due to reaction with dehydroascorbic acid [8-11]. DAF-FM also reacts with superoxide to produce fluorescence species. DAF-FM does not react with peroxynitrite (low concentrations, below 10 μM), nitrite or H_2O_2. However, it has been shown that the fluorescence signal for DAF-FM due to NO is enhanced in the presence of H_2O_2 [8]. More recently, Hoegger's group has shown that DAF-FM forms fluorescent side products during freeze/thaw cycling and in the presence of polyphenols such as catechin and epicatechin [12].

The reaction of DAF-FM with dehydroascorbic acid (DHA) is one of the major issues that needs to be addressed with biological samples due to the presence of higher concentrations of ascorbic acid and DHA in some biological systems [8-10]. The product of this reaction (DAF-FM DHA) has a similar spectroscopic emission profile to DAF-FM T and therefore, it cannot be distinguished from DAF-FM T by spectroscopic methods alone. However, the separation of DAF-FM T from DAF-FM DHA can be

achieved using electrophoretic methods and, for this reason, Sweedler's group employed capillary electrophoresis (CE) and laser induced fluorescence (LIF) detection to quantitate NO production in a single neuron of Aplysia califonica [10,11].

An alternative to CE-LIF is using microchip electrophoresis (ME) with LIF detection. ME allows faster separation and the possibility of future integration of cell culture and single cell cytometry [13-15]. There are several microfluidic devices that have been reported for measurement of NO production [16,17]. DAF-FM DA and fluorescence microscopy was utilized by the Spence group with microfluidic flow devices to monitor extracellular NO release from various types of cells [18-21]. Recently, ME with laser-induced fluorescence (LIF) detection has been utilized for detection of NO [22,23].

The biochemical and physical properties of a population of cells are heterogeneous in nature. It is well known that macrophages generate different phenotypes in the presence of cytokines, endotoxins and other factors [24,25]. To probe these phenotypic differences, single cell analysis is necessary. Flow cytometry is a widely used technique for single cell analysis that has very high throughput. Capillary electrophoresis-based methods have also been developed as an alternative approach for single cell analysis and allows for simultaneous detection of several analytes as well as elimination of interferences [26-30]. More recently, chemical cytometry (single cell analysis) chip-based separation systems have become popular for probing cellular heterogeneity due to their ability for fast separations, high throughput and potential for integration into micro total analysis (μTAS) systems. Ramsey's group pioneered single cell analysis and reported the first design for on-chip single cell lysis followed by electrophoretic separation of intracellular species [31]. This approach has been further advanced by the Albritton and Culbertson groups making it possible to obtain routine measurements from a population of cells [32-36].

In this chapter, intracellular concentrations of NO in native and stimulated Jurkat cells were investigated using DAF-FM DA and ME-LIF. The results described in this chapter were part of a group effort with Emilie R. Mainz (an undergraduate student), Giuseppe Caruso (a visiting graduate student), Eve C. Metto (a graduate student in Dr. Culbertson lab and developed the single cell cytometric device)

and myself. The results of these studies were published in two journals and a conference proceeding, and this chapter combines work described in these publications. The purpose of the studies described in this chapter was to investigate changes in the intracellular concentrations of NO following iNOS activation by bacterial lipopolysaccharide (LPS). First the intracellular NO levels were estimated using a bulk cell experiments before moving to single cell analysis by ME-LIF. Jurkat cells, human leukaemia cells (T-lymphocytes), were used in these studies. Like macrophages, Jurkat cells are known to produce NO through the expression of iNOS but they are nonadherent [37]. To estimate the intracellular NO concentrations in a single Jurkat cell, the amount of NO in a bulk known population of cells was measured using a calibration curve and then divided by the number of cells in the sample. This method was then incorporated into the single cell cytometry system developed by the Culbertson group at Kansas State University [36]. Lastly, the results obtained from bulk cell lysates were then compared to single cell NO measurements.

5.2 Materials and methods

5.2.1 Reagents and materials

Boric acid, sodium borate, lyophilized bovine serum albumin (BSA), Tween-20, acetonitrile (HPLC grade) and ethanol (95%) were obtained from Fisher Scientific (Pittsburgh, PA, USA). Sodium dodecyl sulfate (SDS), anhydrous dimethyl sulfoxide (DMSO), monobasic and dibasic phosphate, 0.4% Trypanblue, and lipopolysaccharide (LPS) were supplied by Sigma-Aldrich (St. Louis, MO, USA). SU-8 10 was purchased from MicroChem Corporation (Newton, MA, USA). The SU-8 developer, 2-(1-methoxy) propyl acetate, was obtained from Acros (Morris Plains, NJ, USA). Silicon wafers, 4 inches in diameter, were purchased from Silicon Inc. (Boise, ID, USA). Sylgard 184 PDMS prepolymer and curing agent was obtained from Ellsworth Adhesives (Germantown, WI, USA). Ultrapure water was generated from a Millipore Synthesis A10 system (Billerica, MA, USA). Penicillin/streptomycin antibiotic solution was obtained from American Type Culture Collection (Manassas, VA, USA). DAF-FM DA probes were purchased from Invitrogen (Carlsbad, CA, USA). 6-Carboxyfluorescein diacetate (6-CFDA) was obtained

from Anaspec (Fremont, CA, USA). DiethylamineNONOate (DEA/NO) for NO standards was purchased from Cayman Chemical (Ann Arbor, MI, USA) and stored at –80 ºC for no longer than six months.

5.2.2 Microchip fabrication

All bulk cell analyses were carried out using 5 cm simple-T PDMS/glass microchips (Figure 5.1). The fabrication of these microchips has been described previously by our group and in chapter 1 [38]. The side and top channels were 0.75 cm long. The width and depth of the channels were 40 and 14 μm, respectively. A similar method was used to fabricate the single cell analysis device except that the chip was constructed completely from PDMS [36]. In this case, the separation channel was 8.0 cm long, 50 μm wide, and 19 μm deep (Figure 5.2A) [36]. Cell lysis was performed with the aid of the separation field (Figure 5.2B). Once the cell is lysed, small charged molecules migrate (DAF-FM is negatively charged) with the electric field while large proteins and membranes travel by pressure driven flow toward the waste [36].

5.2.3 Laser-induced fluorescence detection

In these studies, detection in bulk cell experiments was accomplished using a Nikon Eclipse Ti-U inverted microscope and a 488 nm laser (Spectra-Physics, Irvine, CA) that was focused on the separation channel 85 mm from the end of the channel (Figure 5.3) [23]. For single cell analysis, a 488 nm beam was selected from a multi-line argon-ion laser (Melles Griot Laser Group, Carlsbad, CA) and focused 50 mm downstream from the cell lysis intersection using a Nikon eclipse TS100 microscope (Figure 5.2) (Nikon Instruments, Melville, NY) [36]. A photomultiplier tube (Hammatsu Corporation, Bridgewater, NJ) was used for collection of emission signal, and the signal was amplified by using a SR570 low noise current preamplifier at 1 μA/V (Stanford Research Systems, Sunnyvale, CA) [23,36].

5.2.4 Electrophoresis procedure

ME-LIF experiments of the bulk cell lysate were performed using normal polarity and a run buffer consisting of 10 mM boric acid (pH 9.2) and 7.5 mM SDS. The sample was injected using gated injection [23]. Single cell analysis was accomplished using a run buffer consisting of 25 mM sodium

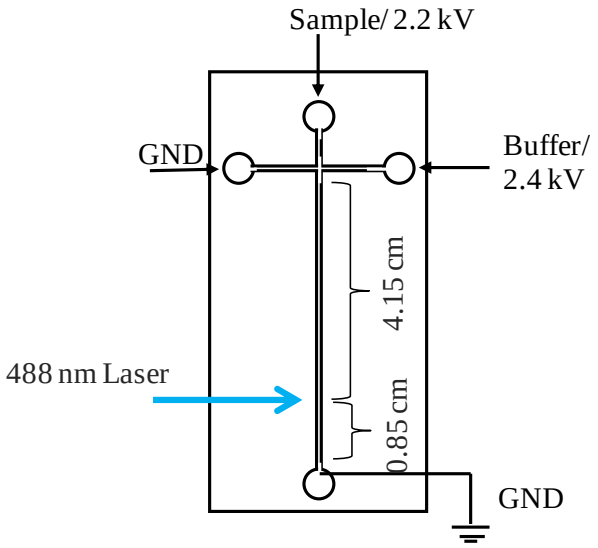

Figure 5.1: A schematic of a simple-T microchip with channel dimensions and electrophoresis voltages used for ME-LIF experiments

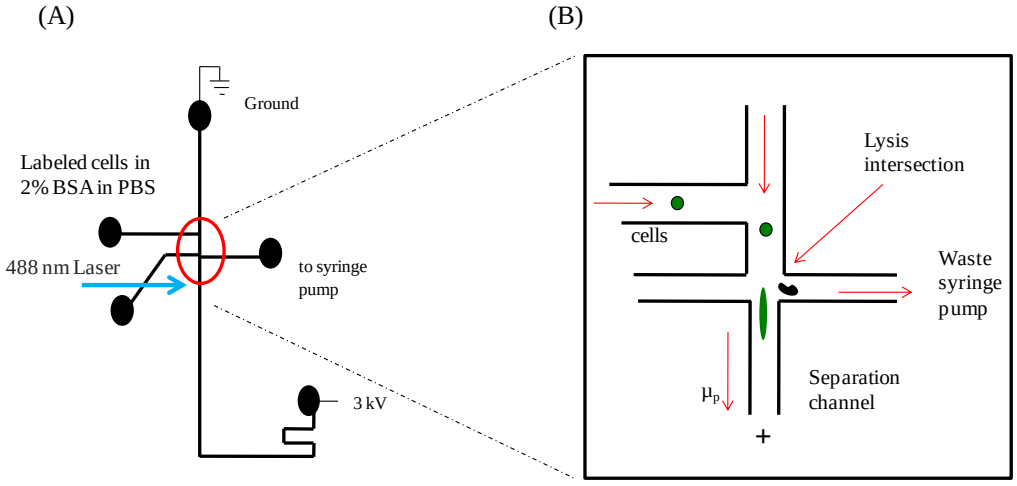

Figure 5.2: (A) The microchip design used for single cell analysis (B) Cell lysis intersection (reproduced with permission from Metto, E. C.; Evans, K.; Barney, P.; Culbertson, A. H.; Gunasekara, D. B.; Caruso, G.; Hulvey, M. K.; da Silva, J. A. F; Lunte, S. M.; Culbertson, C. T. *Anal. Chem.* **2013**, 85 (21), 10188-10195.)

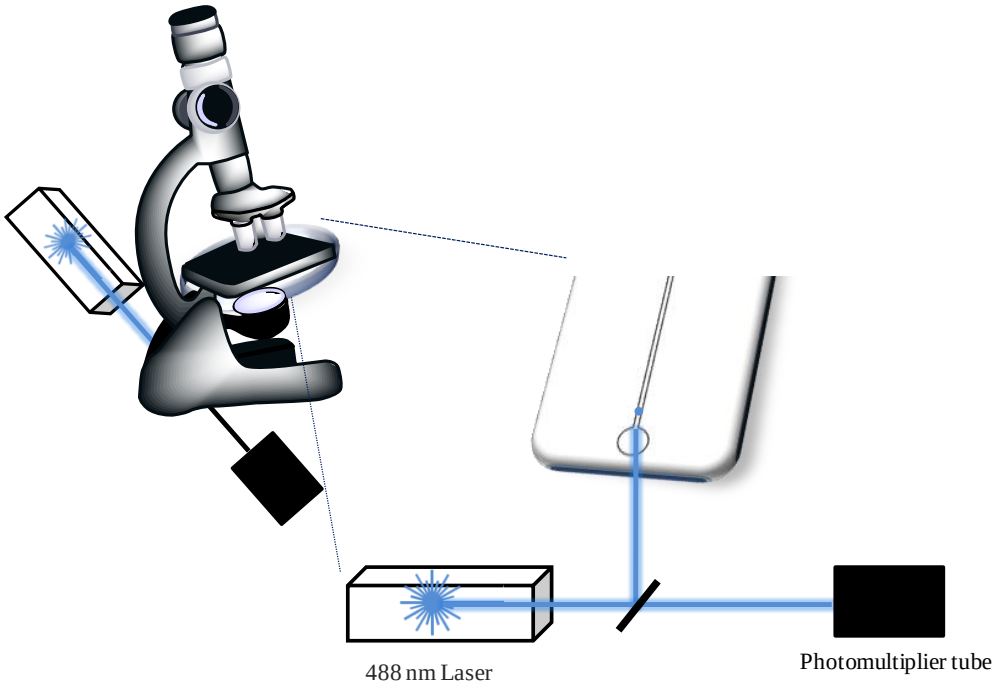

Figure 5.3: A schematic of instrumentation used for ME-LIF

borate, 20% v/v acetonitrile, 2% w/v bovine serum albumin (BSA), 0.6% w/v Tween-20, and 2 mM SDS. In the single cell analysis experiments, cells were transported hydrodynamically into the device using a syringe pump (New Era Pump Systems, Inc., Farmingdale, NY) set to withdrawal mode at a flow rate of 0.25 μL/min [36].

5.2.4 Cell culture and preparation

The Jurkat clone E-6 was purchased from American Type Culture Collection (ATCC, Manassas, VA). The cells were cultured using the recommended procedure and passaged every 3–4 days to avoid overgrowth (Figure 5.4A). The cells then were stimulated to produce NO by the introduction of 1.5 μg/mL lipopolysaccharide (LPS) into the flask. The cells were incubated for 3–4 hr to allow the expression of inducible nitric oxide synthase (Figure 5.4B). A separate group of cells with the same passage number (native cells) was used as a control. For bulk cell ME-LIF experiments, DAF-FM DA was added to the cells following stimulation and they were allowed to incubate for another 15 min. Then 6-CFDA was added and the cells were incubated for an additional 20 min (Figure 5.4B). The cells were then centrifuged, washed with medium, and centrifuged again to produce a cell pellet. The pellet was then lysed in run buffer, centrifuged using a 3 kDa molecular weight cut-off filter, and the filtrate was isolated for ME-LIF analysis (Figure 5.4 B). For single cell analysis DAF-FM DA and CFDA-labeled cells were resuspended in PBS and injected into the chemical cytometry system.

5.2.5 NO quantification

NO quantification in Jurakat bulk cells was accomplished using a calibration curve prepared from DEA/NO. The preparation of the DEA/NO standards was as described in chapter 3. Known NO concentrations (0–4 μM) were reacted with DAF-FM (The DAF-FM has produced by hydrolysis of DAF-FM DA using 0.01 M NaOH prior to mix with NO [8]) and analyzed by ME-LIF. Cell viability was determined using a trypan blue assay.

5.2.6 Preparation of DAF-FM DHA

The dehydroascorbate derivative of DAF-FM (DAF-DHA) was prepared by combining DAF-FM

(A)

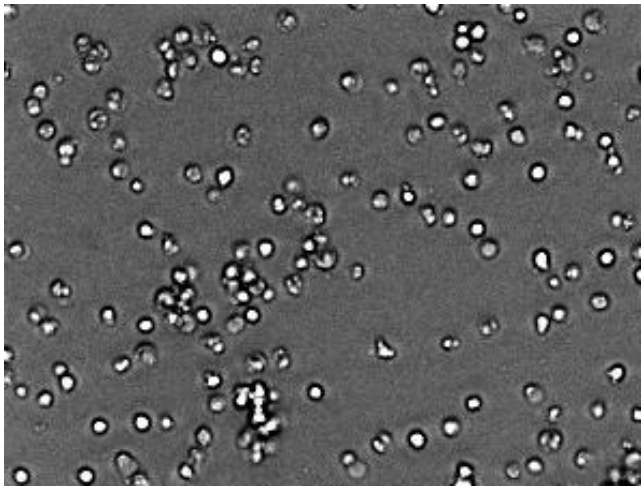

Jurkat cells

(B)

Cell stimulation and sample preparation protocol

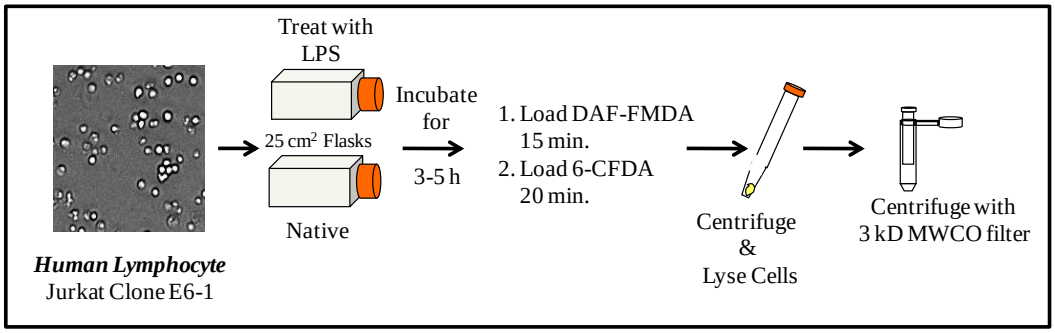

Figure 5.4: (A) An image of Jurkat cells (B) cell stimulation and sample preparation protocol

with a 70-fold excess of ascorbic acid in run buffer. Ascorbic acid (AA) was oxidized to DHA in a high pH boric buffer (9.2) by dissolved oxygen. The DAF-FM (20 μM) was then reacted for about 10 min with the oxidized AA (1.45mM) solution to generate DAF-FM DHA.

5.3 Results and discussion

5.3.1 Bulk cell analysis

DAF-FM reacts with NO to produce a benzotriazole (DAF-FM T) derivative that can be detected by LIF detection (Figure 5.5A). In addition to DAF-FMDA, 6-carboxyfluorescein diacetate (6-CFDA) was used in these experiments as an internal standard to account for cell-to-cell variability and volume (Figure 5.5B). Both dyes are cell permeant and are trapped inside the cell following cleavage of the diacetate groups to produce negatively charged species (DAF-FM and 6-CF). CFDA has been used previously in single cell chemical cytometry experiments and acted as an internal standard [39]. Prior to cell analysis DAF-FM T, DAF-FM DHA and 6-CF were separated using a buffer consisting of 10 mM boric acid and 7.5 mM SDS at pH 9.2 (Figure 5.6). The microfluidic device was then employed for the analysis of bulk native and stimulated Jurkat cells. Figures 5.7A and B show electropherograms obtained for native and stimulated bulk cells respectively. The two peaks were identified by incubating cells individually with either DAF-FMDA or 6-CFDA.

One of the disadvantages of this system is that DAF-FM T and, the parent reagent DAF-FM, co-migrate; however, DAF-FM is weakly fluorescent. Appropriate care was taken to not expose DAF-FM to light, which can produce a fluorescent product [8]. DAF-FM samples were also analyzed prior to cell analysis and an insignificant peak was observed. That is, DAF-FM peak was about 5% of DAF-FM T peak at a concentration of 250 nM. This indicates that the ME-LIF method cannot be used to measure NO concentrations below 12.5 nM. Freeze thaw cycles were also avoided by using 50 μg DAF-FM DA individually packed vials. A new vial was taken for each cell or standard experiment. Figure 5.7A and B also shows a very small peak for DAF-FM DHA in the cell lysates samples. This is because ascorbate-free medium was used in the Jurkat cell culture [40,41].

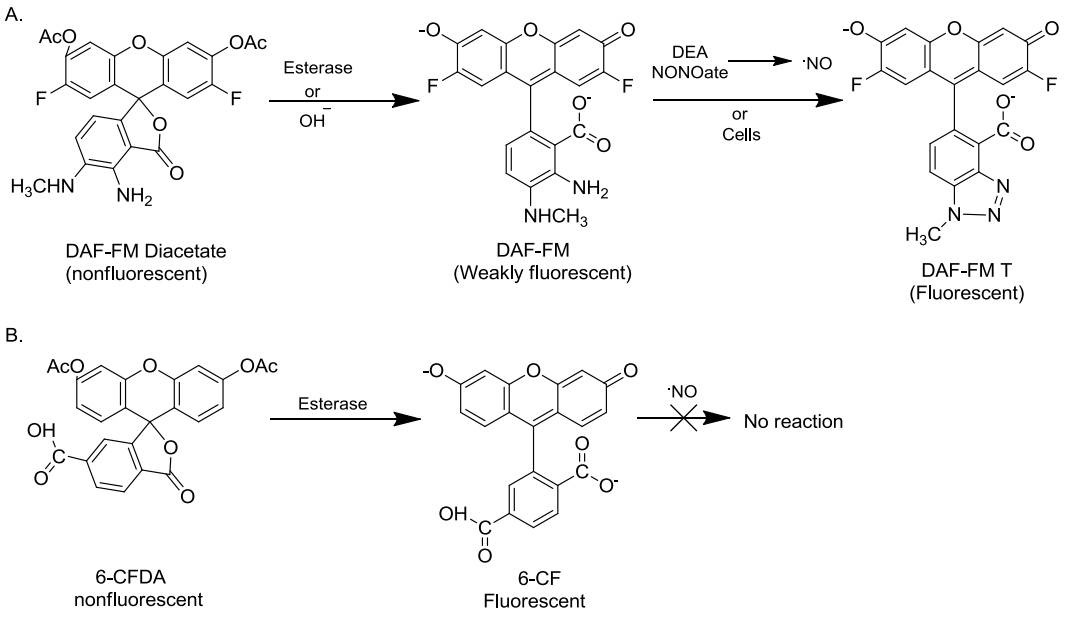

Figure 5.5: Reaction schemes for (A) DAF-FM DA (B) 6-CFDA with NO and intracellular esterase. The figure was adapted from ref. 45

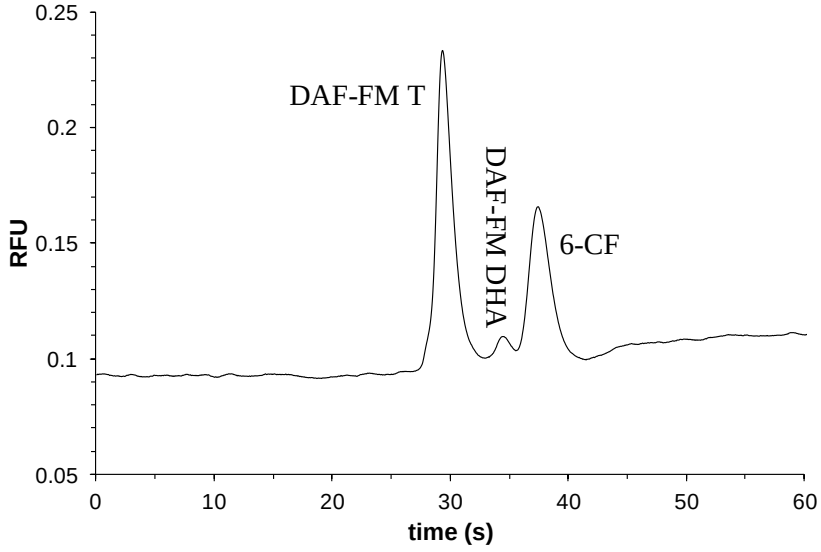

Figure 5.6: Separation of DAF-FM T, DAF-FM DHA, and 6-CF using microchip electrophoresis with laser-induced fluorescence detection. Separation voltage was 2400 V (separation) and 2200 V (sampling). Run buffer consisted of 10 mM boric acid, 7.5 mM SDS, pH 9.2. Separation channel length was 5 cm. The final concentration of 6-CF was 0.024 µM. The DAF-FM DHA peak corresponds to a cellular concentration of ascorbate of 1.45 mM and the DAF-FM T signal corresponds to 200 nM NO.

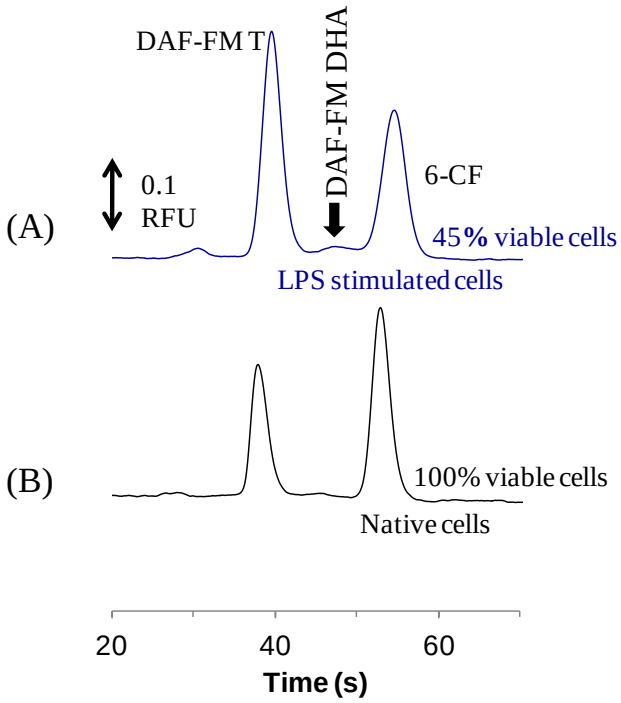

Figure 5.7: Comparison of (A) LPS-stimulated and (B) native cell lysate. Separation conditions were the same as those in 5.6

5.3.2 Quantitative analysis of NO production in Jurkat bulk cell lysates

Quantitative analysis of NO in Jurkat cells was performed using a NO standard prepared from DEA/NO. The amount of NO was calculated using a calibration curve for NO from 0.125 to 4 μM (with a correlation coefficient of 0.998 or higher).The limits of quantification of the ME-LIF method was 125 nM NO standard (S/N of 10). The intracellular NO concentration of a single Jurkat cell was estimated by dividing the total amount of NO produced by the total number of viable cells. The average intracellular NO concentration of a single Jurkat cell was estimated using three separate cell samples. The NO concentration was determined to be 0.55 (±0.13) mM for native cells and 1.48 (±0.43) mM for LPS-stimulated cells. The calculated intracellular NO concentration in a LPS-stimulated cell was significantly higher compared to the calculated NO concentration in a native cell (two sample t-test, $p < 0.05$) (Figure 5.8). These values for NO production are also very similar to those reported by Goto *et al.* for macrophages stimulated with LPS [16]. However the concentrations are much higher than values reported for platelets and erythrocytes where eNOS (not iNOS) is the primary source of NO [19,42]. We also observed considerably high mortality of Jurkat cells (up to 60%) with the LPS-stimulation due to excessive NO production, which has previously been reported [43].

The DAF FM/6-CF ratio can also be used to calculate the relative increase in NO production in LPS-stimulated cells compared to native cells. There was a 2.2 ± 0.2 times increase in NO production in LPS-stimulated cells compared to native cells for the same three cell samples describe above. NO concentrations were calculated using calibration curves and cell counts and indicated that there was around 2.5 fold NO production increase from native to LPS-stimulation.

5.3.3 Single cell analysis

To compare the average intracellular NO production obtained from bulk cell analysis with individual cells, a single cell chemical cytometry device developed by the Culbertson group was used [36,44]. Details of the single cell analysis system can be found in ref. 36 while Figure 5.2 shows the device used for this study. The DAF-FM T/6-CF ratio of each individual cell was obtained for the single

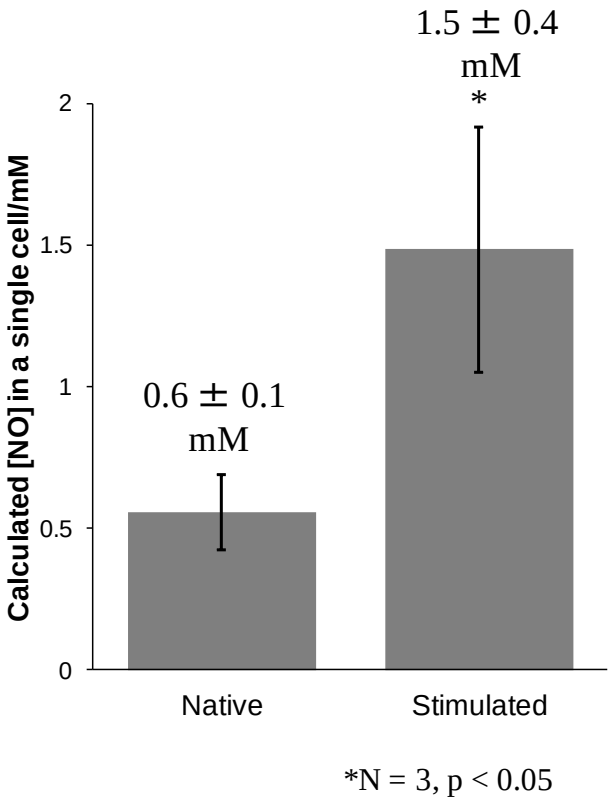

Figure 5.8: Comparison of calculated average NO concentration in a single LPS-stimulated and a native Jurkat cell ($n = 3$, $p < 0.05$). For these calculations, the volume of a Jurkat cell was assumed to be 0.5 pL.

cell studies and are shown in Figure 5.9. It is clear that with the LPS stimulation, the DAF FM T/6-CF ratio shifted to higher values due to higher NO production. The average fold increase in NO production from native to LPS-stimulated cells was 2.3 ± 0.15, which is in a good agreement with the results obtained for the bulk cell lysate (2.2±0.2).

5.4 Conclusion

In this chapter, a ME-LIF method with DAF-FMDA and 6-CFDA was utilized for the quantitation of intracellular NO concentrations in bulk native and LPS-stimulated cell lysates. It was found that the average intracellular NO concentration for a LPS-stimulated single Jurkat cell was 1.5 mM while a single native Jurkat cell produces approximately 0.6 mM of NO during the last 35 min of LPS stimulation. That is rate of NO production in a single Jurkat cell during this period is 8.57 aM/min). The DAF FM T/6-CF ratio can also be used for comparison of the fold increase in NO production in LPS-stimulated versus native cells. The DAF FM T/6-CF ratio for LPS-stimulated versus native cells was 2.22 while the estimated NO concentration was 2.5 times higher in LPS-stimulated cells relative to native cells. This average NO production per cell calculated from bulk cell studies was then compared with NO production in a group of single cells using the single cell chemical cytometry method and a good agreement was observed. During the next phase of this project, we propose to develop a method to detect $ONOO^-$ using a $ONOO^-$ selective fluorescent probe, HK Green and ME-LIF.

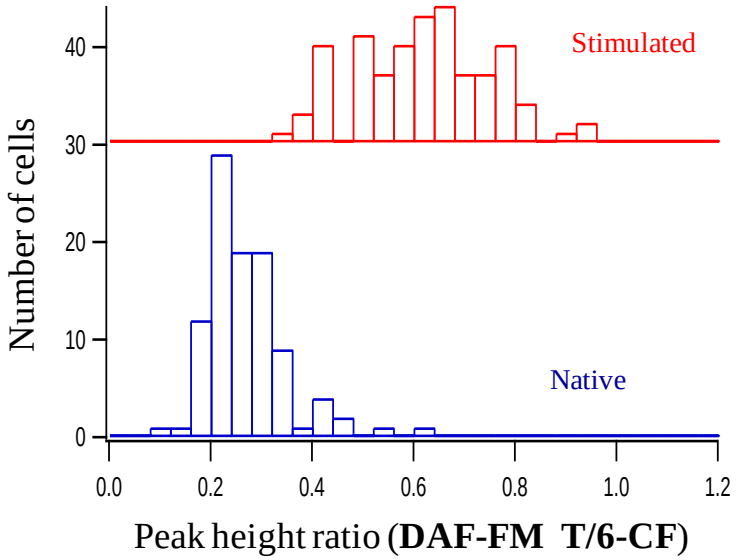

Figure 5.9: A comparison of DAF FM T/6-CF ratios in single LPS-stimulated and native Jurkat cells. The cells were analyzed using the microchip in Figure 5.2. 100 cells were used in each condition for preparation of histogram (reproduced with permission from Metto, E. C.; Evans, K.; Barney, P.; Culbertson, A. H.; Gunasekara, D. B.; Caruso, G.; Hulvey, M. K.; da Silva, J. A. F.; Lunte, S. M.; Culbertson, C. T. *Anal. Chem.* **2013**, 85 (21), 10188-10195.)

5.5 References

1. Miyado, T.; Wakida, S.-i.; Aizawa, H.; Shibutani, Y.; Kanie, T.; Katayama, M.; Nose, K.; Shimouchi, A., High-throughput assay of nitric oxide metabolites in human plasma without deproteinization by lab-on-a-chip electrophoresis using a zwitterionic additive. *J. Chromatogr. A* **2008,** *1206*, 41-44.

2. Miyado, T.; Tanaka, Y.; Nagai, H.; Takeda, S.; Saito, K.; Fukushi, K.; Yoshida, Y.; Wakida, S.-I.; Niki, E., High-throughput nitric oxide assay in biological fluids using microchip capillary electrophoresis. *J. Chromatogr. A* **2006,** *1109*, 174-178.

3. Hetrick, E. M.; Schoenfisch, M. H., Analytical chemistry of nitric oxide. *Annu. Rev. Anal. Chem.* **2009,** *2*, 409-433.

4. Gomes, A.; Fernandes, E.; Lima, J. L. F. C., Use of fluorescence probes for detection of reactive nitrogen species: A review. *J. Fluoresc.* **2006,** *16*, 119-139.

5. Nagano, T., Development of fluorescent probes for bioimaging applications. *Proc. Jpn. Acad., Ser. B* **2010,** *86*, 837-847.

6. McQuade, L. E.; Lippard, S. J., Fluorescent probes to investigate nitric oxide and other reactive nitrogen species in biology (truncated form: fluorescent probes of reactive nitrogen species). *Curr. Opin. Chem. Biol.* **2010,** *14*, 43-49.

7. Ye, X.; Rubakhin, S. S.; Sweedler, J. V., Detection of nitric oxide in single cells. *Analyst* **2008,** *133*, 423-433.

8. Balcerczyk, A.; Soszynski, M.; Bartosz, G., On the specificity of 4-amino-5-methylamino-2',7'-difluorofluorescein as a probe for nitric oxide. *Free Radical Biol. Med.* **2005,** *39*, 327-335.

9. Zhang, X.; Kim, W.-S.; Hatcher, N.; Potgieter, K.; Moroz, L. L.; Gillette, R.; Sweedler, J. V., Interfering with nitric oxide measurements. 4,5-diaminofluorescein reacts with dehydroascorbic acid and ascorbic acid. *J. Biol. Chem.* **2002,** *277*, 48472-48478.

10. Kim, W.-S.; Ye, X.; Rubakhin, S. S.; Sweedler, J. V., Measuring Nitric Oxide in Single Neurons by Capillary Electrophoresis with Laser-Induced Fluorescence: Use of Ascorbate Oxidase in Diaminofluorescein Measurements. *Anal. Chem.* **2006,** *78* (6), 1859-1865.

11. Ye, X.; Xie, F.; Romanova, E. V.; Rubakhin, S. S.; Sweedler, J. V., Production of Nitric Oxide within the Aplysia californica Nervous System. *ACS chem. Neurosci.* **2009,** *1* (3), 182-193.

12. Uhlenhut, K.; Hoegger, P., Pitfalls and limitations in using 4,5-diaminofluorescein for evaluating the influence of polyphenols on nitric oxide release from endothelial cells. *Free Radical Biol. Med.* **2012,** *52*, 2266-2275.

13. Martin, R. S.; Root, P. D.; Spence, D. M., Microfluidic technologies as platforms for performing quantitative cellular analyses in an in vitro environment. *Analyst* **2006,** *131*, 1197-1206.

14. Lin, Y.; Trouillon, R.; Safina, G.; Ewing, A. G., Chemical Analysis of Single Cells. *Anal. Chem.* **2011,** *83*, 4369-4392.

15. Kovarik, M. L.; Gach, P. C.; Ornoff, D. M.; Wang, Y.; Balowski, J.; Farrag, L.; Allbritton, N. L., Micro Total Analysis Systems for Cell Biology and Biochemical Assays. *Anal. Chem.* ACS ASAP.

16. Goto, M.; Sato, K.; Murakami, A.; Tokeshi, M.; Kitamori, T., Development of a microchip-based bioassay system using cultured cells. *Anal. Chem.* **2005,** *77*, 2125-2131.

17. Amatore, C.; Arbault, S.; Chen, Y.; Crozatier, C.; Tapsoba, I., Electrochemical detection in a microfluidic device of oxidative stress generated by macrophage cells. *Lab On A Chip* **2007,** *7*, 233-238.

18. Carroll, J. S.; Ku, C.-J.; Karunarathne, W.; Spence, D. M., Red Blood Cell Stimulation of Platelet Nitric Oxide Production Indicated by Quantitative Monitoring of the Communication between Cells in the Bloodstream. *Anal. Chem.* **2007,** *79* (14), 5133-5138.

19. Halpin, S. T.; Spence, D. M., Direct Plate-Reader Measurement of Nitric Oxide Released from Hypoxic Erythrocytes Flowing through a Microfluidic Device. *Anal. Chem.* **2010,** *82*, 7492-7497.

20. Letourneau, S.; Hernandez, L.; Faris, A. N.; Spence, D. M., Evaluating the effects of estradiol on endothelial nitric oxide stimulated by erythrocyte-derived ATP using a microfluidic approach. *Anal. Bioanal. Chem.* **2010,** *397*, 3369-3375.

21. Genes, L. I.; Tolan, N. V.; Hulvey, M. K.; Martin, R. S.; Spence, D. M., Addressing a vascular endothelium array with blood components using underlying microfluidic channels. *Lab On A Chip* **2007,** *7*, 1256-1259.

22. Wang, Y.; Yin, M., Sensitive and rapid determination of nitric oxide in human serum using microchip capillary electrophoresis with laser-induced fluorescence detection. *Microchim. Acta* **2009,** *166*, 243-249.

23. Mainz, E. R.; Gunasekara, D. B.; Caruso, G.; Jensen, D. T.; Hulvey, M. K.; Fracassi, d. S. J. A.; Metto, E. C.; Culbertson, A. H.; Culbertson, C. T.; Lunte, S. M., Monitoring intracellular nitric oxide production using microchip electrophoresis and laser-induced fluorescence detection. *Anal. Methods* **2012,** *4*, 414-420.

24. Gordon, S., Alternative activation of macrophages. *Nat. Rev. Immunol.* **2003,** *3*, 23-35.

25. Gordon, S.; Taylor, P. R., Monocyte and macrophage heterogeneity. *Nat. Rev. Immunol.* **2005,** *5* (12), 953-964.

26. Cecala, C.; Rubakhin, S. S.; Mitchell, J. W.; Gillette, M. U.; Sweedler, J. V., A hyphenated optical trap capillary electrophoresis laser induced native fluorescence system for single-cell chemical analysis. *Analyst* **2012,** *137* (13), 2965-2972.

27. Cecala, C.; Sweedler, J. V., Sampling techniques for single-cell electrophoresis. *The Analyst* **2012,** *137* (13), 2922-2929.

28. Cruz, L.; Moroz, L. L.; Gillette, R.; Sweedler, J. V., Nitrite and nitrate levels in individual molluscan neurons: single-cell capillary electrophoresis analysis. In *J Neurochem*, 1997; Vol. 69, p 110.

29. Dickinson, A. J.; Armistead, P. M.; Allbritton, N. L., Automated Capillary Electrophoresis System for Fast Single-Cell Analysis. *Anal. Chem.* **2013,** *85*, 4797-4804.

30. Floyd, P. D.; Moroz, L. L.; Gillette, R.; Sweedler, J. V., Capillary Electrophoresis Analysis of Nitric Oxide Synthase Related Metabolites in Single Identified Neurons. *Anal. Chem.* **1998,** *70* (11), 2243-2247.

31. McClain, M. A.; Culbertson, C. T.; Jacobson, S. C.; Allbritton, N. L.; Sims, C. E.; Ramsey, J. M., Microfluidic devices for the high-throughput chemical analysis of cells. *Anal. Chem.* **2003,** *75* (21), 5646-5655.

32. Culbertson, C. T., Single Cell Analysis on Microfluidic Devices. In *Microchip Capillary Electrophoresis*, Henry, C., Ed. Humana: Totowa, NJ, 2006; Vol. 339, pp 203-216.

33. Jiang, D.; Sims, C. E.; Allbritton, N. L., Microelectrophoresis platform for fast serial analysis of single cells. *Electrophoresis* **2010,** *31* (15), 2558-2565.

34. Kovarik, M. L.; Shah, P. K.; Armistead, P. M.; Allbritton, N. L., Microfluidic Chemical Cytometry of Peptide Degradation in Single Drug-Treated Acute Myeloid Leukemia Cells. *Anal. Chem.* Ahead of Print.

35. Lai, H. H.; Quinto-Su, P. A.; Sims, C. E.; Bachman, M.; Li, G. P.; Venugopalan, V.; Allbritton, N. L., Characterization and use of laser-based lysis for cell analysis on-chip. *J R Soc. Interface* **2008,** *5 Suppl 2*, S113-21.

36. Metto, E. C.; Evans, K.; Barney, P.; Culbertson, A. H.; Gunasekara, D. B.; Caruso, G.; Hulvey, M. K.; da Silva, J. A. F.; Lunte, S. M.; Culbertson, C. T., An Integrated Microfluidic Device for Monitoring Changes in Nitric Oxide Production in Single T-Lymphocyte (Jurkat) Cells. *Anal. Chem.* **2013,** *85* (21), 10188-10195.

37. Amin, A. R., Expression of nitric oxide synthase in human peripheral blood mononuclear cells and neutrophils. *J. Inflamm.* **1996,** *47* (4), 190-205.

38. Hulvey, M. K.; Frankenfeld, C. N.; Lunte, S. M., Separation and Detection of Peroxynitrite Using Microchip Electrophoresis with Amperometric Detection. *Anal. Chem.* **2010,** *82*, 1608 -1611.

39. McClain, M. A.; Culbertson, C. T.; Jacobson, S. C.; Allbritton, N. L.; Sims, C. E.; Ramsey, J. M., Microfluidic Devices for the High-Throughput Chemical Analysis of Cells. *Anal. Chem.* **2003,** *75* (21), 5646-5655.

40. Gokhale, P.; Patel, T.; Morrison, M. J.; Vissers, M. C. M., The effect of intracellular ascorbate on the susceptibility of HL60 and Jurkat cells to chemotherapy agents. *Apoptosis* **2006,** *11*, 1737-1746.

41. Ek, A.; Stroem, K.; Cotgreave, I. A., The uptake of ascorbic acid into human umbilical vein endothelial cells and its effect on oxidant insult. *Biochem. Pharmacol.* **1995,** *50*, 1339-46.

42. Ku, C.-J.; Karunarathne, W.; Kenyon, S.; Root, P.; Spence, D., Fluorescence Determination of Nitric Oxide Production in Stimulated and Activated Platelets. *Anal. Chem.* **2007,** *79*, 2421-2426.

43. Nath, N.; Chattopadhyay, M.; Pospishil, L.; Cieciura, L. Z.; Goswami, S.; Kodela, R.; Saavedra, J. E.; Keefer, L. K.; Kashfi, K., JS-K, a nitric oxide-releasing prodrug, modulates ss-catenin/TCF signaling in leukemic Jurkat cells: evidence of an S-nitrosylated mechanism. *Biochem. Pharmacol.* **2010,** *80* (11), 1641-1649.

44. Roman, G. T.; Chen, Y.; Viberg, P.; Culbertson, A. H.; Culbertson, C. T., Single-cell manipulation and analysis using microfluidic devices. *Anal. Bioanal. Chem.* **2007,** *387*, 9-12.

45. J. Johnson and M. T. Z. Spence, The molecular probes handbook: Life Technologies Corporation, 2010.

Chapter 6

Cellular nitrosative stress profiling using microchip electrophoresis coupled to electrochemical detection

This work has been published in the following journal publication:

D. B. Gunasekara, J. M. Siegel, G. Caruso, M. K. Hulvey, S. M. Lunte, "Development of a microchip electrophoresis method with amperometric detection for profiling cellular nitrosative stress markers," *Analyst*, **2014**, 139 (13), 3265 – 3273

6.1 Introduction

There are many different types of immune cells in the human body, with macrophages the primary cell type that is activated as part of an immune response [1,2]. Macrophages produce NO primarily through the activation of iNOS; however, an uncontrolled or large NO production in these cell types results in cellular nitrosative stress, which is a cause of many neurodegenerative and cardiovascular diseases [3,4]. The toxic effects of cellular pro-oxidants produced from NO can be mitigated by the presence of antioxidant molecules in the cell [5,6]. GSH is an antioxidant produced by the cells that can scavenge NO and produce nitrosoglutathione. Also, GSH can react with hydrogen peroxide to form glutathione disulfide. This reaction is catalyzed in the cell by glutathione peroxidase [5,6]. The balance between pro- and antioxidants is important for regulating cellular nitrosative stress [7].

In this chapter, a method that allows the direct detection of NO and its metabolites in macrophages using ME-EC is described. The electrophoretic method permits subminute separation of NO, NO_2^-, and cellular antioxidants as well as potential interferences and other electrochemically active intracellular components (*e.g.*, tyrosine and nitrotyrosine). This approach makes it possible to gather information regarding the overall redox state of the macrophage cells along with NO production. The method was used to investigate NO and intracellular GSH levels in macrophages under native and stimulated conditions. The ME-EC method reported here will be adapted in the future for single cell analysis studies.

6.2 Materials and methods

6.2.1 Materials and reagents

The following chemicals and materials were used as received: SU-8 10 photoresist and SU-8 developer (MicroChem Corp., Newton, MA, USA); AZ 1518 photoresist and 300 MIF developer (Mays Chemical Co., Indianapolis, IN, USA); photolithography film mask (50,000 dpi; Infinite Graphics Inc., Minneapolis, MN, USA); N(100) 100 mm (4”) silicon (Si) wafers (Silicon, Inc., Boise, ID, USA); chrome and AZ1518 positive photoresist coated soda lime glass substrate (4" × 4" × 0.090", Nanofilm, Westlake,

CA, USA); Pt film-coated glass substrates (2000 Å Pt layer over 200 Å Ti) (The Stanford Nanofabrication Facility, Stanford, CA, USA); Sylgard 184 Silicone Elastomer Kit: Polydimethylsiloxane (Ellsworth Adhesives, Germantown, WI, USA); Titanium (Ti) etchant (TFTN; Transene Co., Danvers, MA, USA); epoxy and 22 gauge Cu wire (Westlake Hardware, Lawrence, KS, USA); silver colloidal paste (Ted Pella, Inc., Redding, CA, USA); acetone, 2-propanol (isopropyl alcohol, IPA), 30% H_2O_2, H_2SO_4, HNO_3, NaOH, HCl, and Trypan blue (Fisher Scientific, Fair Lawn, NJ, USA); sodium nitrite, boric acid, tetradecyltrimethylammonium bromide (TTAB), tetradecyltrimethylammonium chloride (TTAC), ascorbic acid (AA), tyrosine (Tyr), reduced glutathione (GSH), sodium azide, potassium iodide, NaCl, lipopolysaccharides from Escherichia coli 0111:B4, and Griess reagent (modified) (Sigma, St. Louis, MO, USA) and buffered oxide etchant (JT Baker, Austin, TX, USA). All water used was ultrapure (18.3 MΩ·cm) (Milli-Q Synthesis A10, Millipore, Burlington, MA, USA).

6.2.2 PDMS fabrication

The fabrication of PDMS-based microfluidic devices has been described previously [8]. Briefly, SU-8 10 negative photoresist (for electrophoresis channels) was spin-coated on a 4 in diameter Si wafer to a thickness of 15 ± 1 μm using a Cee 100 spincoater (Brewer Science Inc., Rolla, MO, USA). The wafer was then transferred to a programmable hotplate (Thermo Scientific, Asheville, NC, USA) for a soft bake at 65°C for 2 min and then 95°C for 5 min. Microfluidic channel designs were created using AutoCad LT 2004 (Autodesk, Inc., San Rafael, CA, USA) and printed onto a transparency film at a resolution of 50,000 dpi (Infinite Graphics Inc., Minneapolis, MN, USA). The coated wafer was covered with the transparency film mask and exposed to UV light (344 mJ/cm^2 for 16 s) using an i-line UV flood source (ABM Inc., San Jose, CA, USA). Following the UV exposure, the wafer was post-baked at 65^{o}C for 2 min and 95°C for 10 min. The wafer was then developed in SU-8 developer, rinsed with IPA, and dried under nitrogen. A final "hard-bake" was performed at 175°C for 2 h. The thickness of the raised photoresist, which corresponds to the depth of the PDMS channels, was measured with a profilometer (Alpha Step-200, Tencor Instruments, Mountain View, CA, USA). PDMS microstructures were made by

casting a 10:1 mixture of PDMS elastomer and curing agent, respectively, against the patterned Si master. A simple-T device containing a 5 cm separation channel (from the T intersection to the end of the separation channel) and 0.75 cm side arms was used for these studies. The width and depth of the electrophoresis microchannels were 40 μm and 14 μm, respectively. Holes for the reservoirs were created in the polymer using a 4 mm biopsy punch (Harris Uni-core, Ted Pella Inc., Redding, CA, USA).

6.2.3 Platinum electrode fabrication

All electrochemical measurements were obtained using 15 μm Pt working electrodes. Electrodes were either fabricated using an in-house magnetron sputtering system (AXXIS DC magnetron sputtering system, Kurt J. Lesker Co., Jefferson Hills, PA, USA) or received from the Stanford nanofabrication facility. Details of fabrication of Pt electrodes provided by the Stanford nanofabrication facility were reported previously [9]. In the Stanford plates, the Pt electrodes were deposited on the top of the glass surface. To obtain better stability, Pt electrodes were fabricated in-house by making a 500–600 nm trench in the glass substrate using a procedure previously reported by our group [10]. Briefly, the electrode designs were created using AutoCad LT 2004 (Autodesk, San Rafael, CA, USA) and printed onto a transparency film at a resolution of 50,000 dpi (Infinite Graphics, Minneapolis MN, USA). The electrode design was then patterned on a chrome and AZ1518 positive photoresist-coated soda lime glass plate. The plate was developed using an AZ®300 MIF (Capitol Scientific, Inc., Austin, TX, USA) solution for 30 s and then baked at 100ºC for 10 min on a programmable hotplate (Thermo Scientific, Asheville, NC, USA). Once the photoresist layer was developed, the exposed chrome layer was the shape of the electrode. This chrome layer was then etched using chrome etchant to expose the glass surface underneath. Next, the glass plate was etched for about 5 min using a 10:1 buffered oxide etchant (JT Baker, Austin, TX, USA) to obtain a 500 to 600 nm trench. It has been observed that if the trench is not deep enough (below 400 nm), the Pt-deposited electrodes are not stable under high applied potentials (greater than +1200 mV) and the Pt electrode flakes off the trench during electrophoresis. The plate was washed thoroughly with $CaCO_3$ and water after buffered oxide etching, and the depth of the trench was

measured using an Alpha-step 200 profilometer (Tencor Instruments). The plate was dried at 100ºC for 10 min and then exposed to an oxygen plasma for 1 min (March Plasmod, Concord, CA, USA). The glass plate was immediately transferred to an AXXIS DC magnetron sputtering system (Kurt J. Lesker Co.). After pumping down the vacuum chamber of the sputtering system to a pressure of 1.0×10^{-6} Torr, a 20-nm Ti layer was deposited (220 V deposition voltage, 40 s deposition time, and 5.0×10^{-3} Torr deposition pressure) and then a Pt layer was deposited (200 V deposition voltage, 17 to 20 min deposition time, and 5.0×10^{-3} Torr deposition pressure). The width and height of the resulting Pt electrodes were measured again using an Alpha-step 200 profilometer.

6.2.4 Solution preparation

All solutions were made using 18 MΩ ultrapure water from a Millipore A10 system. Stock solutions of nitrite (NO_2^-, 10 mM), hydrogen peroxide (H_2O_2, 10 mM), GSH (10 mM), KI (5 mM), NaN_3 (5 mM), and AA (10mM) were all prepared in ultrapure water using appropriate amounts and were stored at 4°C. To dissolve tyrosine (Tyr, 10 mM), the solution was acidified using 1–1.5 M HCl. Subsequent dilutions of each stock solution for use in the microchip system were made in the appropriate run buffer at the time of analysis. For separation and sampling buffer, a boric acid (20 mM) stock solution was prepared and the pH was adjusted to 11 using 10 M or 1 M NaOH solution. The pH-adjusted boric buffer was diluted with other buffer constituents in order to obtain a 10 mM boric solution. The buffer pH was measured after dilution and before adding surfactant. The buffer pH was 10.3–10.7. TTAC (100 mM) stock solution, NaCl (50 mM) stock solution, and ultrapure water were used for buffer dilution.

6.2.5 Chip construction and electrophoresis procedure

PDMS microchips consisting of a simple-T design with a 5 cm separation channel were used for all studies. Amperometric signals were recorded using a 15 μm Pt working electrode against a Ag/AgCl reference electrode, which was placed in the buffer waste reservoir after the separation ground lead (Figure 6.1A). The chip containing the separation channel was aligned and reversibly sealed to the glass

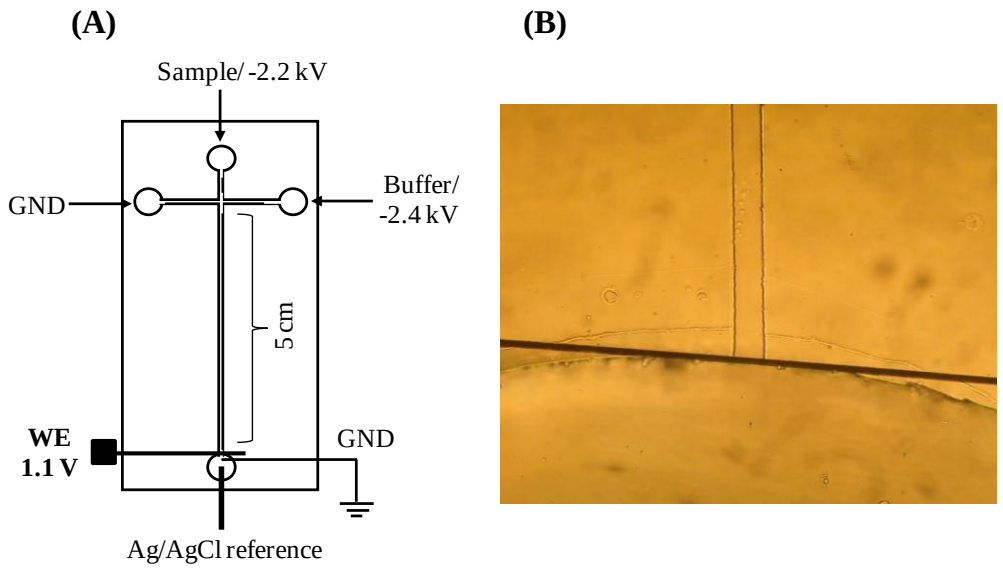

Figure 6.1: (A) Schematic of ME-EC setup with in-channel configuration. (B) Electrode alignment

plate containing the Pt electrode. For in-channel detection, the electrode was placed exactly at the channel end of the separation channel as shown in Figure 6.1B.

Electrophoretic separations were carried out using reverse polarity with TTAC as the cationic surfactant to modify the channel walls. Two negative high voltage Pt leads (Pt wire) were placed in the sample and buffer reservoirs, while two earth ground Pt leads were placed in the sample waste and buffer waste reservoirs. For sampling, -2200 V was employed, while -2400 V was used for the separation. A gated injection was used to inject the sample, with an injection time between 0.5 and 1 s. Boric buffer conditions were evaluated for the separation of nitrite, azide (interference), iodide, tyrosine, GSH, AA, and H_2O_2. To balance the conductivity difference between the cell lysate and separation buffer, 7.5 to 10 mM NaCl was added to the run buffer. The cells were lysed in buffered solution containing surfactant (10 mM boric acid and 2 mM TTAC) without NaCl.

6.2.6 Electrochemical detection

EC detection was accomplished using a modified model of an 8151BP, 8100-K6, or 9051 single- or dual-channel wireless, electrically isolated potentiostat (Pinnacle Technology Inc., Lawrence, KS, USA) operating in a two-electrode format (Pt working; Ag/AgCl reference: Bioanalytical Systems, West Lafayette, IN, USA). The model 8151P, 8100-K6, and 9051 potentiostats have a sampling rate of 5 Hz (Gain = 5,000,000 V/A, Resolution = 30 fA), 10 Hz (Gain = 5,000,000 V/A, Resolution = 27 fA), and 6.5 to 13 Hz (Gain = 5,000,000 V/A, Resolution = 47 fA), respectively. Pinnacle Acquisition Laboratory (PAL or Sirenia) software was used for all data acquisition. The data acquisition was performed via wireless data transmission or Bluetooth from the potentiostat to a computer. A working electrode potential of +1100 mV versus the Ag/AgCl reference was used for all experiments.

6.2.7 Cell culture and preparation

RAW 264.7 cells were purchased from American Type Culture Collection (ATCC, Manassas, VA, USA) and cultured in Dulbecco's Modified Eagle's medium containing 10% (v/v) fetal bovine serum, L-glutamine (2 mM), penicillin (50 IU/mL), and streptomycin (50 µg/mL) (ATCC). The cells were

maintained in a humidified environment at 37°C and 5% CO_2 and cultured in 25 mL polystyrene culture flasks (Fisher Scientific). Cells were passaged every 2–3 days to avoid overgrowth.

6.2.7.1 Stimulation protocol

Stimulation of NO production in cells was accomplished using purified LPS from the *Escherichia coli* line 0111:B4. A freshly prepared 50 µL aliquot of a 10 µg/mL LPS stock solution was added to healthy RAW 264.7 cells in a 25 cm^2 cell culture flask to obtain a 100 ng/mL final LPS concentration and then incubated for 24 h. An unstimulated RAW macrophage cell flask from the same population was incubated under identical conditions and used as a control (native) for each stimulation experiment.

6.2.7.2 Sample preparation

The protocol used for cell analysis is shown in Figure 6.2A. Cells were grown in 25 cm^2 polystyrene flasks until they reached approximately 80% confluence. At the 80% confluence level, there are around 5 million RAW cells in the flask. These cells were stimulated using LPS and, after the stimulation period (24 h with a 100 ng/mL final LPS concentration, Figure 6.2B), cells were harvested using a scraper and centrifuged at 3500 rpm for 2.5 min to make a live cell pellet. Before centrifugation, 250 µL of the cell solution was taken out for cell counting. The supernatant medium was then removed, leaving only the cell pellet. The cell pellet was then washed with 10 mM phosphate buffered saline at pH 7.4. Next the cell pellet was lysed using 250 µL of a lysis buffer containing 10 mM boric and 2 mM TTAC at pH 10.3 to 10.7. Both the high pH and surfactant assisted with the immediate lysis of cells. Higher molecular weight compounds such as proteins and cell membranes were removed by centrifugation of the lysate for 2–7 min using a 3 kDa molecular weight cut-off filter (VWR International, West Chester, PA, USA). The filtered lysate was then loaded into the sample reservoir of the microchip.

For the standard addition studies, four 25 cm^2 cell flasks with the same passage number were harvested and lysed using 1 mL of 10 mM boric with 2 mM TTAC at pH 10.3 (for 1 cell flask, 250 µl of buffer was used). The lysate was divided into five portions, and the internal standard was appropriately added to ensure a final concentration 10 µM. Standard addition concentrations of 15, 30, 60, and 120 µM

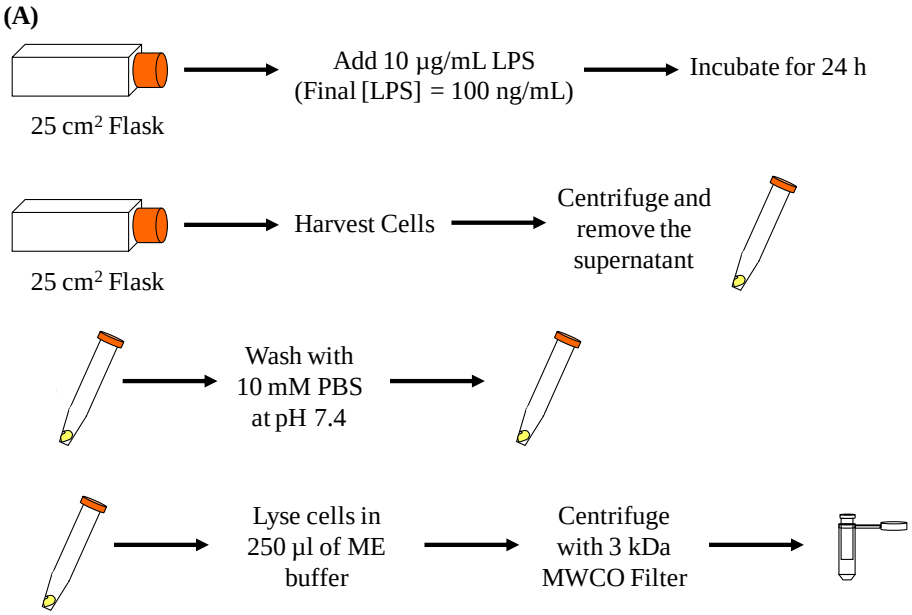

(B)

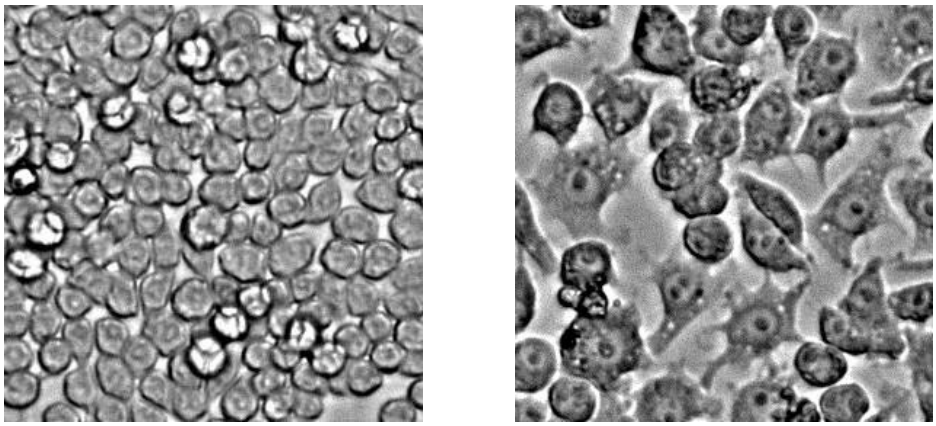

Native macrophages after 24 h

100 ng/mL LPS-stimulated macrophages after 24 h

Figure 6.2: (A) Diagram of the stimulation and sample preparation protocol for RAW 264.7 macrophage cells prior to ME-EC and Griess assay analyses. (B) Images of RAW 264.7 macrophage cells after 24 h without stimulation (left) and with LPS-stimulation (right).

NO_2^- were chosen and the required nitrite volume from a 1 mM nitrite standard was added to the cell lysates. Before adding I^- and NO_2^-, a volume equal to that of the I^- and NO_2^- to be added was removed from the cell lysate.

6.2.7.3 Cell viability

Cell viability was measured using the Trypan blue (Fisher Scientific) exclusion assay and a hemocytometer cell count (C-Chip disposable hemocytometer, Bulldog Bio, Inc., Portsmouth, NH, USA). The RAW cell suspension was diluted using a 1:1 to 1:3 ratio (based on cell density) with a 0.4% Trypan blue solution. The number of viable cells and the cell density were determined using a 4 mm^2 total area hemocytometer. Native RAW cells typically had densities of about 5 million cells in a 25 cm^2 flask.

6.2.7.4 Griess assay protocol

The Griess assay was performed using 96-well plates and a plate reader (Molecular Devices, Spectra Max M5, Sunnyvale, CA, USA). To perform the assay, 100 µL of the filtered cell lysate was added to 100 µL of Griess reagent, left to react for 15 min, after which the absorbance at 540 nm was recorded using the plate reader. A buffer background was always employed for these measurements. For nitrite quantitation, a calibration curve was prepared using nitrite standards from 1 to 50 µM. Cell counts were taken before lysing the cells, and the final nitrite concentration was calculated, taking into account the cell counts.

6.3 Results and discussion

6.3.1 Microchip electrophoresis with electrochemical detection

There are two primary electrode configurations that are used for ME under reverse polarity conditions. The electrode can be placed either slightly inside the channel (in-channel) or outside the channel (end-channel). The advantage of the in-channel configuration is that it allows higher resolution between closely migrating species, which cannot be separated using the end-channel configuration due to band broadening [9]. Therefore, faster separations and shorter analysis times can be obtained using the in-channel configuration. Also, we have observed an increase in sensitivity, lower LOD and a higher number

of theoretical plates with the in-channel configuration compared to the end-channel configuration [9]. However, an important consideration with in-channel detection is that one must take into account the working electrode potential shift that occurs due to the separation voltage when an electrode is placed inside the channel. To minimize this effect in these experiments, the working electrode was placed exactly at the channel end, which still preserves the higher resolution and separation efficiencies characteristic of in-channel detection that are necessary for these studies, but minimizes the potential shift at the working electrode (Figure 6.1B) [9].

6.3.2 Separation buffer optimization

The analytes of interest in our studies of nitrosative stress included NO, NO_2^- (a metabolite of NO), GSH (cellular antioxidant), AA (cellular antioxidant), and tyrosine (amino acid, which is nitrated in the presence of $ONOO^-$). We have previously reported the separation and detection of several of these analytes (nitrite, ascorbic acid, tyrosine, glutathione, and H_2O_2) by ME-EC as compounds that could potentially interfere with the quantitation of NO and NO_2^- in macrophage cell lysates [9]. For the macrophage cell lysate studies described here, the same separation conditions (10 mM boric with 2 mM TTAB) with slight modifications were utilized.

6.3.2.1 Internal standard, surfactant, and interferences

To quantitate the compounds in the cell lysates and increase the precision of the analytical method, iodide was incorporated as an internal standard and, therefore, had to be taken into consideration during the separation optimization procedures. In our previous studies, TTAB was used to reverse the EOF. In these studies, TTAB was replaced with TTAC, where the counter ion is Cl^- instead of Br^-. It was found that bromide can be oxidized to Br_2 at around +1200 mV versus Ag/AgCl, leading to an increase in background current at the EC detector. Bromide, chloride, and nitrite have similar electrophoretic mobilities and, hence, migrate closely. We observed a vacancy peak close to the nitrite peak during initial cell studies due to high Cl^- content. Another species that needed to be separated from the cell lysate components was azide. The molecular weight cut-off filters used for cell lysate filtration were found to

contain a small amount of this compound, which is used as an anti-microbial agent. Under these separation conditions, azide migrated between nitrite and iodide but did not interfere with either measurement.

6.3.2.2 Conductivity issues

During the initial analysis of the cell lysates, it was observed that the sampling current was always higher than the separation current and the high conductivity samples suppressed the nitrite peak due to destacking [11]. A similar suppression in the nitrite signal has been reported in CE when a high conductivity sample was analyzed [12]. To reduce the amount of salt and matrix components present in biological samples prior to CE analysis, solid-phase microextraction [13], acetonitrile addition (acetonitrile lowers the sample conductivity) [12], dialysis [14], and pre-electrophoresis separation [15] have been widely employed.

An alternative approach to avoid nitrite destacking is to increase the conductivity of the separation buffer by using sodium chloride. Figure 6.3A shows the nitrite peak suppression that occurs when standards are prepared in a high conductivity buffer (10 mM boric with 2 mM TTAC and 10 mM NaCl at pH 10.3) and the separation buffer consists of a low conducting buffer (10 mM boric with 2 mM TTAC at pH 10.3). In contrast, Figure 6.3B illustrates that the addition of 7.5 mM NaCl to the separation buffer causes an approximately 3-fold increase in the nitrite signal. This can then be compared to a case where both the sample buffer and separation buffer are low conductivity buffers (10 mM boric with 2 mM TTAC at pH 10.3) (Figure 6.3C). In this last case, the nitrite signal is similar to that seen in Figure 6.3B. These experiments confirmed the destacking of nitrite in high conductivity samples. All three electropherograms used for the comparison studies were recorded with the same microchip, working electrode, and working electrode potential.

6.3.3 Detection of nitrite from macrophage cell lysates

RAW 264.7 macrophage cells are known to produce large amounts of NO through the activation of iNOS. LPS, an endotoxin in negative gram bacteria and an external stimulant, can be used to activate

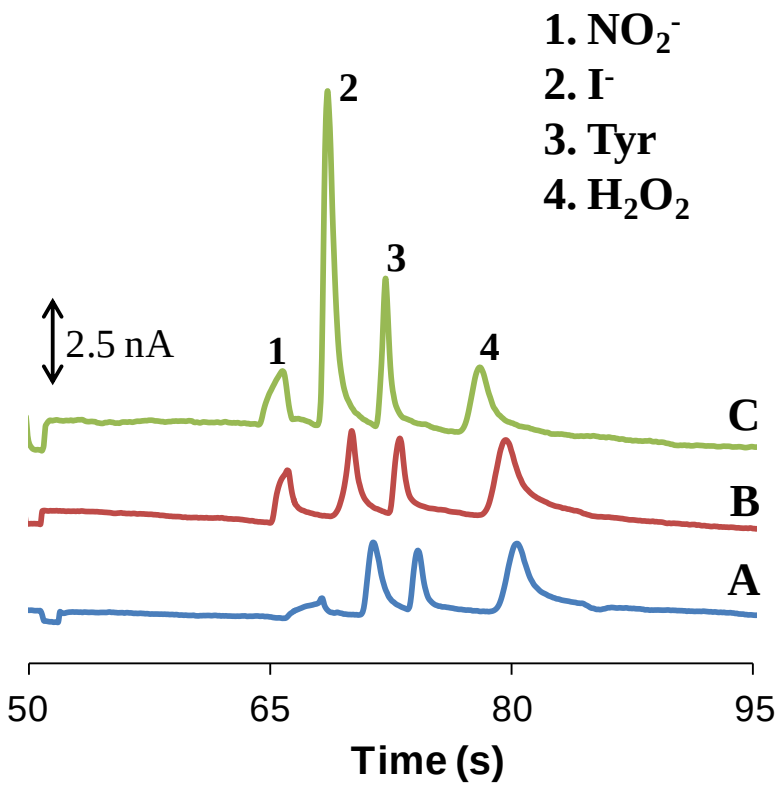

Figure 6.3: Electropherograms of a standard containing 100 µM nitrite, 10 µM iodide (internal standard), 50 µM tyrosine, and 200 µM hydrogen peroxide (neutral marker) using a 10 mM boric acid and 2 mM TTAC buffer at pH 10.3 while varying the sample and run buffer conductivities. (A) High conductivity sample buffer (10 mM NaCl) and normal separation buffer. (B) High conductivity sample buffer (10 mM NaCl) and high conductivity separation buffer (7.5 mM NaCl). (C) No change to the conductivity of the sample and separation buffer.

iNOS [16,17]. It has been reported that RAW 264.7 macrophage cells produce significantly higher amounts of NO in the presence of LPS [16,17]. In these studies, a LPS concentration of 100 ng/mL over 24 h was used for cell stimulation (Figure 6.2A). A substantial difference in physical appearance between native and LPS-stimulated cells was observed, as can be seen in Figure 6.2B.

To compare intracellular NO_2^- produced in stimulated and native macrophage cells, bulk cell lysates were prepared as shown in Figure 6.2A, and analyzed by ME-EC. The Griess assay was also performed to compare with the results obtained with ME-EC. To confirm that NO production was due solely to an increase in iNOS activity, a separate set of cells was exposed to L-NAME, which is a known inhibitor of iNOS, before LPS stimulation and analyzed via Griess assay. These results were compared to those from native and LPS-stimulated cell lysate samples with the same passage number. Each flask contained around 5 million cells, which were lysed in 250 μL of borate buffer (10 mM boric with 2 mM TTAC at pH 10.3 to 10.7) in order to minimize the sample conductivity (Figure 6.3A).

Figure 6.4A shows the electropherograms obtained for native and LPS-stimulated cell lysates using our ME-EC device. The migration times for the first two peaks in the native cell electropherogram were similar to those for nitrite and iodide standards, and the peak identities were confirmed by spiking with standards. Samples were also spiked with azide to further ensure that the nitrite peak does not comigrate with azide during cell studies.

6.3.4 Comparison of nitrite production in macrophage cell lysates using ME-EC and Griess assay

Three different pairs of native and LPS-stimulated cell lysates were analyzed by both the ME-EC and the Griess assay for the comparison of nitrite concentrations. Both methods were used to determine nitrite production increase in LPS-stimulated cells versus native cells (Figure 6.4B). A t-test was performed to compare the two sets of data (Greiss versus ME-EC), and it was found that these two series were statistically insignificant at a 90% confidence level. This shows that the nitrite level detected with ME-EC is similar to that seen in the results of the Griess assay.

The nitrite concentration varied from one sample to another due to the samples having different cell counts. Therefore, the cell counts were taken into account in both the Griess assay and ME-EC studies when calculating the final nitrite concentrations. The nitrite production in a single cell was estimated by assuming that the volume of a macrophage is approximately 0.5 pL. The Griess assay results show that the average intracellular concentrations of nitrite in single unstimulated and LPS-stimulated macrophage cells are 0.63 ± 0.16 mM (0.31 ± 0.08 fmol/cell) and 1.69 ± 1.06 mM (0.84 ± 0.53 fmol/cell), respectively.

In the case of ME-EC analysis, an external calibration curve could not be used for the quantitation of nitrite due to the nitrite peak suppression. Therefore, the method of standard additions was used, employing iodide as an internal standard. Two different ME-EC setups were used for the analysis of these samples, and a standard addition calibration curve of the nitrite/iodide response versus standard addition concentration was plotted. These plots yielded R^2 values of 0.987 and 0.973 resulting in values for intracellular nitrite of 0.58 and 0.83 fmol per cell, respectively. This resulted in an average estimated intracellular nitrite concentration for a single native macrophage cell of 1.41 mM. The average nitrite level in single LPS-stimulated cells was then estimated using the nitrite production increase in LPS-stimulated cells relative to that in native cells, which is a 2.83-fold increase (Figure 6.4B). Consequently, LPS-stimulated cells have a nitrite concentration of approximately 4.00 mM (1.99 fmol per cell). Goto et al. reported similar levels for extracellular nitrite production in single LPS-stimulated macrophage cells using the Griess reagent and a microfluidic device [18].

6.3.5 Direct detection of NO and other electroactive species in macrophage cells

6.3.5.1 NO detection

The reason for employing ME-EC in these studies is the ability to directly detect NO, its metabolite NO_2^-, and other cellular electroactive species (*e.g.*, cellular antioxidents) simultaneously. The overall goal is to implement this in a single cell analysis system in the future. Detection of all these species cannot be achieved with the Griess assay or LIF detection alone.

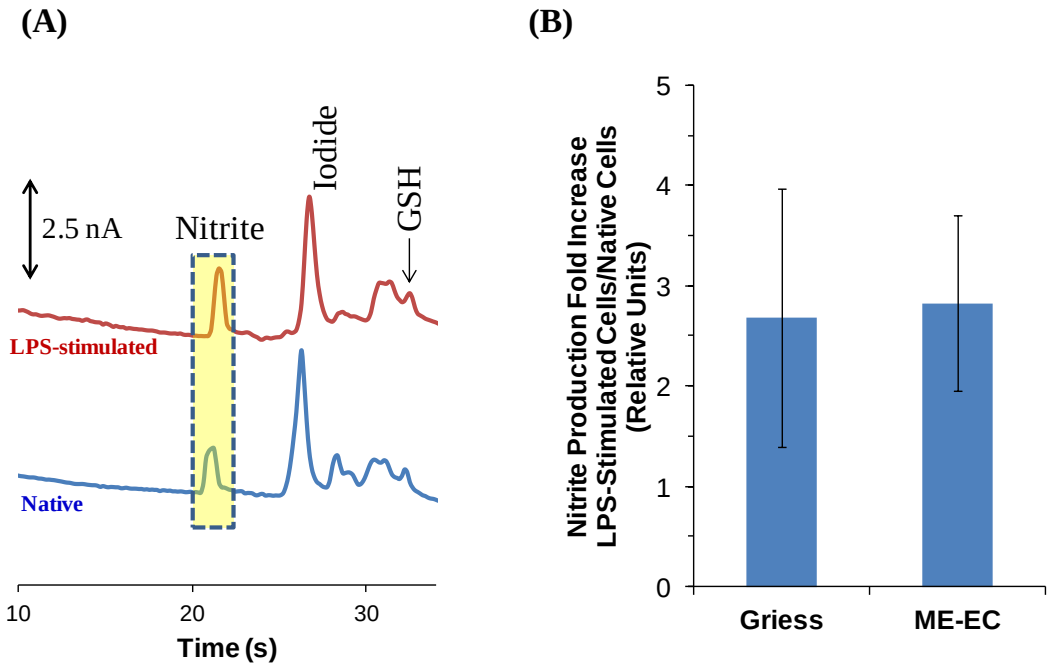

Figure 6.4: (A) Comparison of LPS-stimulated (top) and native (bottom) RAW 264.7 macrophage cell lysates using ME-EC. (B) Comparison of the ME-EC method and the Griess assay for determining the increase in nitrite concentration resulting from a 24 h LPS stimulation relative to the nitrite concentration produced from native cells. The sample was prepared in 10 mM boric acid and 2 mM TTAC buffer at pH 10.3 and the separation was achieved with a 10 mM boric acid, 7.5 mM NaCl and 2 mM TTAC buffer at pH 10.3

When detecting NO in cell lysates, sample preparation steps were streamlined to minimize NO degradation and evaporation. Cells were lysed quickly (10–20 s), and the lysate was centrifuged for only 2 min. Even though nitrite destacks in low conductivity run buffers (run conditions similar to Figure 6.3A), a buffer consisting of 10 mM boric and 2 mM TTAB at pH 11 was used initially for NO detection. The cells were lysed using the same buffer. Also instead of 100 ng/mL LPS, cells were stimulated with 1.5 µg/mL LPS for 6-8 h. This stimulation was used to obtain a high level of NO production in a short period of time. This stimulation also made it possible to perform the experiment in the same day as stimulation. Figure 6.5 shows electropherograms obtained for native and LPS-stimulated cell lysates using this method. In this case, nitrite destacking was not observed and higher nitrite levels were observed in LPS-stimulated cells; however, nitrite destacking was common using these buffer conditions. Migration times for the first three peaks in the native cell electropherogram were similar to those of nitrite, tyrosine, and glutathione standards. Standards of nitrite, tyrosine, and glutathione were also spiked into the cell lyste for peak identification. The migration time of the fourth peak was similar to the neutral marker and this peak quickly disappears over several injections suggesting that the compound is NO.

Figure 6.6 shows electropherograms obtained for native and LPS-stimulated cell lysates following this procedure under modified buffer conditions (10 mM boric with 2 mM TTAC and 7.5 to 10 mM NaCl at pH 10.3-10.7, buffer conditions were similar to Figure 6.3B). It can be seen that the height of the peak that migrates at approximately 30 s decreases over time compared to the internal standard peak. The migration time of the decreasing peak is close to the neutral marker (32.3 ± 2.1 s), and the quick disappearance of this peak over several injections suggests that the compound is unstable. Since cells produce NO following LPS-stimulation due to the induction of iNOS, this peak is most likely NO. The disappearance of this peak is probably due to loss of the gas through the open reservoirs on the microchip or permeation through the PDMS. Nitrite was also detected during these studies, but the NO_2^- peak is very small compared to the NO peak (Figure 6.5 inset), which confirms that NO disappears from the

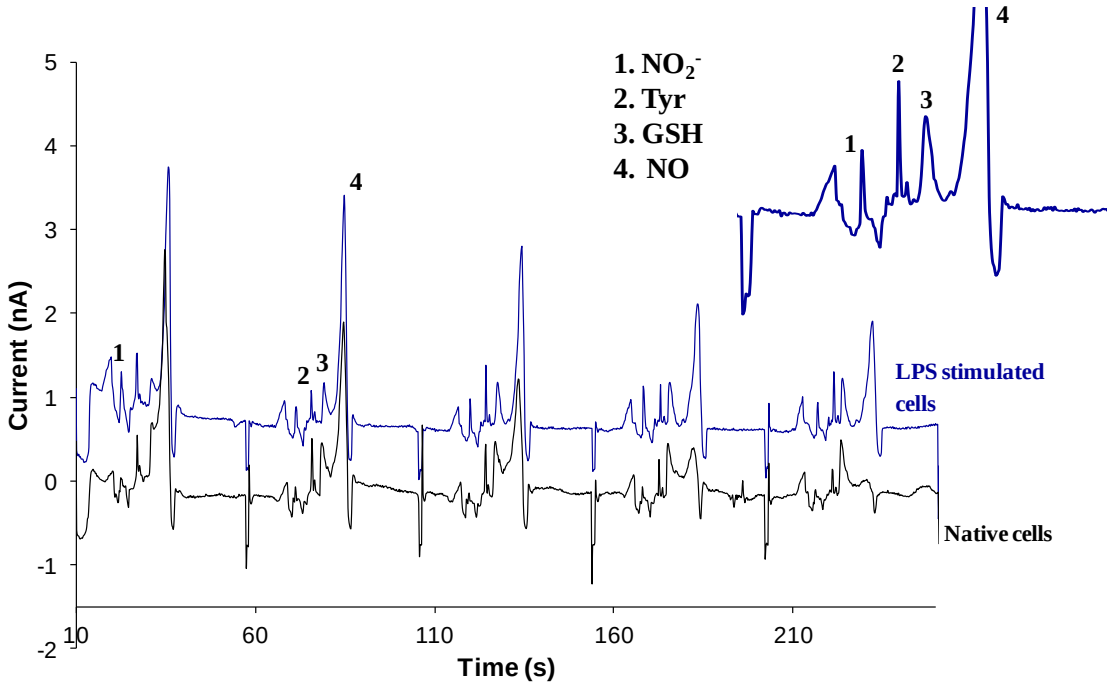

Figure 6.5: Detection of NO in macrophage cell lysate. LPS-stimulated cell lysate (top) and native cell lysate (bottom). Inset is a magnified portion is an electropherogram of the LPS-stimulated cell lysate. The cells were lysed using 500 µL of 10 mM boric acid and 2 mM TTAB buffer at pH 11 and the separation was achieved with a run buffer consists of 10 mM boric acid and 2 mM TTAB buffer at pH 11.

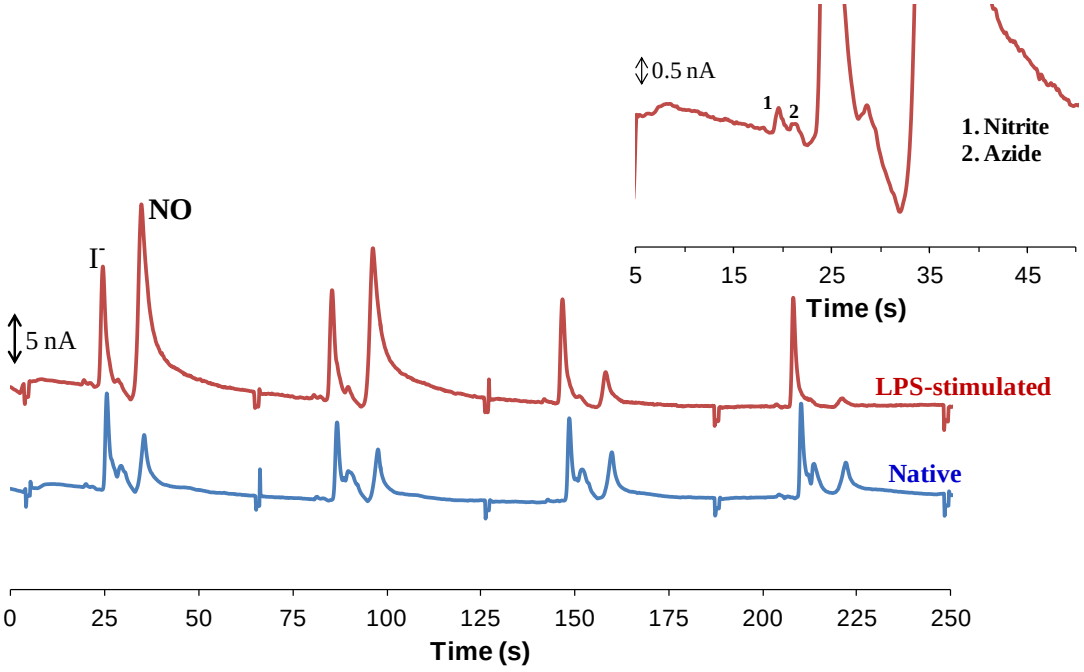

Figure 6.6: Detection of NO in cell lysate. LPS-stimulated cell lysate (top) and native cell lysate (bottom). Inset is a magnified portion of the LPS-stimulated cell lysate. The sample was prepared in 10 mM boric acid and 2 mM TTAC buffer at pH 10.3 and the separation was achieved with a 10 mM boric acid, 7.5 mM NaCl and 2 mM TTAC buffer at pH 10.3.

wells quickly before degradation occur. When the sample preparation time was lengthened, this peak disappeared.

We previously reported a ME method for the detection of NO generated using diethylammine NONOate (DEA/NO) and proline NONOate (PROLI/NO) salts (chapter 3) [19]. The migration time of NO in those studies is comparable to the migration time of the decaying peak in the cell lysates considering the slight variation in chip-to-chip migration times that is expected in PDMS-based systems [19]. It can be seen in the native cell lysate that the last peak does not decay at the same rate as the unstable NO peak seen in LPS-stimulated cell lysate. This indicates that the peak observed in the native cell sample is contaminated with a more stable electroactive species. This species was found to be an interfering filter component that migrates close to the neutral marker (Figure 6.5 and 6.6). Therefore, the NO peak observed in these studies is contaminated.

Currently, the NO peak cannot be used for a quantitative comparison of native and stimulated cells due to the necessity for further peak identification, experimental variability, the presence of interference due to the filters, and, most importantly, the fact that the peak decreases over time due to evaporation and degradation. However, detection of NO will be better accomplished using a single cell analysis microfluidic device where cells are lysed inside the device and the content is immediately analyzed. Since the cell lysis procedure is automated, a single cell cytometric device would provide better precision. Furthermore, a single cell cytometric device eliminates the cell lysate filtering step.

6.3.5.2 Comparison of glutathione levels in native and stimulated cells

Other electroactive species such as tyrosine and GSH were also detected in macrophage cell lysates. However, electropherograms of native and LPS-stimulated cell lysates showed a very small peak or no peak for AA, which agreed with previous ME-LIF studies [20]. Macrophages do not naturally produce AA and an AA free media was used for cell culture. Previous studies reported undetectable levels of AA in RAW macrophage cells [21].

The relative GSH and nitrite levels for three separate LPS-stimulated cell lysates were compared to that of a native cell lysate with the same passage number using the same ME-EC conditions used for nitrite detection. As before, it was found that the nitrite level in LPS-stimulated cells was increased 5.74 ± 2.44 times relative to the native cell lysates. However, the GSH levels showed no significant change (1.30 ± 0.31) when the cells were stimulated with LPS (Figure 6.7). Hothersall *et al.* also observed that GSH levels were not changed when macrophage cells were stimulated with LPS alone. However, they have shown that the GSH level changed when the cells were stimulated with LPS and interferon gamma [22].

6.4 Conclusion

In this chapter, a ME-EC method was optimized for the detection of nitrite, NO, and other electroactive species within macrophage cell lysates. ME-EC makes it possible to obtain more information regarding the overall cellular redox state of the cell. It also provides a separation of interfering species from the analytes of interest that cannot be achieved using classical methods such as the Griess assay and fluorescence imaging. Initially, NO production was detected through the detection of NO_2^- using the ME-EC device. The results obtained for NO_2^- production between LPS-stimulated and native cell lysates using ME-EC were compared to those from the Griess assay. This method was then used for the direct detection of NO and other electroactive species in the cell lysate. An unstable species, which had many of the chemical and physical properties of NO, was detected during these studies. However, the NO peak cannot currently be used for a quantitative comparison of native and stimulated cells. The detection of NO will be better accomplished using a single cell analysis microfluidic device where cells are lysed inside the device and the content immediately analyzed. We have already reported a single cell chemical cytommetric device for NO detection from Jurkat cells using a NO-selective fluorophore [23]. The ultimate goal is to use ME-EC to measure multiple redox-active species in a single cell as an indication of nitrosative stress.

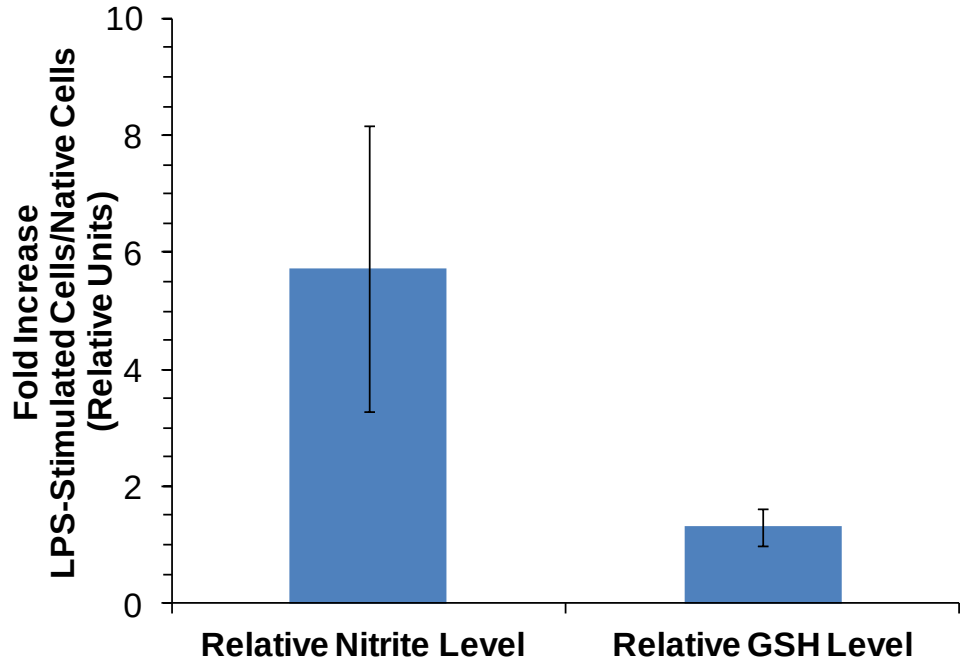

Figure 6.7: Comparison of the nitrite and glutathione (GSH) levels as a result of LPS stimulation relative to that of the native cell lysate. The sample was prepared in 10 mM boric acid and 2 mM TTAC buffer at pH 10.3 and the separation was achieved with a 10 mM boric acid, 10 mM NaCl and 2 mM TTAC buffer at pH 10.7.

6.5 References

1. MacMicking, J.; Xie, Q.; Nathan, C., Nitric oxide and macrophage function. *Annu. Rev. Immunol.* **1997,** *15*, 323-350.

2. Martinez, F. O.; Helming, L.; Gordon, S., Alternative activation of macrophages: an immunologic functional perspective. *Annu. Rev. Immunol.* **2009,** *27*, 451-483.

3. Pacher, P.; Beckman, J. S.; Liaudet, L., Nitric oxide and peroxynitrite in health and disease. *Physiol. Rev.* **2007,** *87* (1), 315-424.

4. Minghetti, L.; Levi, G., Microglia as effector cells in brain damage and repair: focus on prostanoids and nitric oxide. *Prog. Neurobiol.* **1998,** *54* (1), 99-125.

5. Valko, M.; Leibfritz, D.; Moncol, J.; Cronin, M. T. D.; Mazur, M.; Telser, J., Free radicals and antioxidants in normal physiological functions and human disease. *Int. J. Biochem. Cell Biol.* **2006,** *39* (1), 44-84.

6. Zhang, H.; Forman, H. J., Glutathione synthesis and its role in redox signaling. *Semin. Cell Dev. Biol.* **2012,** *23* (7), 722-728.

7. Schulz, J. B.; Lindenau, J.; Seyfried, J.; Dichgans, J., Glutathione, oxidative stress and neurodegeneration. *Eur. J. Biochem.* **2000,** *267* (16), 4904-4911.

8. Hulvey, M. K.; Frankenfeld, C. N.; Lunte, S. M., Separation and Detection of Peroxynitrite Using Microchip Electrophoresis with Amperometric Detection. *Anal. Chem.* **2010,** *82* (5), 1608-1611.

9. Gunasekara, D. B.; Hulvey, M. K.; Lunte, S. M., In-channel amperometric detection for microchip electrophoresis using a wireless isolated potentiostat. *Electrophoresis* **2011,** *32* (8), 832-837.

10. Scott, D. E.; Grigsby, R. J.; Lunte, S. M., Microdialysis Sampling Coupled to Microchip Electrophoresis with Integrated Amperometric Detection on an All-Glass Substrate. *Chem. Phys. Chem.* **2013,** *14* (10), 2288-2294.

11. Boden, J.; Baechmann, K., Investigation of matrix effects in capillary zone electrophoresis. *J. Chromatogr. A* **1996,** *734* (2), 319-330.

12. Friedberg, M. A.; Hinsdale, M. E.; Shihabi, Z. K., Analysis of nitrate in biological fluids by capillary electrophoresis. *J. Chromatogr. A* **1997,** *781* (1 + 2), 491-496.

13. Boudko, D. Y., High-resolution capillary electrophoresis on nitrite and nitrate in biological samples. *Methods Mol. Biol.* **2004,** *279* (Nitric Oxide Protocols (2nd Edition)), 9-19.

14. Haddad, P. R.; Doble, P.; Macka, M., Developments in sample preparation and separation techniques for the determination of inorganic ions by ion chromatography and capillary electrophoresis. *J. Chromatogr. A* **1999,** *856* (1-2), 145-77.

15. Timerbaev, A. R.; Fukushi, K.; Miyado, T.; Ishio, N.; Saito, K.; Motomizu, S., Analysis of highly saline samples by capillary zone electrophoresis: enhanced direct UV detection of inorganic anions using on-capillary preconcentration and clean-up techniques. *J. Chromatogr. A* **2000,** *888* (1+2), 309-319.

16. Lorsbach, R. B.; Murphy, W. J.; Lowenstein, C. J.; Snyder, S. H.; Russell, S. W., Expression of the nitric oxide synthase gene in mouse macrophages activated for tumor cell killing. Molecular basis for the synergy between interferon-gamma and lipopolysaccharide. *J. Biol. Chem.* **1993,** *268* (3), 1908-1913.

17. Held, T. K.; Weihua, X.; Yuan, L.; Kalvakolanu, D. V.; Cross, A. S., Gamma interferon augments macrophage activation by lipopolysaccharide by two distinct mechanisms, at the signal transduction level and via an autocrine mechanism involving tumor necrosis factor alpha and interleukin-1. *Infect. Immun.* **1999,** *67* (1), 206-212.

18. Goto, M.; Sato, K.; Murakami, A.; Tokeshi, M.; Kitamori, T., Development of a microchip-based bioassay system using cultured cells. *Anal. Chem.* **2005,** *77* (Copyright (C) 2013 American Chemical Society (ACS). All Rights Reserved.), 2125-2131.

19. Gunasekara, D. B.; Hulvey, M. K.; Lunte, S. M.; Fracassi, d. S. J. A., Microchip electrophoresis with amperometric detection for the study of the generation of nitric oxide by NONOate salts. *Anal. Bioanal. Chem.* **2012,** 403, 2377-2384.

20. Mainz, E. R.; Gunasekara, D. B.; Caruso, G.; Jensen, D. T.; Hulvey, M. K.; Fracassi, d. S. J. A.; Metto, E. C.; Culbertson, A. H.; Culbertson, C. T.; Lunte, S. M., Monitoring intracellular nitric oxide production using microchip electrophoresis and laser-induced fluorescence detection. *Anal. Methods* **2012,** *4* (2), 414-420.

21. Badrakhan, C.-D.; Petrat, F.; Holzhauser, M.; Fuchs, A.; Lomonosova, E. E.; de, G. H.; Kirsch, M., The methanol method for the quantification of ascorbic acid and dehydroascorbic acid in biological samples. *J. Biochem. Biophys. Methods* **2004,** *58* (3), 207-218.

22. Hothersall, J. S.; Cunha, F. Q.; Neild, G. H.; Norohna-Dutra, A. A., Induction of nitric oxide synthesis in J774 cells lowers intracellular glutathione: effect of modulated glutathione redox status on nitric oxide synthase induction. *Biochem. J.* **1997,** *322* (2), 477-481.

23. Metto, E. C.; Evans, K.; Barney, P.; Culbertson, A. H.; Gunasekara, D. B.; Caruso, G.; Hulvey, M. K.; Fracassi, d. S. J. A.; Lunte, S. M.; Culbertson, C. T., An Integrated Microfluidic Device for Monitoring Changes in Nitric Oxide Production in Single T-Lymphocyte (Jurkat) Cells. *Anal. Chem.* **2013,** *85* (21), 10188-10195.

Chapter 7

Conclusions and future direction

7.1 Conclusions

The main goal of this dissertation was to develop methods based on microchip electrophoresis with electrochemical detection to probe cellular nitrosative stress. To achieve this goal, a fast separation of RNOS and intracellular antioxidants was achieved using reverse polarity conditions. This method makes it possible to detect RNS before they significantly degrade, as well as separate these compounds from intracellular electroactive interferences. High resolution was required for separation of all species and therefore electrochemical detection was performed using in-channel amperometric detection. An isolated potentiostat that was developed by Pinnacle Technology was used for these studies. The ME-EC system with this potentiostat was characterized and it was found that the $E_{1/2}$ of analytes shifted in a negative direction when the electrode was placed inside the channel. This is due to the interaction of the separation voltage with potential applied to the working electrode. To minimize this $E_{1/2}$ shift, the working electrode was placed at the exact end of the channel, which still preserved the higher resolution characteristic of in-channel amperometry by lowering the shift in potential. A separation of nitrite, tyrosine, ascorbic acid, glutathione and hydrogen peroxide was achieved in less than 35 s using this approach.

This method was then applied for the detection of nitric oxide and peroxynitrite. For peroxynitrite detection, commercially available peroxynitrite standards were separated using a high pH run buffer (pH 11), which stabilizes the compound. A quick disappearance (within five consecutive 60 s runs) of the peroxynitrite peak was observed during these studies. In addition to peroxynitrite, nitrite was also present in the peroxynitrite standards and was identified based the comparison of the migration time with nitrite standards. This method was then used to study nitric oxide (NO) generation from NONOate salts. NONOate salts degrade under low pH conditions to produce NO. Diethyl amine and proline NONOate salts were used in these studies. Three peaks were detected in the electropherograms correspond to nitrite (due to oxidation of NO), the NONOate parent molecule and NO. NO was identified by its migration time (it migrates with the neutral marker) and rapid disappearance as a function of time. Since an open sample

reservoir was used in the microchip, it was found that NO dissipated quickly leading to a low conversion of NO to nitrite in the sample.

To further identify RNOS in standards and biological samples, two dual-electrode strategies were developed. The first consisted of two 15 µm working electrodes in the series electrode configuration. This configuration was evaluated due to the ease of its integration into simple-T microchips. However, with this configuration, oxidation at the first electrode and the signal difference due to electrode placement with relation to the channel needed to be taken into account when calculating the current ratio. A mathematical correction can be performed to correct for the observed current ratios following an electrode characterization experiment. However, each analyte needs to be evaluated separately in this characterization experiment, which is disadvantageous if this method is applied for the detection of an unknown compound or labile species. The second strategy that was investigated was a dual-parallel configuration that has been previously used for generation of current ratios in CE. The dual-channel microchip design reported by the Hahn group was utilized for this case and no correction was needed. Both of these electrode configurations were used to characterize the purity of commercially available peroxynitrite ($ONOO^-$) standards. During these studies, it was observed that most commercially available $ONOO^-$ samples were contaminated with H_2O_2, which is a precursor used for $ONOO^-$ synthesis.

Before applying this method to cellular analysis, a ME system with laser induced fluorescence detection was developed using a NO selective fluorophore, DAF-FM, for quantification of intracellular NO. DAF-FM (non fluorescent) reacts with NO and produces DAF-FM T, which is highly fluorescent. However, DAF-FM also reacts with dehydroascrobic acid (DHA) and produces DAF-FM DHA, which is spectrally similar to DAF-FM T. Therefore, a separation of DAF- FM T, DAF-FM DHA and an internal standard, 6-CFDA, was developed using ME with LIF detection prior to cell analysis experiments. Jurkat cell were used for the cell studies as they are known to produce NO through activation of iNOS and are non adherent. The NO concentrations inside a single Jurkat cell were quantified using combination of a calibration curve and cell viability counts. The intracellular NO concentrations of native and LPS-

stimulated cells was estimated to be 0.6 and 1.5 mM respectively, which is statistically different ($N = 3$, $p < 0.05$) with NO production 2.5 times higher in LPS-stimulated cells compared to native cells. The internal standard 6-CFDA was used to correct for differences in the volume of the cell and therefore, the DAF-FM T/6-CF ratio can also be used for comparison of NO production increase. Using this ratio, 2.2 times higher NO production was observed in LPS-stimulated cells compared to native cells. The ME-LIF and cell stimulation protocol was then transferred to Kansas State University for single cell analysis analysis experiments using a chemical cytometric device developed by the Culbertson lab. The estimated average intracellular NO production for a single Jurkat cell from the bulk cell studies was compared to the average NO value obtained from the single cell studies with good agreement. However, the distribution of intracellular NO production could only be observed in the single cell analysis studies.

Next, the ME-EC method was used for determination of RNOS in macrophage cells. Macrophage cells were used since they are known to produce large amounts of NO. Initially, 10 mM boric with 2 mM TTAB at pH 11 was used for the separation of standards of nitrite, tyrosine, ascorbic acid, glutathione and H_2O_2. This separation buffer was slightly modified to contain 7.5 to 10 mM NaCl. Cell lysis was performed with a buffer without NaCl. NaCl was added separation buffer to balance the conductivity of the separation buffer with the cell lysates to avoid nitrite desatcking. Additionally, iodide was used as an internal standard in these studies. Initially, nitrite production was compared between LPS-stimulated and native cells lystes. It was found that there was approximately 2.8 times higher nitrite production in LPS-stimulated cells when compared to native cells. Then the sample preparation procedure was expedited to see if we could detect NO in the sample. A quickly decaying peak that migrated with the neutral maker was observed during these expedited studies, confirming the presence of NO. In addition to nitrite and NO, glutathione and tyrosine were also detected in the cell lysates. The intracellular GSH and nitrite levels were compared for cells with LPS-stimulation and under native conditions and no statistically significant increase in glutathione levels (90% confidence) was observed even though nitrite level increased 5.7 times.

7.2 Future directions

7.2.1 Immediate future goals

7.2.1.1 Identification of electroactive species in cell lysates

The immediate future goal is the application of ME with dual-electrode electrochemical detection to confirm the peak identity of species detected during bulk cell analysis. Preliminary experiments have been performed using 10 mM boric and 2 mM TTAB at pH 11 as both the lysis and separation buffers. These conditions are slightly different from those used in chapter 6. Also, instead of 100 ng/mL LPS for 24 h, 1.5 µg/mL LPS for 6-8 h stimulation was used, which makes it possible to perform the cell stimulation and ME-EC analysis on the same day. Current ratios were recorded using both the dual-series and dual-parallel electrode configuration (Chapter 4). Generation of a current ratio is relatively simple in the dual-parallel configuration; however, electrode alignment is much more difficult. Electropherograms obtained using ME-EC with the dual-parallel configuration are shown in Figure 7.1. Table 7.1 lists the current ratios and migration times for the peaks in the macrophage cell lysates compared to standards. The current ratio for the first peak in cell lysates is similar to that of nitrite, however the migration time is slightly different. The fist peak could therefore be azide (azide migrates after nitrite), which has a current ratio similar to that of nitrite. Due to nitrite destacking under these conditions (conductivities of the cell lysate and separation buffer are not equal in this set of experiments), the determination of a nitrite peak ratio is difficult. The decaying peak (5) shows current ratio of 0.21, meaning that it is difficult to oxidize species and potentially NO. In these studies the working electrode potentials were chosen to be +950 mV and +1100 mV for identification of the more difficult to oxidize species, such as nitrite and NO. For identification of Tyr, AA and GSH, different working electrode potentials need be used. In addition to recording and obtaining current ratios for peaks from cell lysates, standards of analytes will be spiked into cell samples to verify migration time and the current ratios will be recorded to make sure the current

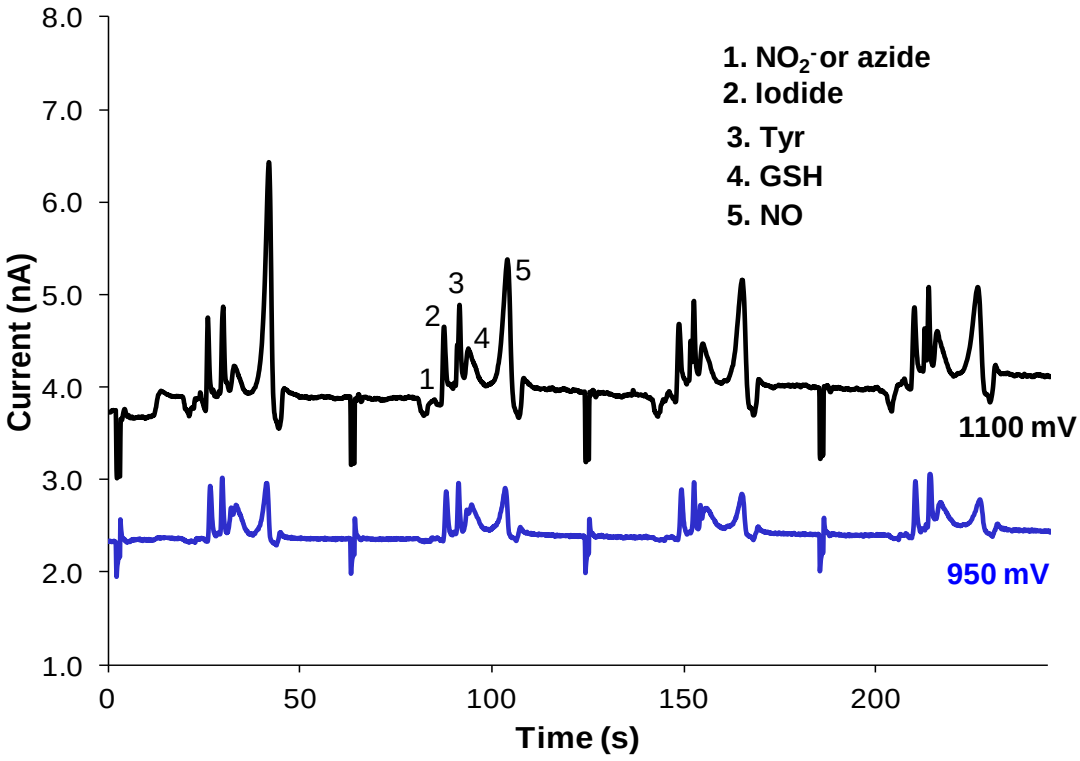

Figure 7.1: Eelectropherograms of native macrophage cell lysates using dual-parallel electrodes. The cells were lysed using 250 µL of 10 mM boric and 2 mM TTAB buffer at pH 11 and the separation was also achieved using the same buffer. WE-1 = +1100 and WE -2 = +950 mV versus Ag/AgCl reference electrode were used.

Table 7.1: Comparison of corrected current ratios and migration times of native macrophage cell lystes and standards. The standard deviation was calculated using the same sample and three consecutive injections in the same microchip (n = 3)

Species	Migration time	Cells I_{950}/I_{1100}	Standards I_{950}/I_{1100}	Migration time	Standards
1	18.3 ± 0.1	0.24 ± 0.03	0.21 ± 0.03	20.8 ± 0.5	Nitrite
2	22.9 ± 0.1	0.63 ± 0.06	0.74 ± 0.03	21.3 ± 0.2	Iodide
3	26.6 ± 0.1	0.65 ± 0.03	0.76 ± 0.02	27.1 ± 0 .2	Tyrosine
4	31.5 ± 0.4	0.66 ± 0.43	0.52 ± 0.08	30.2 ± 0 .2	GSH
5	34.7 ± 0.1	0.24 ± 0.02	1.98 ± 0.06	40.4 ± 0.8	H_2O_2

ratios of peaks in cell lystes do not change.

7.2.1.2 Development of single cell chemical cytometric device

The detection of NO will be accomplished more effectively using a single cell analysis microfluidic device where cells are lysed inside the device and the content is immediately analyzed. A single cell chemical cytommetric device for NO detection from Jurkat cells using a NO-selective fluorophore was described in chapter 4. This device can be modified to incorporate an electrode for ME-EC analysis [1]. A schematic of the modified chemical cytommetric device is shown in Figure 7.2. Jurkat cells are nonadherent cells and easier to handle in a single cell cytometric device than macrophages and will be used for initial studies. Therefore, bulk Jurkat cells were analyzed using the ME-EC method developed in chapter 2 as an initial experiment before moving into single cell studies. A comparison of the ME-EC electropherograms of native and LPS-stimulated Jurkat cell lysate is shown in Figure 7.3. Similar to macrophage cells, NO, GSH and tyrosine peaks were detected during these studies. An LPS concentration of 3 µg/mL was used in these experiments and therefore a low cell viability due to excessive NO production was observed (see chapter 5). The ultimate goal is to use ME-EC to measure multiple redox-active species in a population of individual cells as an indication of nitrosative stress.

7.2.2 Long term future goals

7.2.2.1 Biological studies

The devices developed here can be applied to biological studies, such as determining the effect of oxidized LDL, cytokines, omega-3 fatty acids, and other activating agents on NO release and the production of RNOS in monocyte-derived macrophages using a single cell chemical cytometric device. Monocytes are recruited into the intima due to chronic inflammation and then differentiated into macrophages to regulate high LDL concentrations in intima [2-4]. These transmigrated monocytes can

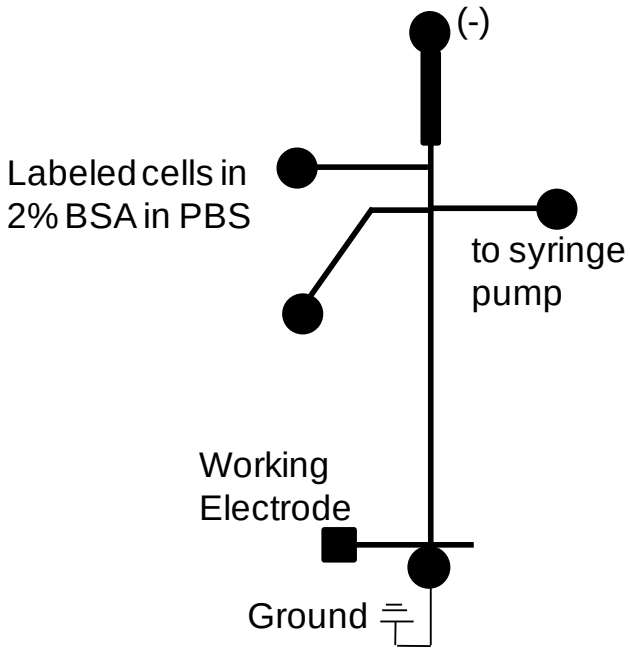

Figure 7.2: A schematic of modified single cell analysis device

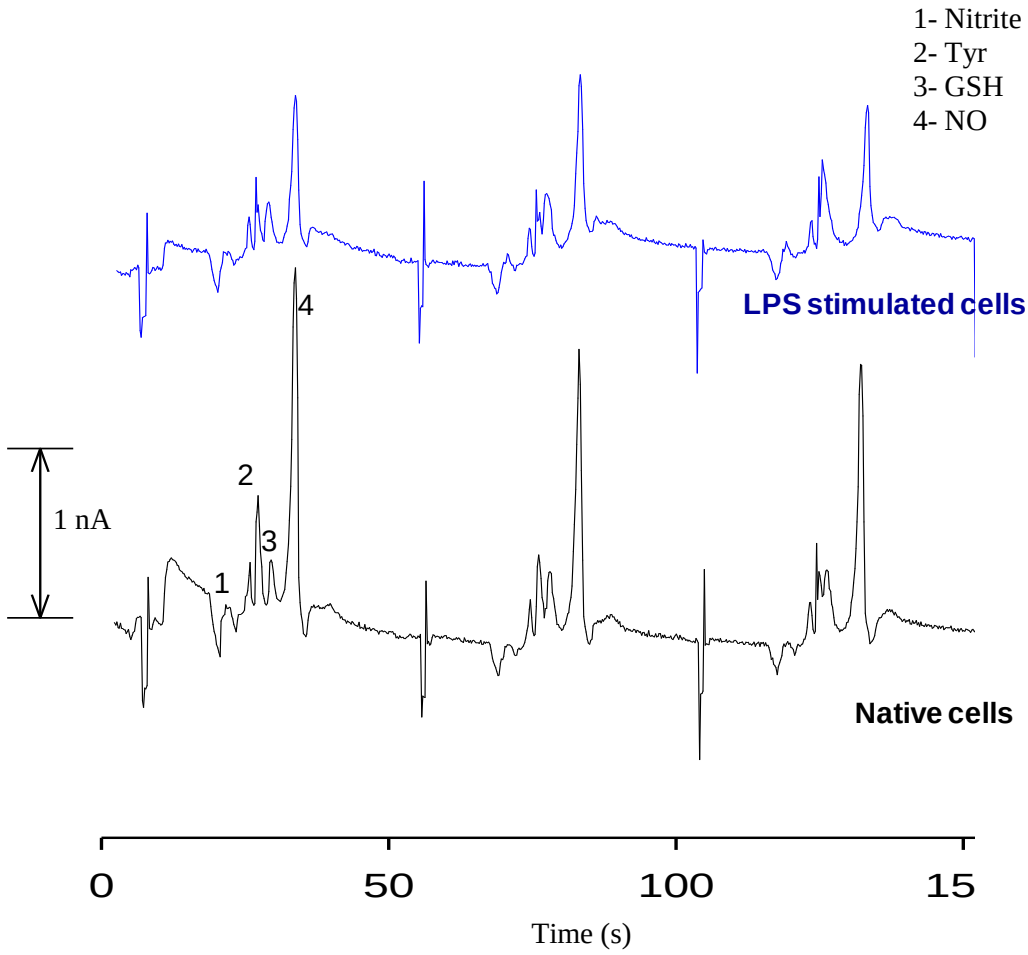

Figure 7.3: (A) Comparison of LPS-stimulated and native Jurkat cell lysates using ME-EC. A LPS concentration of 3 µg/mL for 6 h was used in these experiments. The sample was prepared in 10 mM boric acid and 2 mM TTAB buffer at pH 11 and the separation was also achieved using the same buffer.

differentiate into several different phenotypes, with M1 and M2 macrophages being the two main subpopulations [2,4,5]. M1 macrophages are pro-inflammatory and are produced from monocytes exposed to granulocyte-macrophage colony-stimulating factor (GM-CSF). On the other hand, M2 is an anti-inflammatory macrophage that is produced when the monocyte is exposed to macrophage colony-stimulating factor (M-CSF) [6]. When inflammation is more prevalent, the predominant subpopulation will be M1 macrophages; however, as the healing and regulatory processes occur, there is a shift to the M2 phenotype [5,7].

The M1 subpopulation plays an important role in plaque buildup, and is known to produce large amounts of RNOS that can cause apoptosis of cells and damage to nearby tissues. However, there is less knowledge about the effects of various cytokines (IFN-ɣ and interleukins), LDL, omega-3 fatty acids, etc. on the ratio of subpopulations of macrophages in the plaque buildup and their RNOS production. This is due to the fact that both RAW murine macrophages (adherent cells) and J774 nonadherent macrophages have been the subject of many RNOS-related studies. Therefore, a high throughput single cell chemical cytometric device could be utilized to probe how these substances affect RNOS production in macrophage phenotype subpopulations.

One of goals in this part of the project is to mimic the physiology of an artery using a monolayer of endothelial cells and then determine the amount of RNOS production by macrophages and foam cells that are differentiated from transmigrated monocytes through the endothelial layer using a microfluidic device.

7.2.1.2 Fundamental interests: bipolar electrochemistry

When an electrode is placed in an electric field, the electrode behaves as a bipolar electrode. Both oxidation and reduction reactions occurred simultaneously at the two ends of the bipolar electrode. Bipolar electrodes can be used to convert the electric (electrochemical) signal into a fluorescent or other optical signal where photons are measured instead of electrons. This can potentially be used as a detector

for ME (Figure 7.4) that will result in lower limits of detection due to lower background. We are currently exploring this approach in our laboratory.

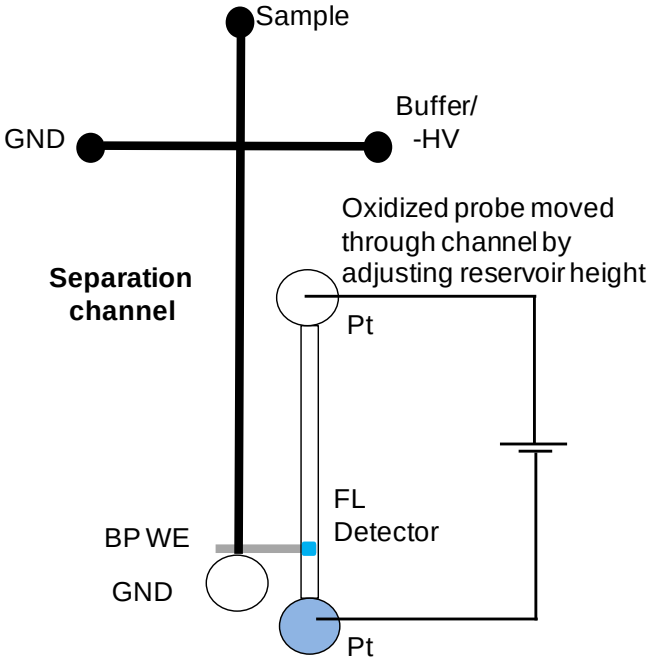

Figure 7.4: Proposed ME coupled bipolar electrode set up for conversion of an electrochemical signal into fluorescence signal

7.3 References

1. Metto, E. C.; Evans, K.; Barney, P.; Culbertson, A. H.; Gunasekara, D. B.; Caruso, G.; Hulvey, M. K.; Fracassi, d. S. J. A.; Lunte, S. M.; Culbertson, C. T., An Integrated Microfluidic Device for Monitoring Changes in Nitric Oxide Production in Single T-Lymphocyte (Jurkat) Cells. *Anal. Chem.* **2013,** *85* (21), 10188-10195.

2. Wilson, H. M., Macrophages heterogeneity in atherosclerosis - implications for therapy. *J. Cell. Mol. Med.* **2010,** *14*, 2055-2065.

3. Lilly, L. S.; Harvard Medical, S., *Pathophysiology of heart disease : a collaborative project of medical students and faculty*. Wolters Kluwer/Lippincott Williams & Wilkins: Baltimore, MD, 2011.

4. Wolfs, I. M. J.; Donners, M. M. P. C.; de, W. M. P. J., Differentiation factors and cytokines in the atherosclerotic plaque micro-environment as a trigger for macrophage polarisation. *Thromb. Haemostasis* **2011,** *106*, 763-771.

5. Mantovani, A.; Garlanda, C.; Locati, M., Macrophage Diversity and Polarization in Atherosclerosis: a question of balance. *Arterioscler. Thromb. Vasc. Biol.* **2009,** *29*, 1419-1423.

6. Waldo, S. W.; Li, Y.; Buono, C.; Zhao, B.; Billings, E. M.; Chang, J.; Kruth, H. S., Heterogeneity of human macrophages in culture and in atherosclerotic plaques. *Am. J. Pathol.* **2008,** *172*, 1112-1126.

7. Wilson, H. M.; Barker, R. N.; Erwig, L.-P., Macrophages: promising targets for the treatment of atherosclerosis. *Curr. Vasc. Pharmacol.* **2009,** *7*, 234-243.